Rise and fall of an ice-cored moraine

A case study from Semskfjellet, Saltfjellet, northern Norway - investigating the role of hydrological processes in the decay of an ice-cored moraine

Master Thesis in Physical Geography

Sofie Jordheim

Department of Geography

University of Bergen

May 2022

Cover photo: The southern ridge of the ice-cored moraine, overlooking the proglacial lake towards the glacier on the eastern flank of Semskfjellet. Photo: Anna de Bode 14.09.21

Abstract

Deterioration of ice-cored moraines damming proglacial lakes may cause local natural hazards. Thus, it is crucial to study and understand their dynamics in a changing climate for mitigation. This study investigated the role of hydrological processes in the decay of an ice-cored moraine at Semskfjellet, Saltfjellet, northern Norway. Fieldwork was carried out during the summer of 2021. Hydrological investigations of the lake and surface streams running along the margin of the moraine were used to infer the environment of the subsurface water pathways and provide insights into the internal structure of the moraine. Remote sensing analysis was used for studying changes in surface elevation over time to assess the rate of de-icing. Dating of moraine ridges and geomorphological mapping further aided in improving the understanding of the formation and development of ice-cored moraines.

The lichenometric dating suggests that the ice-cored moraine was formed during the Little Ice Age and that the proglacial lake emerged at the beginning of the 20th century. The research showed the ice-cored moraine to be in a process of transition, with backwasting and downwasting processes being apparent across the moraine. The internal structure of the moraine influences to what extent the moraine functions as a barrier to the proglacial lake. A threshold possibly connected to the presence of ground ice and/or an ice core in the moraine creates a cyclical and seasonal drainage pattern for the pro-glacial lake which is affected by changes in air temperature, glacial ablation, and water temperature.

The presence of the lake and subsurface waterflow play an important role in the decay of the ice-cored moraine, as it contributes to the melting of ice in the moraine and initiates backwasting and downwasting processes. The central section of the moraine is more influenced by subsurface waterflow and has undergone the highest rates of surface elevation change, compared to the southern and northern sections.

Finally, a conceptual model for the life cycle of this ice-cored moraine system in relation to glacier-permafrost interaction and hydro-geomorphological processes was proposed. In the future, the rate of decay is expected to be heterogenous across the moraine. The scale of full de-icing might be long and possibly connected to the lifespan of the glacier and proglacial lake. Further research of the internal structure of ice-cored moraines and their association with other active processes is encouraged to create a better understanding of the impact of climate change on these ice-cored moraine systems and associated risks of geohazards.

Sammendrag

Nedbrytning av iskjernemorener som demmer bresjøer utgjør en mulig naturfare. Det er derfor viktig å studere og forstå hvordan dynamikken i iskjernemorener påvirkes av endringer i klima, for å kunne forebygge og minimere risiko. Denne studien har undersøkt hvilken rolle hydrologiske prosesser spiller i nedbrytningen av en iskjernemorene ved Semskfjellet, Saltfjellet i Nordland. Feltarbeidet fant sted sommeren 2021. Hydrologiske undersøkelser av innsjøen og overflateavrenning langs marginen til morenen ble brukt som indikatorer for miljøet som dreneringen går gjennom i morenen, for å få innsikt i den interne strukturen. Fjernanalyse ble benyttet for å studere endringer i høydeforskjeller over tid, for å si noe om hvor raskt utsmeltingen foregår. Datering av morenerygger og kvartærgeologisk kartlegging bidro videre til å bedre forståelsen av hvordan iskjernemorener dannes og utvikler seg.

Lichenometridateringene hentydet til at iskjernemorenen stammer fra Lille Istid og at bresjøen ble dannet på begynnelsen av 1900 tallet. Studien viste at iskjernemorenen er i en overgangsfase, med tegn på både horisontal og vertikal nedsmelting. Til hvilken grad morenen fungerer som en barriere for bresjøen synes å påvirkes av den interne strukturen. En terskel som muligens er knyttet til tele i bakken og/eller en iskjerne i morenen har skapt et mønster av en syklisk og sesongbasert drenering av bresjøen. Dreneringsgraden påvirkes videre av endringer i lufttemperatur, breablasjon og vanntemperaturen i bresjøen.

Bresjøen og dreneringen av vann gjennom morenen spiller en viktig rolle for degraderingen av iskjernemorenen ettersom det bidrar til å tine isen inne i morenen, samt setter i gang massebevegelser relatert til vertikal og horisontal nedsmelting. Den sentrale delen av morenen synes å ha vært mest påvirket av undergrunnsdreneringen, og høyden på overflaten synes å ha endret seg mest her, til sammenligning med den nordlige og sørlige delen av morenen.

En konseptuell modell for livssyklusen til denne iskjernemorenen i sammenheng med bre-permafrost interaksjoner og hydrogeomorfologiske prosesser er foreslått. Hastigheten på nedbrytningen av morenen ventes å fortsette å være heterogen for de ulike delen av morenen i fremtiden. Tidshorisonten for en fullstendig nedsmelting kan være lang og er muligens knyttet til breen og bresjøens eksistens. Videre forskning som ser nærmere på den interne strukturen til iskjernemorener og deres tilknytning til andre aktive prosesser anbefales for å skape en bedre forståelse av hvordan naturfarer tilknyttet iskjernemorener påvirkes av klimaendringer.

Acknowledgements

Table of Contents

List of figures

placed in the lake, while the air temperature was recorded by a barometer placed on the shore of the lake.

List of tables

1 Introduction

In recent decades, permafrost thaw and glacial retreat due to climate change have been observed in high mountain areas across the world (Hock *et al.* 2019). The thawing of permafrost and recession of glaciers are altering these landscapes, leading to a destabilization of previously stable areas. There have been numerous observations of alterations in the physical environment, from thawing of peat palsas leading to the emergence of slump holes, slope processes becoming more active with an increase in detachment slides, and streams and rivers finding new ways in the now unfrozen ground, making them disappear from the surface (Mathismoen, 2020; Hipp *et al.* 2014). Glaciers cover about 0,7 % of Norway and are vital for water management and hydropower, as well as being important for tourism. Glaciers are sensitive indicators of climate change and because of the ice-cap hypsometry of Norwegian glaciers, Norwegian glaciers are especially sensitive to changes in surface mass balance (Lilleøren & Etzelmüller, 2011). Andreassen *et al.* (2020) mapped glacier change in mainland Norway since the 1960s, and the general trend shows that, despite heterogenous results of mass balance and extent changes from year to year, Norwegian glaciers are disappearing. Proglacial lakes are also growing in both number and size, which again is associated with more frequent floodings, landslides, and other cascading events. Higher risks of glacier lake outburst floods (GLOFs) are associated with diminishing glaciers and affect the runoff of downstream areas, in addition to changing the visual landscape (Åkesson *et al.* 2017; Beniston *et al.* 2018). Glacierized and snow dominated catchments are also important fresh water sources for plants, wildlife and for local communities (Penna *et al.* 2014).

In the IPCCs special report on the Ocean and Cryosphere in a Changing Climate, second chapter on High Mountain Areas, Hock *et al.* (2019) highlight that glacial retreat and thaw and degradation of permafrost will increase during this century. Near surface permafrost is expected to degrade significantly in the Arctic over the next century, and especially for areas south of 70° north. It is likely that this will have widespread implications for the hydrology, ecology and emissions of greenhouse gases. It is further expected that the arctic terrestrial freshwater systems will go through a transition from a surface water dominated system to a system dominated by groundwater (Frey & McClelland, 2009). The risk of natural hazards associated with changes in the cryosphere is projected to increase in both frequency and

magnitude (Hock *et al.* 2019). A better understanding of the origin of runoff and the interactions between glacial meltwater, streamflow and periglacial features are critical for assessments of risks of natural hazards, mitigation of such risks and good management of water sources in the mountain regions (Penna *et al.* 2014).

Considering the time of transition that we are in, it is becoming increasingly important to have insight into the dynamics and process regimes associated with features of the cryosphere and how they interact with other physical features and processes. Even if both glacial and periglacial processes are present and influential in the landscape formation of high mountain areas, these features are often studied separately (Haeberli, 2005). Integrated research shows that there are a range of interactions between these features, from dynamics connected to freeze-thaw cycles, to energy- and sediment fluxes of meltwater streams, and landform development (Moorman, 2005). As a warming climate is contributing to the de-icing of glacial landforms; more integrated research of glacier-permafrost interactions is needed to better assess the risks associated with the deformation and decreasing stability of landscapes in alpine areas (Haeberli, 2005).

Ice-cored moraines are landforms which formation and preservation depend on glacier-permafrost interactions (Østrem, 1964). Because of the presence of ice at the core, ice-cored moraines have been considered rather stable landforms. There is now however an increasing amount of literature showing that these landforms are de-icing due to the current climatic forcing (see for example Krüger & Kjær, 2000; Schomacker & Kjær, 2008; Ewertowski, 2014). Moraines also play an important role in the groundwater flow and storage processes of glacial catchments, and the interactions between hydrological processes and de-icing influences the spatial distribution and rate of de-icing. Glacial lakes dammed by ice-cored moraines further complicates the picture of glacier-permafrost interactions and poses a serious threat of geohazards in many areas (Falátková, 2016; Richardson & Reynolds, 2000). When modelling the response of glacial catchments to climate change, the influence of permafrost within moraines represents a challenge. Little is for example known in terms of the relationship between the extent of buried and ground ice, melt rate and climate change (Langston *et al.* 2011). The melt out and deterioration of ice-cored moraines and debris covered glaciers damming proglacial lakes may lead to local natural hazards with floods and landslides, which

may be a threat to local communities and infrastructure. Therefore, it is crucial to study and understand the dynamics and process regimes connected to how they are impacted by a changing climate to mitigate for potential geohazards related to them (Clague & Evans, 2000; Quincey *et al.* 2005; Quincey *et al.* 2007; Schomacker, 2008).

This study investigates the role of hydrological processes in the decay of an ice-cored moraine system at Semskfjellet, Saltfjellet, northern Norway. The system consists of a retreating cirque glacier and a proglacial lake dammed by an ice-cored moraine. There is to my knowledge, no previous case studies of ice-cored moraines on Saltfjellet, and thus this project may be seen as a pilot study for this in the area.

1.1   Research questions

This research project aims to gain a holistic understanding of the formation, development, and degradation of the ice-cored moraine system with a focus on the role of hydrological processes, to assess how it may develop in the future under the current climatic forcing. A multifaceted approach combining hydrological investigations with geomorphological mapping, lichenometric dating and remote sensing techniques is applied and explores the following research questions:

- *When and how was this ice-cored moraine system established?*

- *What pathways of surface and subsurface hydrology exist around the ice-cored moraine and what is their role in this system?*

- *What may be inferred about the internal structure of the ice-cored moraine from hydrological investigations of the lake and surface streams, aided by remote sensing analysis?*

- *What is the role of hydrological processes in the decay of the ice-cored moraine and how may climatic changes influence the rate of decay and future development of this system?*

2 Theoretical background

2.1 Glacier-permafrost interactions

The landscape of high mountain areas of Norway is shaped by both glacial and periglacial processes (Lilleøren & Etzelmüller, 2011). Despite both domains being important parts of the cryosphere, glaciers and permafrost have been regarded as different fields and thus tends to be studied separately. This is because glaciers and permafrost have been deemed mutually exclusive and that glaciers in permafrost environments were considered slow moving and non-erosive. However, more recent integrated research has shown that there are a range of interactions between glaciers and permafrost (Haeberli, 2005; Waller *et al.* 2012), spanning from dynamics associated with freeze-thaw cycles to energy- and sediment fluxes of meltwater (Moorman, 2005). Thus, there is an increasing need to better understand how these features interact and affect each other under the current climatic forcing.

Harris and Murton (2005) bring forward that glacier-permafrost interactions depends on proximity, and it is for example common with aggradation of permafrost in the forelands of retreating glaciers (Lilleøren *et al.* 2013). Haeberli *et al.* (2017) highlight that the degradation of permafrost happens at a slower rate than the retreat of glaciers, and that glacier- and permafrost landscapes are undergoing a transformation or are going to transform within decades into landscapes that are sparsely vegetated, consisting of bare bedrock, loose debris, several new lakes, and slopes with slowly degrading permafrost. Observations have also been made of reduced stability of steep and icy mountain slopes; stemming from stress redistribution due to de-buttressing from disappearing glacier ice in addition to changes in the mechanical strength and hydraulic permeability of the mountain sides because of permafrost degradation (Haeberli *et al.* 2017). The current glacier-permafrost landscapes found in the high mountain and polar areas may as of such be termed transitional landscapes that are in a state of disequilibrium (Slaymaker, 2009).

2.2   Permafrost

Permafrost is a thermally defined phenomenon, and an area is described as a permafrost zone if the ground temperature is at or below 0 ℃ for a period of two consecutive years or more (Gisnås *et al.* 2017; Haeberli *et al.* 2006). Permafrost enables the preservation of ground ice and influences the rate and extent of creep in the ground (Haeberli *et al.* 2006). Above the permanently frozen ground, there is an active layer which thaws during the summer and refreezes during the winter. The depth of the active layer tends to range from a few decimeters to several meters (Humlum, 1997). Permafrost is present as continuous (90-100%), discontinuous (50 – 90 %) or sporadic (10-50 %), and its extent relies to a large degree on latitude, continentality and altitude. These determinants further set the conditions for the climatic factors, such as mean annual air temperature and precipitation. In addition, local environmental conditions such as aspect influence the incoming solar radiation, and surface conditions - such as the depth and longevity of the snow cover and the type of vegetation, will play a part in whether an area will have permafrost or not (Haeberli *et al.* 2010; Gisnås *et al.* 2017). Hock *et al.* (2019) bring to light that there are few observations of permafrost and that it is heterogeneously distributed within and among mountain regions. As it is a subsurface phenomenon, it is also difficult to observe remotely. Distribution and changes to the presence of permafrost is therefore not understood as well as for glaciers, and in many places, it may only be inferred (Gruber *et al.* 2017).

In Scandinavia, there are four types of landforms that may be regarded as an indication of the presence, or former presence, of permafrost: ice-cored moraines (Østrem, 1964; Lilleøren & Etzelmüller, 2011), rock glaciers (Shakesby *et al.* 1987; Lilleøren, & Etzelmüller, 2011), palsas (Seppälä,1994; Sollid, & Sørbel, 1998) and ice-wedge polygons/patterned ground (Svensson, 1962; Svensson, 1992). Permafrost landforms can be significant for local geomorphic, hydrological (Jones *et al.* 2019) and biological conditions and they also play a role in the global climate system by altering atmospheric and aquatic fluxes of greenhouse gases through the permafrost carbon feedback. Increased attention is being yielded towards the implications of the permafrost carbon feedback, as the permafrost thaws, gases stored in the permafrost, including methane, carbon dioxide and nitrous oxide are being released into the atmosphere (Hock *et al.* 2019).

Permafrost degradation may be theorized at various scales and the different forms of degradation may impact the hydrology of a system in different ways: an overall thawing of permafrost can lead to large-scale reductions in the extent of permafrost. This is associated with continuous permafrost and long time scales; which in turn can have an effect on deep groundwater contributions to streams and rivers. Secondly, increases in the depth of the active layer inducing increases in the mid- to late- season interaction between surface waters and soils. Thirdly, development of thermokarst, which stems from surface thawing of ice-rich ground, leading to loss of volume from melting ice and subsequent creation of depressions in the surface from thaw slumping. Thermokarst processes bring about a more local response, but with potentially more dramatic hydrological impacts (Frey & McClelland, 2009).

Haeberli *et al.* (2017) highlight that the landscape of high mountain areas is rapidly changing due to the current climatic changes. In areas with degrading permafrost, several new lakes are appearing, and the long-term slope stability is reduced as surface and subsurface ice disappears. The relative run-off from thawing of permafrost is also expected to be greater in arid areas where permafrost is more abundant and as permafrost reacts less rapidly than glaciers, the landscapes are likely to be more affected by permafrost thaw in the future (Hock *et al.* 2019). In sum, this leads to a growing risk for humans and infrastructure in polar and high mountain areas. During recent decades, the rates of permafrost warming in Scandinavia, the European Alps and on the Tibetan Plateau have been exceeding the warming rates of the late 20th century (Hock *et al.* 2019). Summer heat waves have been connected to extreme increases in the active-layer thickness and the degradation of permafrost is further accelerated by water percolations (PERMOS 2016; Luethi *et al.* 2017). Hock *et al.* (2019) highlight that the thaw and degradation of permafrost will increase during this century.

2.3   Thermal regime of glaciers.

The thermal regime of a glacier is shaped by the environmental setting as well as the extent and dynamics of the glacier. The distribution of cold and temperate ice within the glacier is important for basal sliding, the material rheology and the englacial and subglacial hydrology of the glacier (Wilson and Flowers, 2013). The thermal regime of a glacier is deemed temperate if the ice is at the pressure melting point (PMP), and there is water and ice coexisting and an interstitial liquid content up to ~9% by volume, except for a seasonally cold surface layer in

the ablation area (up to 15 m thick) (Pettersson *et al.* 2004; Irvine-Fynn *et al.* 2011). When the ice is temperate at the base, it means that water will be present and allows for ice movement through basal sliding and subglacial erosion, such as abrasion. Glacial landforms formed under temperate conditions are usually flow aligned, such as flutes and eskers, which are formed in subglacial meltwater channels. For cold based glaciers, winter cooling will keep the temperature of the ice below the PMP, and geothermal heat is usually not sufficient to cause melt, exhibiting negligible interstitial water. With a cold based glacier-bed interface, the glaciers are considered to be frozen to the bed due to the high adhesive strength of cold ice (Irvine-Fynn *et al.* 2011). Ice movement in cold based glaciers is mainly caused by internal deformation. This allows for the preservation of old landforms and relict landscapes, e.g. blockfields (Kleman, 1994). However, the assumption of cold-based glaciers as completely non-erosive may be questioned as field observations have shown that limited sliding is possible far below the pressure melting point. This in turn has implications for glacier dynamics and associated geomorphological landforms (see e.g. Waller, 2001). Still, the observed sliding might be considered so small that it may be considered insignificant for short-term glacier dynamics, even if it may play a role in the frame of a geological timescale (Cuffey *et al.* 1999; Waller, 2001).

Polythermal glaciers are complex in the sense that they contain sections of both temperate and cold ice. The thermal state of polythermal glaciers may vary from almost completely cold based to almost completely temperate. Numerous geophysical surveys have shown that the location of the cold-temperate ice transition zone (CTZ) varies greatly, further underpinning the complexity of thermal regimes of polythermal glaciers (Blatter & Hutter, 1991; Irvine-Fynn *et al.* 2011). Figure 2.1 shows some idealized representations of thermal ice distributions of polythermal glaciers, and it is important to keep in mind

Cold ice
Temperate ice
Transient thermal layer
--- Cold-temperate transition zone (CTZ)
ELA
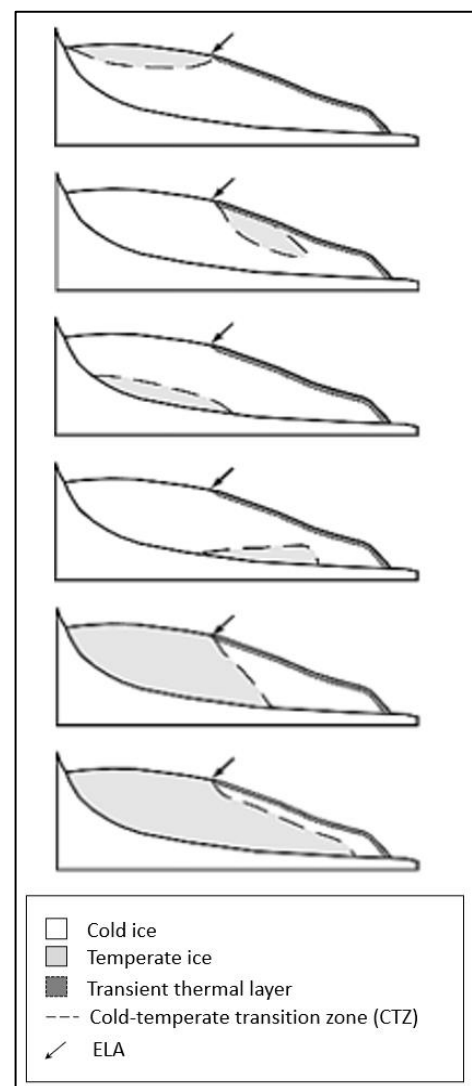
Figure 2.1 Schematic representation of various polythermal regime configurations of polythermal glaciers. The ELA, where the surface mass balance is zero, is indicated by arrows (Modified figure from Irvine-Fynn et al. 2011)

that real ice masses may have even more spatial variations in thermal structure and that areas of temperate ice within polythermal glaciers may be patchy (Murray *et al.* 2000; Irvine-Fynn *et al.* 2011). Irvine-Fynn *et al.* (2011) highlight that there are still some challenges in terms of understanding the complexity of the thermal regime of glaciers, as the distribution of temperate and cold ice within a glacier is difficult to distinguish (e.g. Brown *et al.* 2009), the transition between temperate and cold ice is gradual (Blatter, 1987) and that strain heating may lead to variations in space (Hutter, 1982) or time (Jania *et al.* 2005; Irvine-Fynn *et al.* 2006).

Etzelmüller & Hagen (2005) argue that glaciers terminating in a stable terrestrial permafrost environment will be either cold or polythermal, as the marginal zones of the glacier are affected by the presence of permafrost and will have a cold frontal snout. Storglaciären in Sweden is an example of such a polythermal glacier (Pettersson *et al.* 2004). Temperate ice may be created in the accumulation zone during spring through the refreezing of meltwater, while a near surface layer of cold ice is created in the ablation zone during winter. However, in summers with high rates of ablation, the cold frontal layer may melt away (Etzelmüller & Hagen, 2005). Formation of ice-cored moraines marginal to polythermal glaciers of this type is widespread in eastern Scandinavia (Lilleøren & Etzelmüller, 2011).

2.3.1 Changing thermal regime of glaciers

Climatic change might lead to a switch in the thermal regime of a glacier, with retreat and thinning of polythermal glaciers being influential in changing the thermal regime. Austre Brøggerbreen on Svalbard is an example of a glacier which experienced a thermal adjustment from a polythermal glacier into a completely cold based regime, due to sustained retreat and thinning. Depending on the location and local climate of the glacier, thinning and retreat of glaciers in response to rising mean annual air temperatures may lead to either a reduction or an increase in the proportion of cold ice (Irvine-Fynn *et al.* 2011), as outlined in fig.2.2. Irvine-Fynn *et al.* (2011), emphasize that the time frame for thermal switching at various depths still needs to be explored further.
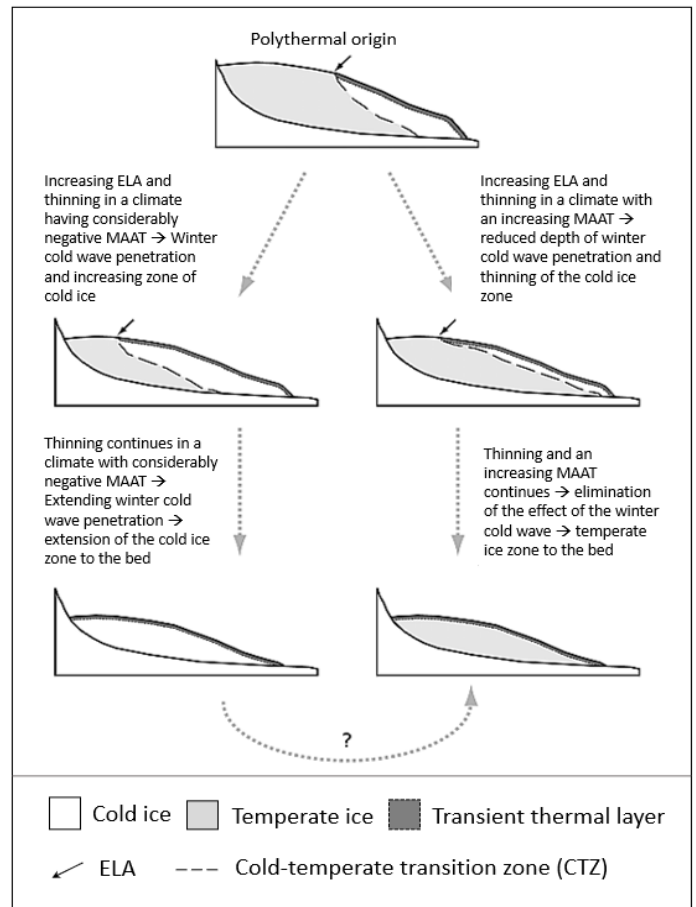
Figure 2.2 Figure showing the impact of glacial retreat and thinning on thermal regime. With a warming climate, it is unclear if a cold glacier may switch to a temperate state if winter cooling disappears. (Modified figure from Irvine-Fynn et al. 2011)

2.4. Ice-cored moraines

The first descriptions of ice-cored moraines in Scandinavia were by Østrem (1959;1964) and may be defined as ice marginal landforms containing a discrete body of glacier ice and/or frozen sediment placed by a glacier (Østrem, 1959; Evans, 2014). The formation and preservation of ice-cored moraines are associated with glacier-permafrost interactions and these landforms are typically found in front of small valley- and cirque glaciers in north-eastern (leeward) aspects. A common trait is that they consist of steep and oversized ridges and that there is a perennial snowbank running along the margin of the distal moraine ridge (Østrem, 1964; Østrem & Arnold, 1970). The height of ice-cored moraines may be considered an indicator of the former elevation of the glacier surface when the moraine was formed. Ice-cored moraines may be either fully or partially ice-cored, depending on their formation. The

formation of ice-cored moraines is usually associated with glacier-permafrost interactions (Etzelmüller & Hagen, 2005), and ice-cored moraines are often used as indicators of permafrost zones (Lilleøren & Etzelmüller, 2011). Østrem (1964; 1971) put forward that in Scandinavia, if there are large moraine ridges found in front of small retreating mountain glaciers with an elevation clearly higher than the glacier and a surface curvature with distinct changes, the moraine will most likely be ice-cored. Ice-cored moraines are also generally found on gently sloping or relatively horizontal ground (Østrem, 1971).

Even if most ice-cored moraines are associated with glacier-permafrost interactions, it is worth noting that these landforms are not exclusively found in permafrost environments. Ice-cored moraines may also form under non-permafrost conditions, such as in front of large surging glaciers (Driscoll, 1980), or in areas with high production of material and sedimentation rates, e.g. from volcanic eruptions (Krüger & Kjær, 2000), or due to flooding events by meltwater covering the ice with sediments (e.g. Moorman & Michel, 2000). However, ice-cored moraines formed in a non-permafrost environment, are unstable as they experience rapid mass wasting and thus have a rather short lifespan, often disintegrating within decades (Driscoll, 1980; Krüger & Kjær, 2000). Ice-cored moraines in permafrost environments are on the other hand considered stable landforms, and if the debris cover remains thicker than the depth of the active layer, the ice will be shielded from atmospheric processes and may even be preserved for millennia (Etzelmüller & Hagen, 2005).

2.4.1 Formation of ice-cored moraines

A thick continuous debris cover on the frontal part of a polythermal glacier has a significant effect on glacial ablation and retreat rate, which might lead to the formation of ice-cored moraines. Several factors are determining for the formation of ice-cored moraines. The magnitude of glacier strain and ice velocity, the thickness and ductileness of the subglacial sediment, as well as the thickness and rheology of the permafrost in the area. Furthermore, a source of material is needed. Cirque glaciers commonly have steep headwalls surrounding the glacier and active slope processes lead to accumulation of supraglacial debris. This supraglacial debris may then be transported supraglacially or englacially towards the glacier margin. The formation of ice-cored moraines in Scandinavia is linked to polythermal glaciers with a cold based frontal zone, frozen to the bed, and a higher temperate zone. This thermal structure allows

for basal ad-freezing of subglacial material and glacio-fluvial material, and transportation of material as debris bands englacially and sub-glacially in the temperate part of the glacier. In the temperate to cold ice transition zone (TCZ), sediments which have been transported sub and englacially are transported along shear planes towards the glacier surface at the front of the glacier, leading to an accumulation of coarse debris at the glacier terminus (Østrem, 1959; 1964; 1971; Etzelmüller & Hagen, 2005; Lilleøren & Etzelmüller, 2011). The mechanism responsible for the uplift of sub- and englacial debris bands is debated, and Moore *et al.* (2013) highlight that either folding near the margin or thrusting of rapid-flowing ice over slow marginal ice are some mechanisms which may be responsible for the uplift of sediments. However, Monz *et al.* (2022) propose that these debris bands originate at the base of the glacier and are uplifted through one of these mechanisms: 1) refreezing of meltwater near the thermal transition of basal ice, or 2) by injection into tensile fractures periodically opened at the base because of high fluid pressure and freezing. Monz *et al.* (2022) further argue that the separation of the debris from the base is due to introduction of ice beneath the debris bands as a result of high fluid pressure and freezing, and it is then transported forward due to basal shear and upwards because of longitudinal compression and then revealed by surface thinning.

Thick debris covers on glaciers are known to significantly reduce the rate of ablation as it insulates the underlaying ice from atmospheric processes (Østrem, 1959; Mattson *et al.* 1991). However, a very thin supraglacial debris layer may lower the albedo of the glacier and speed up the net melt rate. Supraglacial debris with a thickness over ca. 2 cm insulates ice and leads to a lower net melt on the debris covered parts of the glacier compared to the surrounding debris free ice (Østrem, 1959). It is therefore possible for degrading ice to survive for a long period of time under a protective debris cover (Krüger & Kjær, 2000). Thus, if cold based conditions prevail in the frontal zone of the glacier, ice might be preserved beneath the debris cover. For the debris cover to accumulate and form moraines, the glacier snout is believed to be rather stagnant during this period (Østrem, 1964). As the glacier continues to retreat, the ice-cored moraine may become detached from the glacier. If the thickness of the debris cover exceeds the depth of the active layer in a permafrost zone, this detached part of the glacier may thus become a part of the local permafrost (Berthling, 2011; Kellerer-Pirklbauer, 2017).

An ice-cored moraine may also become further enlarged after it has detached from the glacier through the incorporation of nival ice and material stemming from perennial snow patches forming along the margin and between the moraine ridges. This is due to backwasting processes, which incorporates these perennial snow patches and associated material into the moraine (Østrem, 1964; Johnson, 1971). Refreezing of percolating meltwater is another process which may be contributing to the formation of ground ice between the morainic material (Østrem, 1964). Østrem (1964) argues that most of the ice-cored moraines in Scandinavia are made from a combination of incorporated snowbank ice and/or glacial ice.

Another mechanism which contributes to the preservation of an ice core is Balch ventilation (Thompson, 1962). Balch ventilation is a cooling mechanism which is based on air convection, creating voids of cool air in the debris cover, contributing to the preservation of the ice core. Snowbanks forming along the margin of ice-cored moraines further contributes to Balch ventilation as it hinders the cold air from escaping (*ibid.*).

2.4.2 Degradation of ice-cored moraines

In general, degradation of ice-cored moraines happens actively by mass movements and melting of dead-ice, or passively through solely degradation of the ice-core as a result of dead-ice melt (Schomacker, 2008; Ewertowski & Tomczyk, 2015). The main melt processes in ice-cored moraines are backwasting and downwasting (see fig. 2.3). Backwasting is defined as lateral retreat of near-vertical ice-walls or ice-cored slopes (Pickard, 1984; Krüger, 1994; Krüger & Kjær, 2000; Schomacker, 2008). Downwasting is defined as thinning of bodies of ice from the top and/or bottom (Krüger, 1994; Krüger & Kjær, 2000; Schomacker & Kjær, 2007; Schomacker, 2008), though downwasting by bottom melt only happens in non-permafrost environments (Schomacker, 2008).

When ice-cores diminish, the sediment cover will be reworked, due to backslumping, as well as other features of sedimentation, e.g. fall-sorting, sinkholes and extension fractures. (Kjær & Krüger, 2001). Gravitational sorting in ice-cored slopes tend to produce boulder accumulation at the foot of the slope and is a sign of backwasting and mass movement processes being more abundant than downwasting processes. Kjær & Krüger (2001) suggest that the extent of

backwasting may be linked to the aspect of the slope, with southern facing slopes retreating faster than northern facing slopes. In areas where backwasting is abundant, depletion of fine sediments from the debris-cover parent material can be spotted in cycles of sediment flows (Schomacker, 2008). The de-icing progression of isolated dead-ice blocks may lead to sinkholes developing at the base of the slope, and thus having backslumping upslope. Boulders are then located in depressions or at the crest of the hill, due to fall sorting (Kjær & Krüger, 2001). The degradation of the moraine happens because of a combination of ablation of the ice core, local development of thermokarst and slope failure. Thermokarst is regarded as the fastest form of ice core degradation and develops as circular and linear depressions over conduits of meltwater. The penetration of meltwater further enhances the melting of the ice core. Water may also accumulate in sinkholes leading to wasting of the side walls by thermodenudation and undercutting of ice cliffs (Richardson & Reynolds, 2000). Formation of ponds tend to be locally concentrated, but may wander laterally on the moraine (Pickard, 1983). Thermokarst formation stems from a combination of internal melt processes and external input of water, for example from rain or external throughflow of meltwater in the ice-cored moraine (Johnson, 1971).
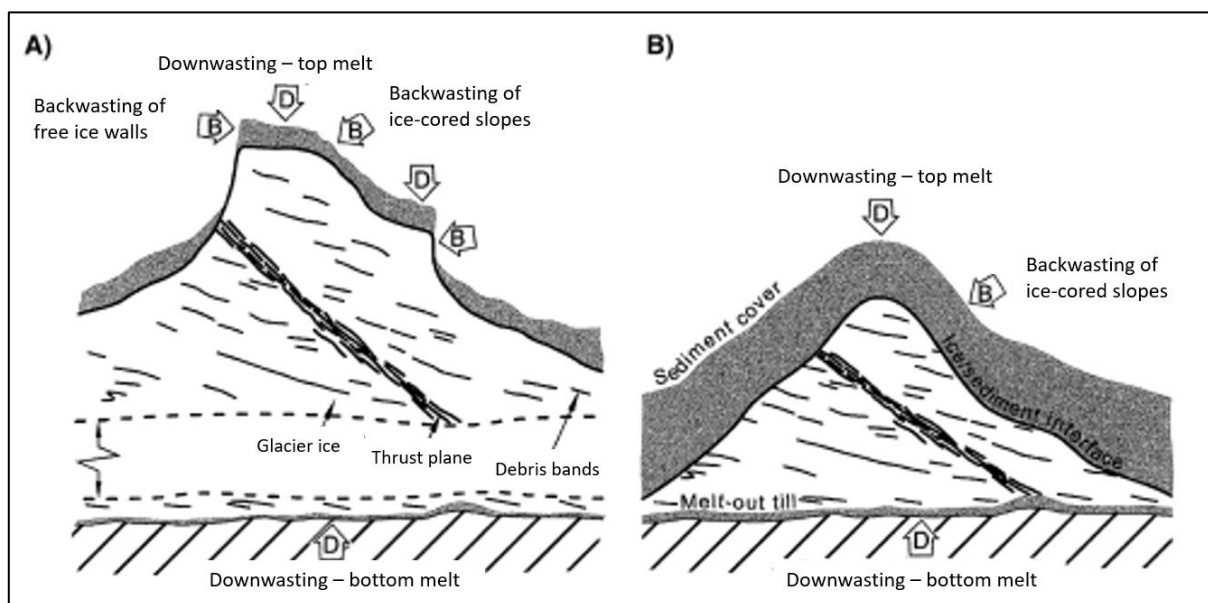
Figure 2.3 Shows the main processes of degradation related to de-icing of a fully ice-cored moraine (A) and partially ice-cored moraine (B) (Modified figure from Kjær & Krüger, 2001).

Schomacker (2008) argues that the properties of the debris cover, and the climate govern the processes and speed of melting in ice-cored moraines. Factors such as the mean annual air

temperature, average summer air temperature, mean annual precipitation, mean summer precipitation and the annual sum of positive degree days were correlated with backwasting rates at ice cliffs in dead-ice areas of fourteen different sites around the world, stretching from Yukon in Canada, to Antarctica, Svalbard, Iceland, the Himalayas and New Zealand. Changes in the mean annual air temperature were found to correlate the most with rates of backwasting. However, the correlation between melt rates and climate parameters were found to be rather low. The lowest rates of backwasting were found in cool, dry climates, and the highest rates in humid, temperate climates. Schomacker (2008) thus stresses that topography and processes such as mass movements by gravity and liquefaction are important for the melt rate and associated backwasting, as it contributes to reduce the shear strength of the debris-cover. Finer debris covers absorb more heat than coarse blocky materials, and in areas with more fine-grained materials heat from incoming solar radiation will be transferred more efficiently. A coarser debris matrix is on the other hand more susceptible to infiltration of rainwater and external throughflow. Percolation of this water through the coarser matrix may also contribute to the melting of ice in the moraine (Mattson & Gardner, 1991).

As the downwasting of the ice core progresses with time, the ablation rate may decrease. This is due to the simultaneous melt out of englacial material with downwasting, hence the debris cover becomes gradually thicker over time. Temperature variations may still be an influential forcing factor for ablation, but processes other than ice melt will play a larger part in the degradation of the ice-cored moraine (Brook and Paine, 2012).

The geomorphic state of the moraine might indicate if backwasting or downwasting processes are the dominant processes of degradation. For example, gravity sorting of sediments may hint to backwasting being a dominant process. Differential melt out of different sections of the moraine is likely, due to various aspect orientations and heterogenous thickness of the debris cover across the moraine. A stepwise lowering with a gradual levelling of the moraine might also be observed if downwasting is the dominating process of degradation (Kjær & Krüger, 2001). Hummocky moraines are generally considered to be the final stage of degradation of ice-cored moraines (e.g. Krüger, 1994; Kjær & Krüger, 2001; Schomacker, 2008; Lilleøren & Etzelmüller, 2011).

2.5   Proglacial hydrology

Proglacial streams are fed by the melting of snow and glacier ice, precipitation, release of englacially stored water and groundwater flow. High seasonal and diurnal variability are controlled by glacier ablation and the presence of permafrost. During the ablation season the base flow is characterized by cycles of raising and falling discharge associated with atmospheric processes driving glacial melt. Variations in discharge are associated with fluctuations in air temperature and precipitation and tends to increase at the beginning of the melt season and decline at the end of the summer season and decrease rapidly in the autumn. Rivers and lakes may work as heat sources for the surrounding frozen ground and have taliks in their proximity (Benn and Evans, 2010: p. 83). Sediment transfer in high mountain areas comes from storage and release of sediment through glacial, fluvial and periglacial processes (Irvine-Fynn *et al.* 2005).

2.6   Proglacial lakes

Proglacial lakes may form in topographic bedrock depressions or when surface runoff is limited by terminal moraines. The matrix of terminal moraines with fine grained material and coarse blocky material hinders the infiltration of the proglacial runoff, and the presence of permafrost or a core of buried glacier ice further impedes the waterflow, leading to the damming of a proglacial lake. Proglacial lakes are directly linked to glacier dynamics and work as a temporary storage of glacial meltwater and sediments. Lakes fed by glacial meltwater have similar diurnal and annual water level fluctuations to proglacial streams, with the highest water levels occurring in the periods with the highest levels of glacial ablation, usually around July/August. Climatic conditions in the catchment of the lake thus plays a large role in controlling the hydrological regime of the inflow of the lake (Benn and Evans, 2010: p. 86).

If a glacier is in direct contact with a proglacial lake, it may have a strong influence on the mass balance, flow velocity and thermal regime of the glacier (Carrivick and Tweed, 2013). Beneath deep proglacial lakes which does not freeze to the bottom in the winter, taliks may also develop (Rowland *et al.* 2011; Ling *et al.* 2012). The longevity of a proglacial lake primarily depends on the stability of the moraine damming the lake, but the lake also plays a role in the disintegration of the moraine. Lakes may for example contain enough energy to

induce thaw and melting of ground ice and ice cores in moraines damming proglacial lakes (Marsh & Neumann, 2001). The failure of moraine dams may be initiated by incision or overtopping (Clague & Evans, 2000). Glacial lake outburst floods (GLOFs) involve the abrupt and rapid release of large amounts of water, leading to a partial or complete draining of the lake. The mechanisms triggering GLOFs may be event based, for example from ice avalanches landslides or rockfall into the lake triggering a wave which overtops the moraine damming the lake. Contrastingly, a GLOF may also happen when a gradual increase in the instability of the moraine dam reaches a climax, for example by de-icing of an ice core or piping, leading to water surging within fast expanding tunnels. An influx of meltwater from an upstream glacier dammed lake might also trigger a GLOF. If overtopping, GLOFs tend to leave a clear morphological legacy with V-shaped incisions in the dam. The likelihood of a GLOF in a glacier is related to the morphology and internal characteristics of the dam, in addition to the size, hypsometry and hydrology of the reservoir, lastly the proximity to slopes that are susceptible to mass wasting (Clague & Evans, 2000).

2.7   Frozen ground hydrology

Frozen ground generally has a lower hydraulic conductivity compared to unfrozen ground (Williams & Smith, 1989), and may act as an impermeable barrier to the flow of groundwater (Waller *et al.* 2012). The development of the active layer in permafrost areas is significant for the hydrology of the catchment, as the depth of subsurface flow will follow the depth of the active layer, with a concentration of waterflow along the impermeable permafrost table (Pecher, 1994; Cooper *et al.* 2011). As permafrost restricts the ability of water to percolate into the subsurface, the runoff in basins where permafrost is present will respond quickly to events of snowmelt and rainfall. In areas with permafrost and perennially frozen ground, sources of sediments to proglacial streams are not just dependent on variations in discharge, but the presence of ground ice may also provide spatially and temporally discontinuous sediment sources (Irvine-Fynn *et al.* 2005). Interacting seasonal dynamics of permafrost and hydrology impacts the timing and quantity of transport of water (Bowling *et al.* 2000). Up to 80-90 % of the total annual river discharge may happen during a 2-3 week interval when snow melt dominates in the seasonal spring melting in high-latitude watersheds (Linell & Tedrow, 1981). This effect becomes more apparent with the size of watersheds (McNamara *et al.* 1998). Regardless of if an area is underlain by seasonally frozen ground or permafrost, melt water will

be restricted to shallow flow parts during the spring melting of snow and ice. Later in the summer, permafrost characteristics, such as the depth of the active layer and the absence or presence of permafrost, have a larger impact on the depth at which the water flows through soils. If the depth of the active layer is rather shallow, water flow will be kept relatively near the surface and there will be more interaction with organic-rich soils, while a deeper or absent active layer opens for a greater flow of water through more mineral rich soils (Frey & McClelland, 2009). Streams may also locally disappear into the subsurface of more coarse materials, such as proglacial till, and re-surface downstream (Pourrier *et al.* 2014; Flett *et al.* 2017).

2.8   Moraines and subsurface hydrology

Moraines and talus slopes may play an important role in the groundwater flow and storage in alpine watersheds (Roy & Hayashi, 2009). The flow of water in moraines is buffered and causes a delay in the overall discharge of glacial meltwater in a watershed (Caballero *et al.* 2002; Langston *et al.* 2011). The subsurface and groundwater flow depends on the internal structure of the moraine and ice-cored moraines may function as storages and groundwater aquifers. The hydrological pathways of an ice-cored moraine can be complex due to the matrix of unsorted sediments and ice. The diverging permeability of fine and coarse materials, in addition to buried glacial ice, bedrock and ground ice – with the dynamics of the seasonal active layer in the surface layers adding another layer of complexity to the subsurface environment (Langston *et al.* 2011). Streams exiting on the distal side of an ice-cored moraine may also have multiple sources. It can for example be deep groundwater stemming from melting of an ice core, rain or meltwater from snow which have infiltrated the moraine, or drainage of proglacial lakes (Roy & Hayashi, 2009).

3 Study area

3.1 Location of study area

The study area is located on the north-eastern flank of Semskfjellet, inside the Svartisen-Saltfjellet national park on Saltfjellet, northern Norway (see fig. 3.1). Semskfjellet has an elevation of 1531 m a.s.l. and a retreating glacier is situated on its north-eastern flank. In front of the glacier there is a proglacial lake dammed by an ice-cored moraine at an elevation of around 1200 m a.s.l. The glacial foreland is marked by glacial activity and periglacial features. The bedrock in the area is mainly granitic gneiss, though quartzite, mica and graphite slate and graphite gneiss also occur (NGU, 2021). The climate, elevation and observed periglacial features of the area suggests that the study area is located in a zone of discontinuous or sporadic permafrost. This is also linked to the limit for alpine permafrost in northern Norway being around 800–1000 m in the western part of northern Norway, and that the permafrost limit decreases with elevation eastwards (Etzelmüller & Hagen, 2005; Lilleøren & Etzelmüller, 2011; Gisnås *et al.* 2017).
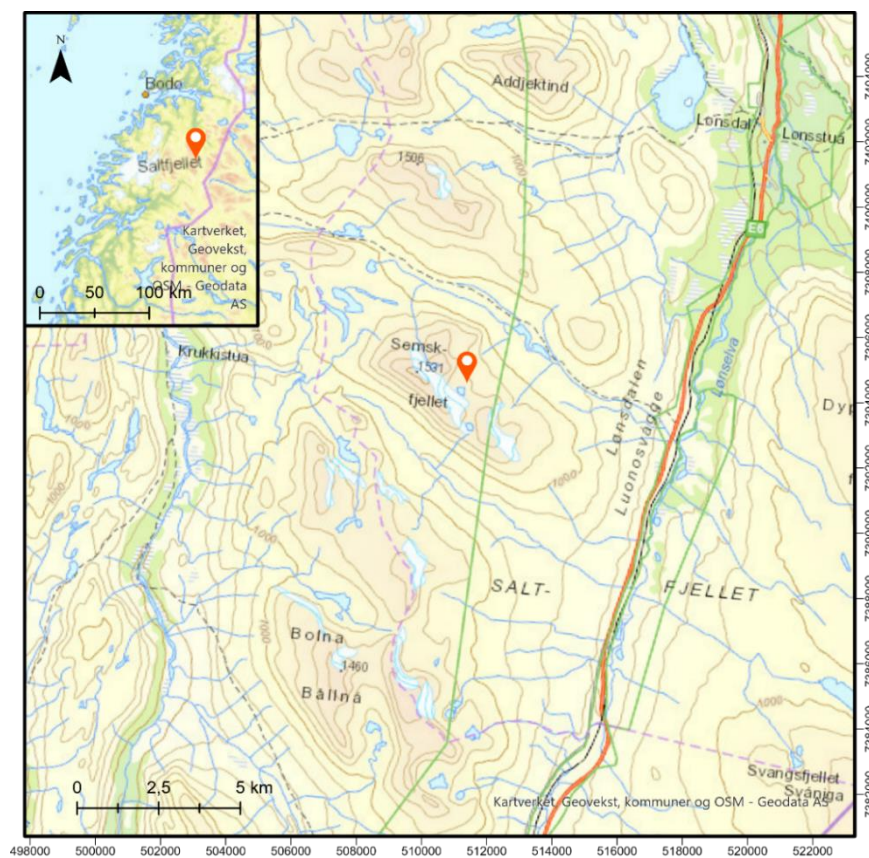
Figure 3.1 Location of study area on the north-eastern flank of Semskfjellet

3.2   Climate

Saltfjellet has a typical dry inland climate with large temperature variations between the summer and winter season. Average precipitation is about 750 - 1000 mm per year and the mean annual air temperature is between - 1 to -3 ºC, according to the normal for 1991 – 2020 (MET, Kartverket, NVE, 2022a/b). The mean annual air temperature (MAAT) for the study area from 1957 – 2021 shows a trend of an increase in the mean annual air temperature over the last 64 years (fig. 3.2).

It is worth noting that Semskfjellet is situated on the border between two catchments, where it becomes drier northeast of the peak towards Saltdal, and wetter when moving westward towards Svartisen and the coast (see fig. 3.3). This is highlighted by looking at the average annual precipitation data from the four closest weather stations from 1957-2021, which are located in the surrounding catchments and show large variations between the stations for each year (fig. 3.4). For the 1991 – 2020 normal, the mean annual snow depth for the field area is between 150 – 400 cm of snow and the water equivalent of the snow being on average 500-1000 mm per year (MET, Kartverket, NVE, 2022c).
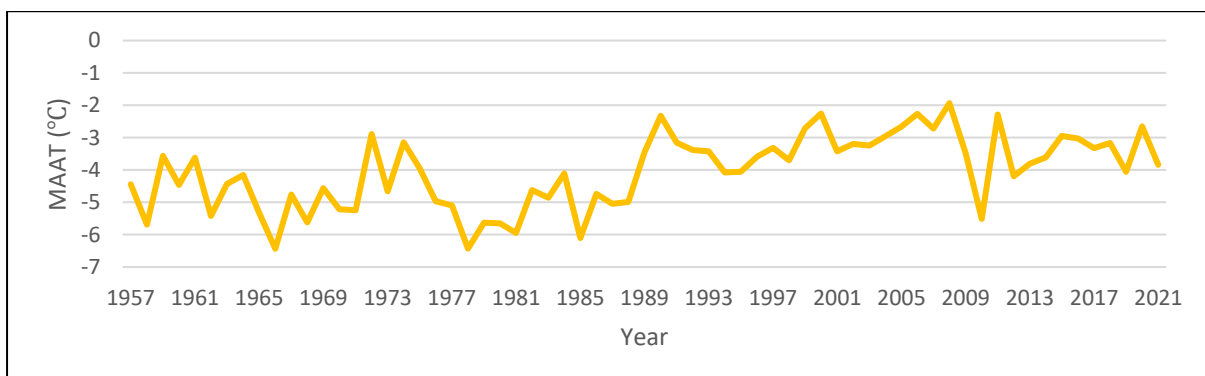
Figure 3.2 Mean annual air temperature 1957-2021 for the study area, MAAT is based on interpolated temperature data from nearby weather stations, interpolation performed by NVE. - Data acquired from the senorge.no portal - MET, Karverket, NVE, 2022a).
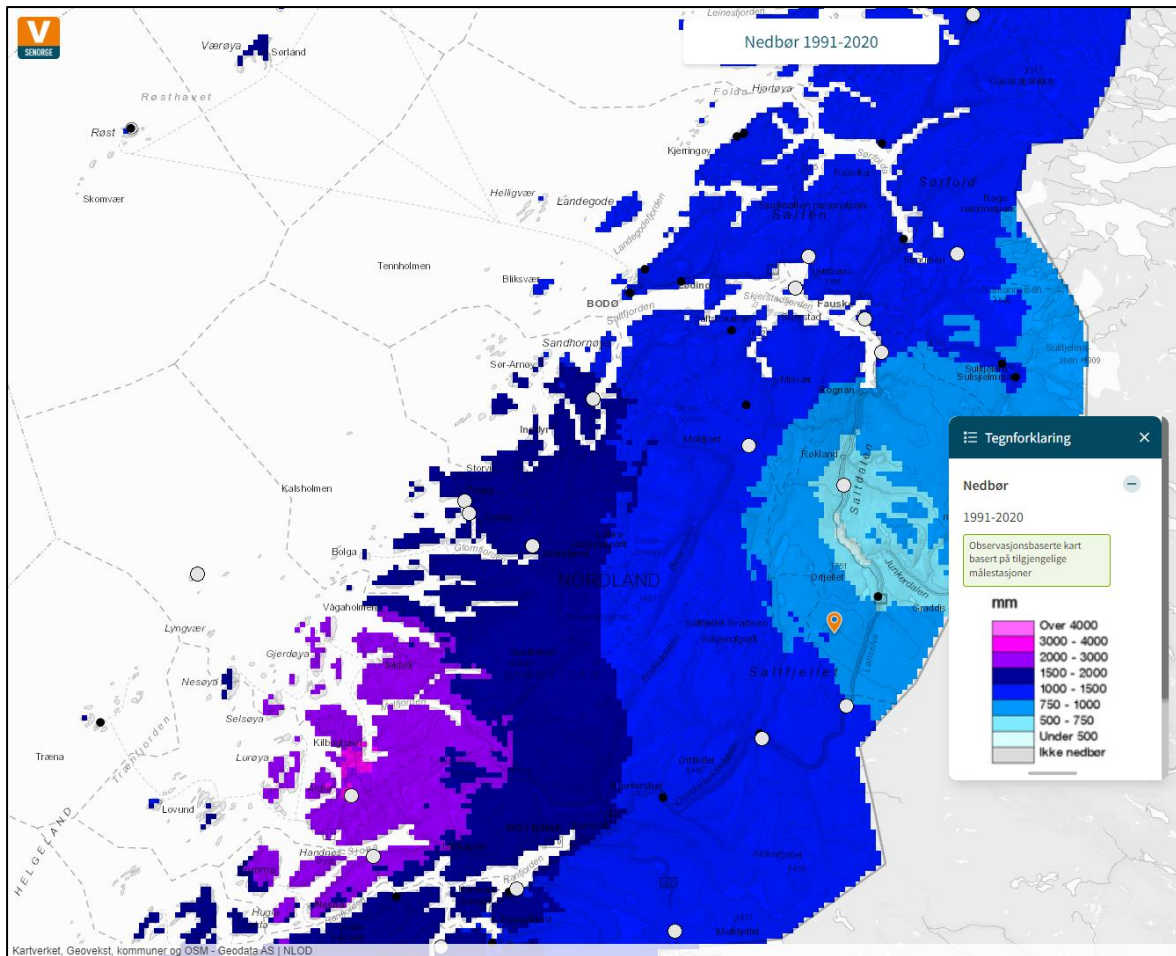
Figure 3.3 Map showing the precipitation normal for 1991 -2020, field area marked by orange marker showing that the mean annual precipitation is around 750 – 1000 mm per year for the field area. White and black dots on the map represent locations of weather stations (figure from the senorge.no portal by MET, Kartverket, NVE (2022b) Retrieved: 12.04.2022.)
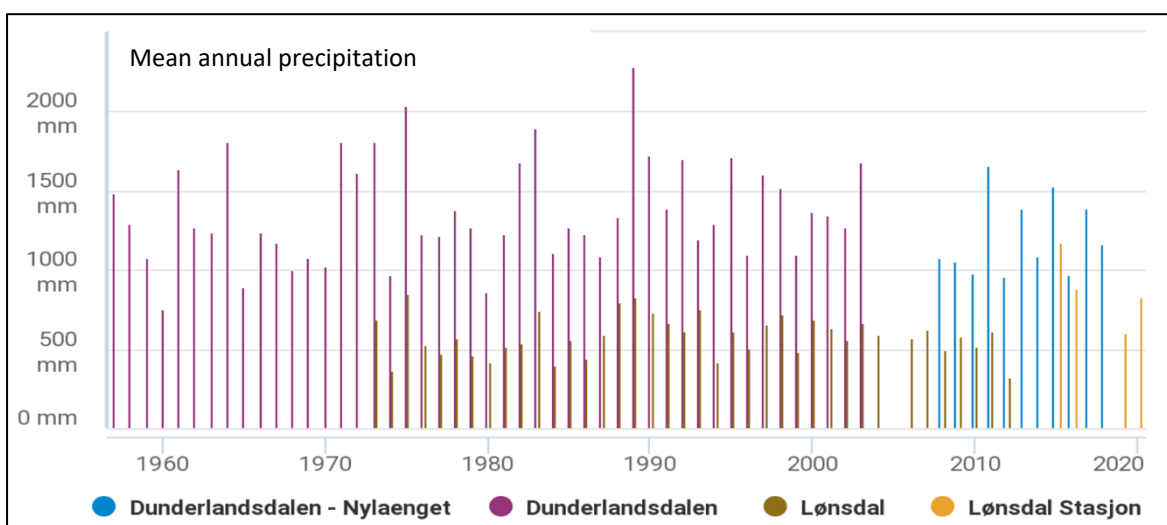
Figure 3.1 Mean annual precipitation from 1957-2021 from the weather stations closest to the field site, each color represents a different weather station (figure from MET (2022) seklima.met.no, Norsk klimaservicesenter, Retrieved 12.04.2022).

3.3   Historical documentation of fluctuations

Historical documentation shows signs of glacial retreat the last century. Fig. 3.5 indicates the extent of the glacier back in 1898, when the spatial extent was considerably larger than today. Aerial imagery from 1968 – 2019 exhibits that the glacier has retreated significantly during the latter half of the last century and that the surface area of the lake has increased (fig. 3.6).
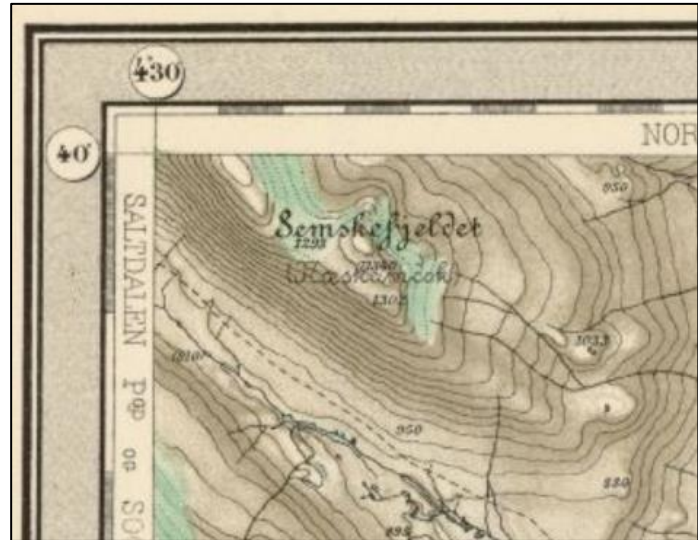
Figure 3.5. Outcrop of historical map from 1898 showing the extent of the glacier at the time (light turquoise markings in top left corner). (Kartverket (Norges Geografiske Oppmåling): Heliogravyre 1:100 000, L15 Nasa, O.Lier, 1898).
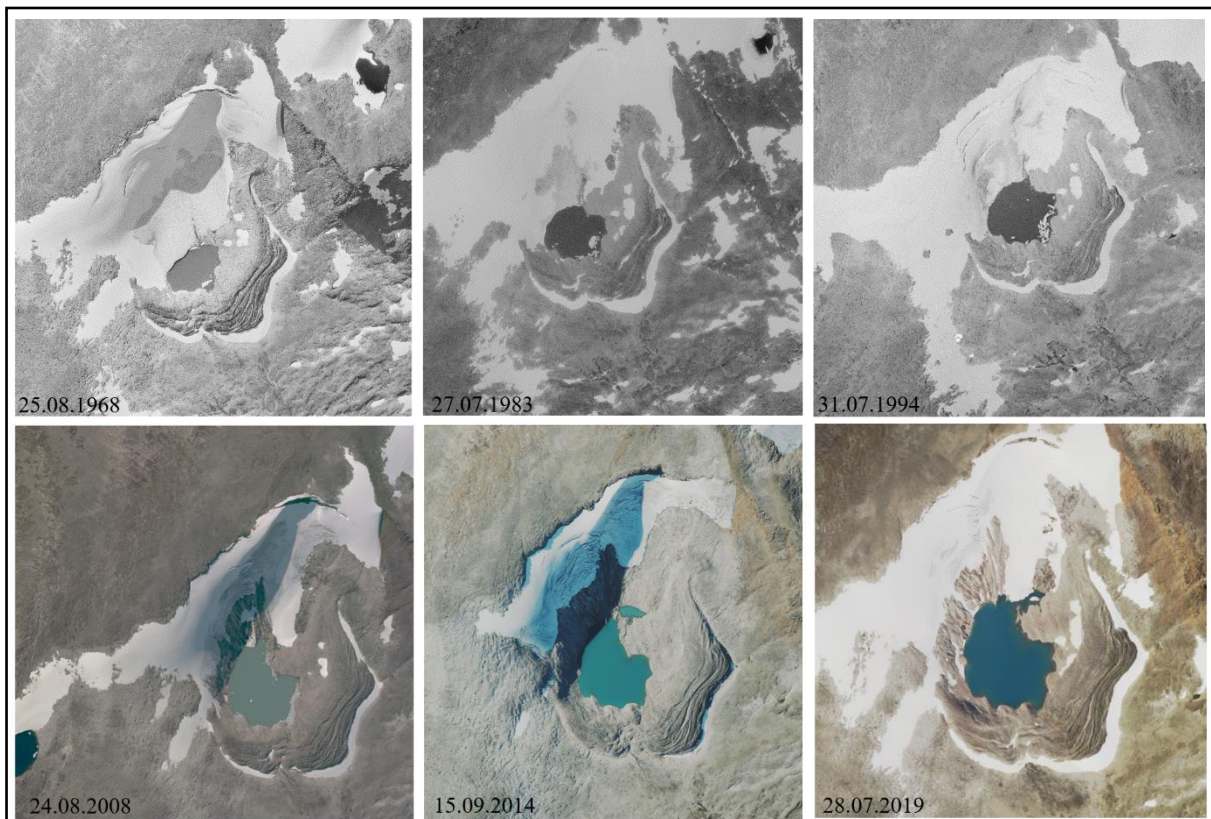
Figure 3.6. Shows the evolution of the glacier and ice-cored moraine from 1968-2019, aerial imagery from Kartverket.

4 Methodology

The methodology used a range of methods to gain a holistic understanding of the development and process regime of the ice-cored moraine system, combining hydrological investigations with geomorphological mapping, lichenometric dating and remote sensing techniques (see fig. 4.1 for an overview).

The hydrological investigations intended to map the spatial distribution and environment of subsurface water pathways in the moraine. This was done to assess the role of ground ice in this system, and in particular how the presence of ice influences lake drainage and deformation of the landform. The geomorphological mapping was used to create an inventory of the processes which have shaped and are forming the landscape in the area. Special attention was given to the influence of glacial and periglacial landforms in the system, to better understand

Figure 4.1. Overview of methodology

how these processes and features may be linked. Photogrammetry and DEM generation from historical aerial imagery from 1968 were compared to a DEM from 2019 to quantify surface elevation change of the glacier and moraine over time. Interferometric Synthetic Aperture Radar (InSAR) data from the portal *InSAR Norway* was investigated to gain insight into changes in surface elevation in recent years and assess the influence of the current climatic forcing on the stability of the ice-cored moraine. Lastly, lichenometric dating was performed on the moraine ridges to learn more about when and how this ice-cored moraine system was formed.

4.1 Geomorphological mapping

To better understand the processes which have shaped and are active in the study area, geomorphological surveys were performed in the field. These were supplemented by digital remote sensing analysis of aerial imagery and a digital elevation model (DEM). The geomorphological mapping in the field was performed with the assistance of the app *FieldMove Clino* by *Petroleum Experts Limited* using a smartphone. This app allows for georeferencing of photos and makes it easier to combine photos and notes in a spatial format. Observations of landforms and landscape features of interest were photographed and recorded in this app. The field observations were then compared to digital aerial imagery of the study site and a digital elevation model (DEM) from 2019 (available from Høydedata.no), as well as a slope raster generated from said DEM in *ArcGISPro* (fig. A10 in appendices). The field observations also involved smaller excavations in the moraine and other landforms to investigate the stratigraphy and grain size of the various features. The geomorphological map was produced using the *ArcGISPro* software by *Esri,* following the colours and nomenclature developed by the Norwegian Geological Survey.

4.2 Hydrological investigations

4.2.1 Monitoring of water level and temperature of the lake and streams summer 2021

Lake level changes were monitored throughout the summer season with a digital time lapse camera of the type: *Brinno TLC2000 Pro*. The camera was set up 26.06.21 (as seen on fig. 4.2), on the south-eastern moraine ridge (see location on fig. 4.3), taking pictures of the lake two times a day. Four *TD-diver (DI801)* loggers from *van Essen Instruments* recording water temperature

Figure 4.2 Set-up and position of the time lapse camera overlooking the pro-glacial lake.

and pressure were also installed on the same day. One logger was installed in the lake and three loggers in streams below the moraine. One barometer (*Baro-diver DI800 from van Essen Instruments*) was also installed on the shore of the lake, recording air temperature and barometric pressure. The location of the loggers, camera and barometers can be seen on fig.

4.3. The loggers recorded pressure and temperature at 30 min intervals from 26.06.21 – 15.09.21, with a precision of +/- 0,5 cmH_2O for pressure and +/- 0,1°C for temperature (NovaMetrix LLC, 2022). The logger in the lake was attached to a long string secured to a rock a few meters up on the shore and the loggers in the streams were attached to a small rock using string and electric tape and placed at a water depth of about 10 cm (see fig 4.4. for setup).

When returning to the field site on 25.07.21, the logger in the lake was moved a few meters higher up, as the lake level had increased by several meters, and I feared I would have to swim after it if left in the same position. Data was also retrieved from the logger 03.08.21, leading to a small change in the position of this logger. On 03.08.21, logger LN was moved to a nearby stream as the stream had run dry. The first position of logger LN is named LN1, while the second position is named LN2 (see fig. 4.3.). Logger LL was moved to a new stream named position 005, on 09.08.21, as the in-situ sampling of temperature and conductivity of stream 005 had showed very consistent results. Position 005 was in a deeper hole between two rocks. After retrieving the loggers, the data was transferred to the *Field Diver software* by *van Essen,* and the pressure measurements of the four diver loggers were compensated in accordance with the air pressure recorded by the barometer.
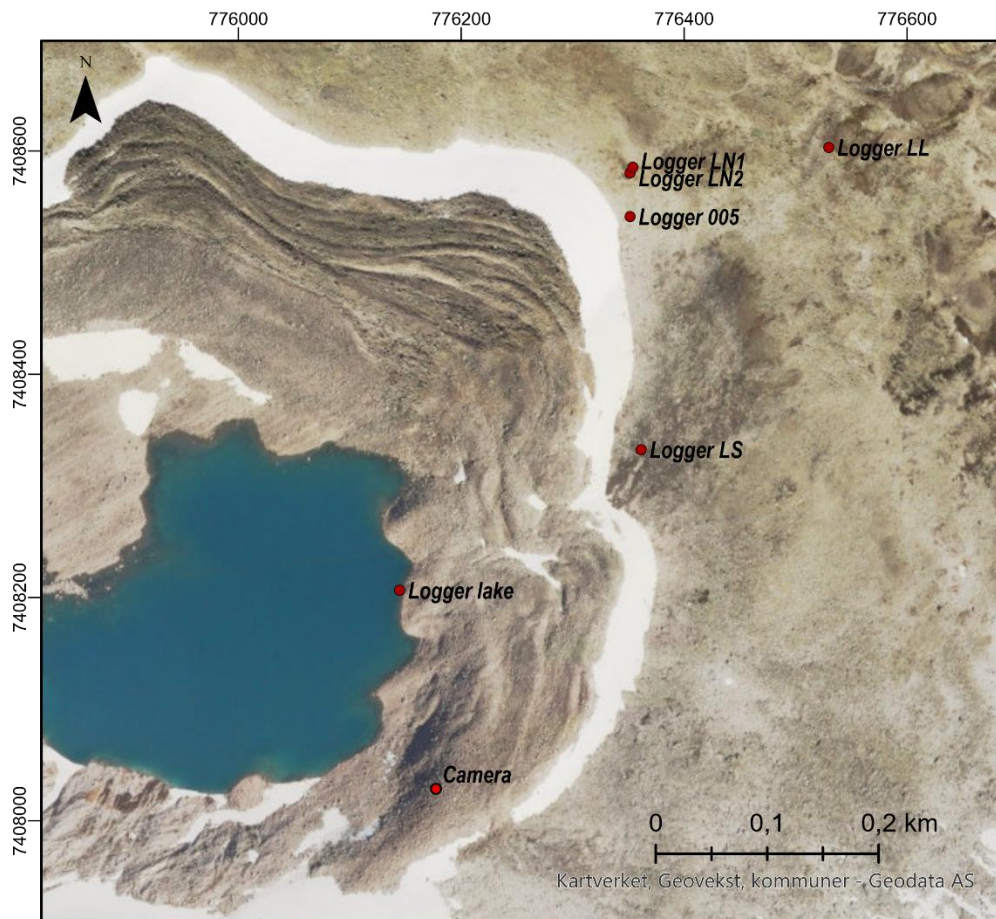
Fig. 4.3 Shows the positions of the camera and diver loggers in the lake (Logger lake) and streams (LS, LL, LN1, LN2 and 005). Logger LN was placed at LN1 from 26.06.21 – 03.08.21, and then moved to position LN2 from 03.08.21 – 15.09.21. Logger LL remained from 26.06.21 – 09.08.21, after which it was moved to 005 from 09.08.21 – 15.09.21.
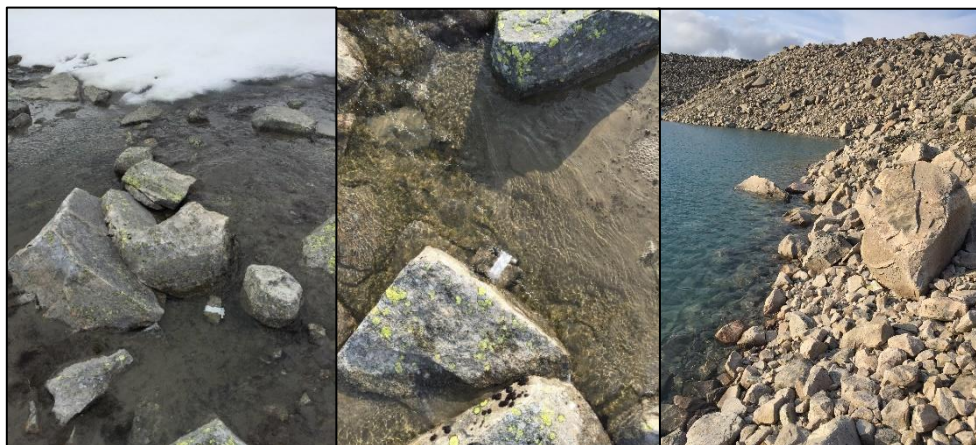
Fig 4.4. Set-up of the loggers in streams (left and middle), taped to rocks about 10 cm below the water surface. Right photo shows the set-up of the logger in the lake with strings with a length of about 6 m attached to a rock on shore (under the big rock) connected to the logger placed a few meters out in the lake.

4.2.2 In-situ temperature and conductivity measurements of the lake and streams

Measurements of electrical conductivity is often used in glacial hydrological studies to distinguish between various water sources, such as glacial meltwater, ground water flow, snow melt or precipitation (see for example Rutter *et al.* 2011; Zuecco *et al.* 2019; Miesen *et al.*, 2019). Variations in the conductivity may hint to the source of the streams and its subsurface pathways, as the electrical conductivity is a measure of the concentration of solutes in a stream, and thus the degree of sedimentation in the water (Zuecco *et al.* 2019). Similarly, differences in water temperature might be used to deduce the subsurface environment of the groundwater pathways. Lower water temperatures in the streams below the moraine could be seen as indications of the presence of ice; with the source of the stream either being from ice-melt or from groundwater running through channels of ice within the moraine. Higher water temperatures could on the other hand be indications of the stream flowing through an ice-free environment below the surface (Roy and Hayashi, 2009; Miesen, 2019).

To infer the environment of subsurface hydrological pathways and map the temporal and spatial distribution of streams throughout the summer, in-situ measurements of water temperature and electrical conductivity were performed at several intervals throughout the summer season in the lake and streams, as outlined in table 4.1. The spatial distribution of streams and in-situ temperature and conductivity measurements of the streams in front of the moraine were performed using a portable handheld conductivity meter of the type WTW Cond 3110 SET1 with automatic

Table 4.1. Sampling times of in-situ measurements of temperature and conductivity of streams and the lake.

Date	Time of day
26.06.2021	Afternoon (14.00 - 16.00)
25.07.2021	Evening (17.30 - 20.40)
26.07.2021	Morning (09.45 - 10.30)
28.07.2021	Evening (20.20 - 21.30)
29.07.2021	Midday (12.20 - 14.20)
03.08.2021	Evening (lake only) (17.30)
04.08.2021	Afternoon (13.15 - 16.00)
05.08.2021	Morning (10.45 - 11.45)
09.08.2021	Midday (13.00 - 14.00)

temperature compensation of 1413 µS/cm at 25 °C, paired with the four electrodes measuring cell TetraCon® 325. The accuracy of the meter is +/- 0,1 °C for temperature and +/- 0,1 µS/cm for conductivity (WTW Weilheim GmbH, 2008), and the accuracy of the measuring cell is +/- 0.2 K (Xylem Analytics Germany GmbH, 2018). The methodological approach was to sample every stream which appeared along the margin of the moraine throughout the season. Thus, the

number of measurements for each stream varies between one and nine, depending on the longevity of the stream this season. It is worth noting that the number of streams exiting the moraine increased considerably throughout the summer. On 26.06.21 only three streams were sampled, while eight streams were sampled 25.07.21 and a total of 28 streams were sampled 09.08.21. The sampling locations are outlined on fig. 4.5. The measurements were performed at various times of the day to record for diurnal variations. All measurement positions were photographed and recorded with GPS position.
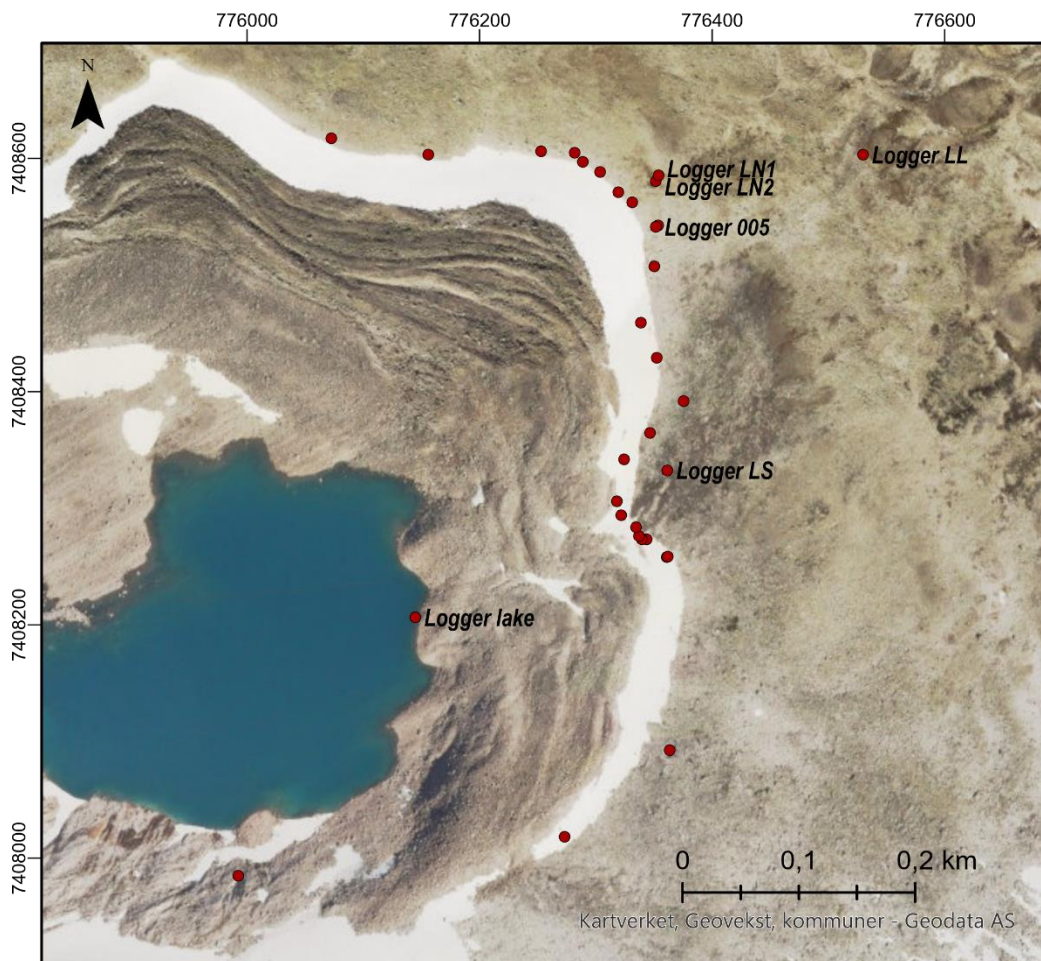
Figure 4.5 Sampling locations for in-situ temperature and conductivity measurements from surface streams exiting the moraine and logger positions. The snow patch retreated more during the summer season than the background aerial imagery from 2019 indicate.

4.2.3 Stable water isotopes

Stable water isotopes in precipitation vary across temporal and spatial scales and analysis of isotopes may reveal information of environmental and climatic dynamics. As stable isotopes

do not decay into other elements, they can be good tracers of hydrological processes, since they are naturally preserved in bodies of water, snow, and ice (Dansgaard, 1964; Kendall *et al.* 2014). Analysis of stable oxygen and hydrogen isotopes is a useful technique for determining the provenance of water in proglacial systems, for example to distinguish between groundwater flow and glacial runoff, or various ice facies (see e.g. Theakstone, 2003; Yde *et al.* 2016; Appleby *et al.* 2017; Zuecco *et al.* 2019). Thus, water and snow were sampled in this study for analysis of stable water isotopes to complement the other hydrological measurements of temperature and electrical conductivity and contribute to a more comprehensive understanding of the interaction between snow, ice, and water in this proglacial catchment.

4.2.3.1 Theoretical background

Isotopes are variations in the number of neutrons in an atom giving atoms different mass and reaction rates (Bradley, 2014: p. 129). The most common stable oxygen isotopes are ^{16}O, ^{17}O, ^{18}O, with ^{16}O being the most abundant isotope (99,76 %). ^{1}H and ^{2}H (deuterium, D) are the two stable hydrogen isotopes and ^{1}H is the most abundant (99,98 %). Fractionation of stable water isotopes happens during phase changes of water and the reaction stems from the difference in potential energy between 'heavy' and 'light' isotopes in a molecule. An isotope of an element is considered 'heavy' if it has a larger number of neutrons, and thus a higher atomic mass. Isotopic fractionation occurs in any thermodynamic reaction due to the differences in reaction rates for different molecules leading to a redistribution of the isotopes (Dansgaard, 1964). As there are disproportionate concentrations of isotopes, isotope fractionation is expressed as a ratio (R) between the most abundant and rare isotopes (Clark & Fritz, 1997: p. 22-23):

$$R = \frac{rare\ isotope\ abundance}{abundant\ isotope\ abundance}$$

The $^{18}O/^{16}O$ ratio is not reported directly, but as the deviation of the δ of the ratio in comparison to a standard of reference. The notification of δ-Values is written as permil (‰) deviation from the reference. For example, the ratio of stable oxygen isotopes is expressed as $\delta^{18}O$, and the stable hydrogen isotope as δD. The reference standard for stable water isotopes is the Vienna Standard Mean Ocean Water (VSMOW) and is given by the following equation by Fritz and Fontes (1980):

$$\delta = \frac{R_{sample} - R_{reference}}{R_{reference}} \times 1000 \; \text{‰}$$

For example, if δD = -60 ‰, there are 60 ‰ less of the heavy isotopes of D (deuterium) than the reference standard, and depletion of δD.

There is a correlation between the fractionation of $\delta^{18}O$ and δD in freshwaters on a global scale. This is represented through the relationship termed the Global Meteoric Water Line (GMWL) which was described by Craig (1961)

$$\delta D = 8 \; x \; \delta^{18}O + 10$$

The GMWL represents the equilibrium conditions of the fractionation of $\delta^{18}O$ and δD under saturated conditions, and it shows that the isotopic composition of meteoric waters have a predictable behaviour. The deviation from the global equilibrium is known as deuterium-excess (d). Based on the GMWL, Dansgaard (1964) defined deuterium excess as

$$d\text{-}excess = \delta D - 8 \; x \; \delta^{18}O$$

D-excess is used when studying the moisture supply of various locations, giving indications of evaporation and condensation. The GMWL represents equilibrium conditions, and if the offset value of a sample is 10, it is thus located on the GMWL. While a sample which has been subject to evaporation, will plot below the GMWL, having a d-excess value of <10. Low d-excess is indicative of more arid and cold conditions, while high values suggest more humid conditions (Dansgaard, 1964).

Isotopes in precipitation

Generally, water containing lighter isotopes evaporate easier than heavier isotopes, while water containing heavier isotopes have higher rates of condensation. As of such, evaporation leads to an enrichment of the remaining water in heavy isotopes, while precipitation leads to the remaining vapor being depleted of heavy isotopes. Heavy isotopes tend to freeze easier and take longer to melt than light isotopes. Thus, snowpacks and bodies of ice will be enriched in heavy isotopes in melt periods (Dansgaard, 1964; Clark & Fritz, 1997). Differences in isotopes

occur at spatial and temporal scales, and is affected by changes in latitude, altitude, distance from source of moisture, seasonality, and changes in climate (Dansgaard, 1964; Ambach *et al.* 1968; Fisher, 1990).

This is further reflected in the global hydrological cycle, producing spatial and temporal variations in precipitation for $\delta^{18}O$ and δD, with isotopic depletion of water vapor towards the poles. As warm air masses are being transported from the equator towards the poles, the air masses cool down, making the precipitation enriched in ^{18}O, leaving the remaining vapor partly depleted in ^{18}O. Thus, with further condensation, the precipitation will gradually contain less ^{18}O when it reaches the polar regions. Similarly, with increasing continentality and altitude, ^{18}O in precipitation decreases. This effect is amplified by colder temperatures and isotope variability thus rely on seasonality (Dansgaard, 1964; Bradley, 2014: p.143). Ice core records have also revealed that temperature and $\delta^{18}O$ variability correlate with seasonal and climatic changes, which may be identified in isotopically distinct layers revealing inter-annual climate fluctuations. Summer horizons can be identified by being isotopically enriched in ^{18}O, while the winter layers are more depleted (Clark & Fritz, 1997: p. 75-76).

Stable water isotopes in glacial-hydrological studies

In glacial hydrological studies, stable water isotopes have been used to investigate seasonal variations and to trace the provenance and residence time of water in different sections of glacial meltwater systems, to gain a better understanding of the development and dynamics of glacial drainage systems (Theakstone, 2003). It is common to perform stable isotope analysis together with other measurements, such as discharge, temperature, electrical conductivity, or solute content, as it gives a more holistic image of the correlation of the dynamics of glacier hydrology (see for example, Theakstone, 2003; MacDonald *et al.* 2016; Penna *et al.* 2017).

Studies of water isotopes in glacial hydrological studies have shown that different water sources within a catchment may be isotopically distinct, depending on the origin and pathway of the stream. For provenance studies, it might be useful to distinguish between glacial ice, snow, meltwater, groundwater and precipitation (e.g. Theakstone & Knudsen, 1996; Yde *et al.* 2016). Theakstone & Knudsen (1996) used $\delta^{18}O$ to determine the origin of glacial meltwater

of Austre Okstindbreen, northern Norway, and table 4.2 is an example showing the range and mean values of $\delta^{18}O$ of various sources in a glacial catchment

Table 4.2. Shows the range and average values of $\delta^{18}O$ in ‰ of water sources in a glacierized catchment, Austre Okstindbreen, northern Norway. (Adapted from Theakstone & Knudsen (1996): p. 534)

Source	Range (‰)		Mean (‰)
	min	max	
Glacier ice	-12.8	-10.8	-11.6
Ice meltwater	-12.7	-10.5	-11.9
Snow (May)	-21.8	-7.2	-12.8
Snow (July)	-15.6	-8.7	-11.5
Snow meltwater	-13.8	-10.5	-12.1
Rain water	-15.5	-6.5	-10.5

4.2.3.2 Sampling and data processing of the stable water isotopes

A total of 67 samples of water (62) and snow (5) were collected for analysis of stable water isotopes (see fig. 4.6. for sampling locations). The samples were collected in 30 ml polypropylene bottles. Before sampling the water, bottles were rinsed three times in the stream. The snow samples were collected at 6 or 30 cm depth of the snowpack. Every stream was sampled 1-2 times between 25.07.21 – 04.08.21, depending on the longevity of the stream coming out of the moraine. The stream with loggers and the lake were sampled three times 26.06.21, 25.08.21 and 04/05.08.21. The snow samples were collected 1-2 times, 26.06.21 and 25.07.21. The lower streams and Namnlauselva down in the valley were sampled once, for comparison to the samples taken along the margin of the moraine. The samples were taken at various times of the day, at the same times that can be seen in table 4.1, having the same sampling times of in-situ measurements of temperature and conductivity of the streams coming out of the moraine.

The water samples were analysed at FARLAB (Facility for advanced isotopic research and monitoring of weather, climate and biogeochemical cycling) at the University of Bergen, for $\delta^{18}O$, δD, and d-excess, using a mass spectrometer. The precision of the measurements were 0,4-0,5 ‰ for δD and 0,06 ‰ for $\delta^{18}O$, giving a precision of 0,6-0,7 ‰ for d-excess.

Analysis of stable water isotopes should preferably be compared to a local or regional meteoric water line. However, there are very limited records of the isotopic composition in precipitation for Norway and Sweden, with GNIP (Global Network of Isotopes in Precipitation) data of longer-term studies only stemming from the 1960s and 1980s. The only GNIP site in Norway was in Lista (IAEA/WMO, 2021), which has a very different environmental setting from the alpine, continental climate of this study site and was therefore not deemed adequate to use for comparison in this study. Thus, due to the limited amount of monitoring stations and lack of available precipitation data to establish a local meteoric water line, the results of this study were compared to the global meteoric water line.
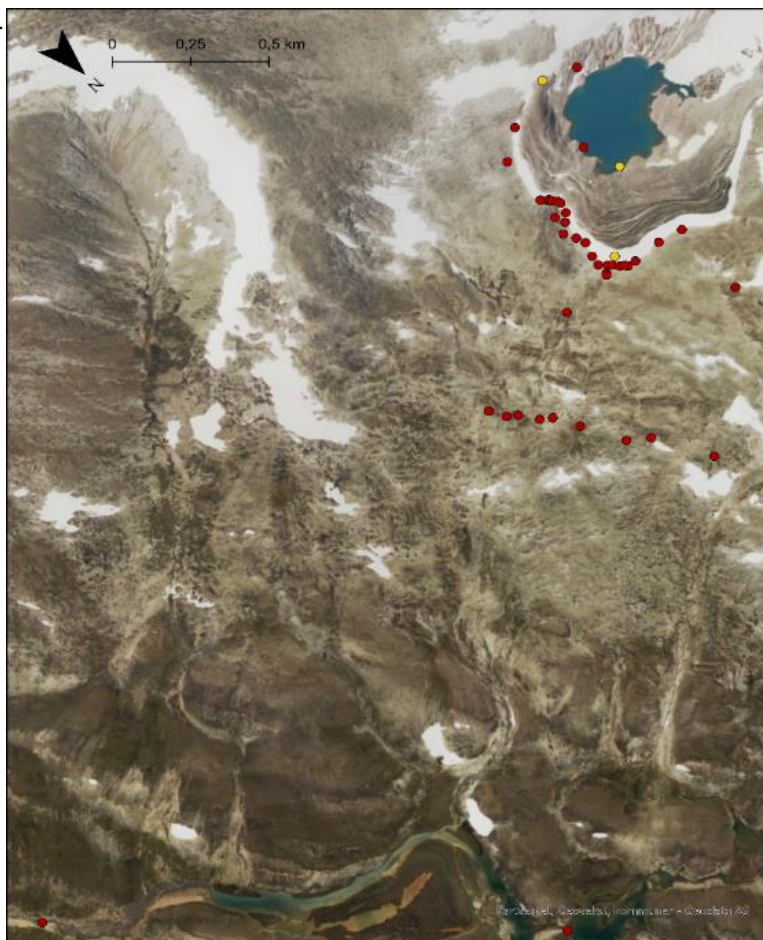
Figure 4.6. Locations for sampling of water (red) and snow/ice (yellow) for stable oxygen isotope analysis

4.3　Photogrammetry for studying landform deformation over time

To quantify deformation on the ice-cored moraine over time, surface elevation changes between 1968 and 2019 were computed from differencing Digital Elevation Models (DEMs). Historical aerial imagery from 1968 were used to photogrammetrically create a DEM, which was then compared to a DEM based on image matching from summer 2019 accessed through the Høydedata portal.

4.3.1 DEM generation

DEMs can be made from historical aerial imagery using the principle of photogrammetry. Photogrammetry makes use of soft-copy triangulation and image-based terrain extraction algorithms on overlapping photos to produce DEMs (Chandler, 1999; Lane *et al.* 2000; Westoby *et al.* 2012).

Four aerial photographs from August 1968 were acquired from Kartverket that covered the study area. The imagery was processed using CATALYST OrthoEngine. The following processing steps were performed in OrthoEngine: removal of image lens distortions, georeferencing and orthorectification. The first step of the processing is related to the interior orientation of the imagery and involved finding the interior camera orientations from the calibration report, such as focal length, size of the image, radial distortion, in addition to manually adding fiducial marks to delineate and set the borders of the scanned analogue photos. Secondly, to perform bundle adjustment for the relative orientation between the imagery and the exterior orientation, the relationship between the image pixels and real-world coordinates were established through ground control points (GCPs). The GCPs were manually located in all the photos with reference to orthophotographs and a high-resolution DEM accessed through the Høydedata portal. "Stable points" in the terrain, such as bedrock etc., were selected as GCPs. Between 5 and 12 GCPs were identified for each of the images. This was followed by an automatic calculation of tie points in the images, to solve the relative orientation between the images. Then the tie points were manually refined and thinned based on the residual values of the tie points, leading to the removal of less accurate tie points, and new tie points were added manually in areas with few points. The residuals for the tie points and GCPs were less than 1 pixel after the refining and thinning. Then orthorectification was performed based on a 1 m DEM from Høydedata from 2019, with a bilinear resampling and a resampling interval of 2. Following this step, an orthomosaic was generated to examine and evaluate the results. Then

to assist with the image matching for the DEM generation, epipolar images were generated. Generating epipolar images significantly reduces the processing speed of the co-registration between the two DEMs and increases the likelihood of correct matches. Epipolar images reprojects the images giving them a common orientation and makes features in the different images to be lined along a common x-axis (Wang *et al.* 2021). Then a DEM was generated using the Semi-Global Matching (SGM) extraction method, a low smoothing filter and mountaineous terrain type.

4.3.2 Co-registration of the DEMs

In order to compare DEMs and assess the surface elevation change over time between them, it is further important to make an absolute orientation adjustment by co-registering the DEMs together. If DEMs are not co-registered then the surface elevation results can be obscured by biases in the co-registration (Nuth & Kääb, 2011). Co-registration was performed using the demcoreg python module (https://github.com/dshean/demcoreg) written by Shean *et al.* 2016. The module performed first a linear correction using the method set out by Nuth & Kaab (2011) which normalises dh/slope and then compares it to the aspect of the DEMs over stable terrain, thus removing linear co-registration biases over stable terrain (Nuth & Kääb, 2011). Subsequently, a third order polynomial was fitted to the data to remove non-linear tilt biases. A manually generated shapefile of "unstable terrain", such as water, snow and shaded areas in the imagery was used as a mask when running the co-registration: So that these areas were not considered as points to base the co-registration of the various imagery on, as the elevation change results would not be reliable in these areas. The 1968 DEM was used as the master DEM, while the 2019 was the slave DEM, giving the change in surface elevation for the last 51 years. The co-registration resulted in linear shifts in the directions of X, Y and Z of -2,65 m, 2,09 m and -2,06 m, respectively and non-linear shifts of X, Y and Z of -1,5 m, 2,02 m and -1,99 m.

4.4   InSAR for studying deformation over shorter time scales

Interferometric Synthetic Aperture Radar (InSAR) data available through InSAR Norway, from 2015-2020 was studied to investigate how active the deformation on the moraine has been in more recent years. InSAR analysis estimates surface deformation and can give precise

measurements of surface displacement over larger areas with a precision down to mm scale. The technique is based on the phase difference between SAR image pairs acquired at different times. This allows for the extraction of the line-of-sight (LOS) projection of the displacement between the two images. The ascending and descending orbits allows for conversion of the movement from the LOS geometry in more than one direction, horizontal (east-west) and vertical (up-down). However, due to the acquisition geometry of the near polar orbiting, surface movement in the north-south direction is not easily deduced (Manzo *et al.* 2006; Kunz *et al.* 2022). InSAR Norway is controlled by the Norwegian Geological Survey and is an open, interactive map portal which shows the average yearly surface movement in mm/year, measured along the line-of-sight of the satellite. InSAR Norway uses Sentinel 1A and B radar satellite imagery, allowing for a time interval down to 6 days between the imagery. The Sentinel-1 national dataset was processed using Persistent Scatter Interferometry (NGU, 2022, 25. February).

The InSAR data from the national service provided by NGU was investigated in this study. One big limitation is that InSAR does not work on snow due to decorrelation between images, thus only imagery from June to October is used (NGU, 2022, 25. February).

4.5   Lichenometry

Lichenometric dating was performed for a selection of moraine ridges to gain insight into the age of this system. Lichenometry is based on the principle that lichen are one of the first colonizers on rocks after an area undergoes deglaciation, and as they grow at a specific rate; the size of lichen can give an indication of when the area became ice free. The size of lichen may thus be used to approximate the age of moraines and give an indication of the rate of deglaciation (Beschel, 1961). According to Armstrong (2014), lichenometry is a useful method for dating surfaces in areas above the treeline, such as in alpine environments where lichen growth is slow, and the lichen have a long lifespan. Surfaces of up to thousands of years old may be dated using this method, but lichenometry is mostly regarded as useful and accurate for dating surfaces from the last 500 years (*ibid*).

As climatic differences influence the growth rate of lichen, it is common to establish local growth curves of lichen based on for example historical records of glacial extent, e.g. photographs, maps or written sources. If this does not exist for the study area, it is possible to create an indirect growth curve based on the size of lichen on geomorphic surfaces of known

ages, such as gravestones from the local area (Bickerton & Matthews, 1992). Indirect growth curves may have a higher uncertainty, depending on the proximity of the area, as climatic differences might occur and the substrate of the rock of the lichen may differ from where the growth curve was established. The estimations of lichen age may therefore only be considered as an estimate of the minimum age of the moraine ridges (Winkler, 2003; Bradley, 2014; p. 129).

4.5.1 Lichenometric measurements and age estimations

A digital calliper was used to measure the size of the lichen *Rhizocarpon geographicum* (see fig. 4.7*).* When measuring the size of lichen, the diameter of the longest axis of individual thalli is recorded. To ensure precision in dating, irregularly shaped thalli were rejected from sampling as they might be merged thalli (Bickerton & Matthews, 1992; Winkler, 2003). Lichen sizes were recorded in seven transects

Figure 4.7. Measuring the size of Rhizocarpon geographicum using a digital calliper.
Photo: George Young

across the moraine ridges, mainly in the north-eastern section of the moraine, as the ridges were easier to distinguish in this area. At each spot, a sample size of the five largest lichens spotted were measured in sections of about 5 x 5 m at each ridge, and the GPS positions were recorded for each site. See fig. 4.8 for the positions of all sampling sites.

The average lichen size of the five largest lichens from each sampling site was used to estimate the age of each of the moraine ridges. As there were no previously dated surfaces and investigations of historical maps were not detailed enough to give an indication of previous glacier extent for this study area, an indirect growth curve established by Winkler (2003) for Øvre Beiarnbre, approximately 38 km west of Semskfjellet, was used to approximate the age of the moraine ridges

$$\log (y + 150) = 0.003\,3 + 2.2343$$

Where x equals the average lichen size and y equals the age of the lichen. Winkler (2003)'s dating curve is based on a relative age dating technique, where lichen measured on gravestones at the cemeteries in Beiarn and Høyforsmoen were used to establish the curve and compared

to a local control point at Øvre Beiarnbre. To estimate a date for lichen colonisation on the individual ridges, the calculated lichen age was subtracted from 2021.
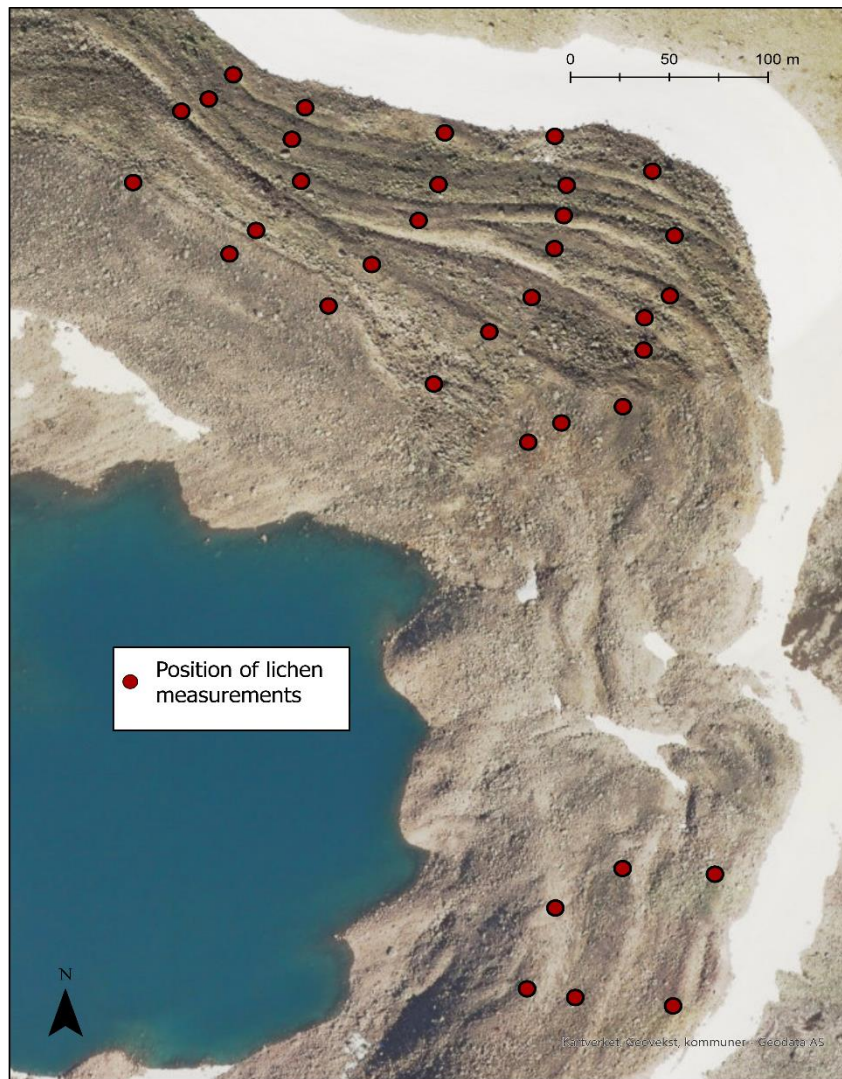
Figure 4.8. Sampling sites for lichenometric measurements.

5 Results

5.1   Landscape inventory

This section provides an overview of the main features in the field area.

5.1.1 The glacier and proglacial lake

The glacier is a relatively small, diminishing cirque glacier with the remains located on the steep north-eastern slope of Semskfjellet, stretching from an elevation of *ca.*1400 m a.s.l. down to the proglacial lake below at about 1200 m a.s.l. The total area of the glacier is about 0,45 km^2 (estimated from a 1 m DEM from Høydedata). The contemporary glacier may be temperate, this conclusion is based on substantial crevassing occurring on the glacier surface and the presence of liquid water (see fig. 5.1). There is also a prominent bergschrunde present at the top of the glacier, which can be seen on the third photo from the top on fig. 5.1. Avalanche events have also been observed from the central section, see bottom photo on fig. 5.1 from September 2021. The proglacial lake has a total area of about 0,094km^2 (estimated from a 1 m DEM from Høydedata) and it is fed by subglacial meltwater streams from the glacier (fig. 5.1). The proglacial lake is dammed by the marginal moraine, and the water does not have a clear outflow from the lake.

Figure 5.1., Pictures of the glacier from summer 2021, top photo taken from the northern ridge of the moraine 28.07.21, second photo taken from the south-central side by the lake 05.08.21, third photo showing a clear Bergschrunde at the top of the glacier 28.07.21, bottom photo showing avalanche event in the central section 15.09.21. Photos by Sofie Jordheim.

5.1.2 The ice-cored moraine

The moraine complex has a total area of about 0,18 km^2 (estimated from a 1 m DEM from Høydedata) and dams the proglacial lake. The moraine ridges are over dimensioned, with heights ranging up to 30-40 m above the surrounding terrain (see fig. 5.2 and 5.3). The material on the moraine consists of an assemblage of various grain and rock sizes from fine sand to boulders of several meters in diameters (fig 5.4). The ridges in the northern and southern part of the moraine are quite well defined, while the terrain is more hummocky in the central section (see fig. 5.4). The moraine is scattered with depressions and can be deemed rather unstable terrain, as mass wasting were apparent from all moraine ridges. Vegetation is generally sparse. Lichen dominates on top and in-between some of the ridges, especially in the northern section, and a few occasional plants were observed. A snowbank runs along the edge of the distal side of the moraine (fig. 5.3 and 5.5). Inspection of aerial imagery revealed that it mostly remains intact throughout the melt season (see section 3.3). However, field observations in the summer of 2021 showed that large sections of the snow patch disappeared in the latter part of the melt season this year. Pro-nival ridges also surfaced as the snowbank melted back over the summer (fig. 5.5). The moraine is assumed to be ice-cored, even if ice has not been observed in the field, due to the form and size of the moraine ridges, the presence of the snowbank along the margin and as the moraine is located in what is likely to be a permafrost zone (see section 3.1). On the distal side of the moraine, there are several meltwater springs emerging from the subsurface of the moraine, forming an array of braided meltwater channel.

Figure 5.2 The moraine seen from the south. Photo by Sofie Jordheim 28.07.21.

Figure 5.3 The moraine seen from the southern moraine ridge 26.07.21 (left) (person for scale), the northern section showing the demarcation of the ridges, photo taken with a UAV 15.09.21 (right).

Figure 5.4 Moraine ridges mainly consisting of large boulders (person for scale on the photo on the left), more hummocky terrain in the central section (photo on the right). Photos by George Young and Sofie Jordheim 25-26.07.21.

Figure 5.5 Emergence of pro-nival ridges from the snow patch running along the margin of the moraine. Photos by Sofie Jordheim, 28.07.21

5.1.3 The glacial foreland

The glacial foreland shows signs of current and past glacial and periglacial processes which have shaped the area. There is a quite distinct change between glacial and glaciofluvial deposits in the foreland, as might be seen by the change in colour from green to grey along a horizontal centerline of fig. 5.6. A rather thin layer of till covers most of the upper forefield, as well as bedrock in some sections. The lower section has a considerably thicker layer of till which is mostly moss or grass covered. Water was observed to flow on the surface when the till was finer grained, and below the ground under coarser till. Periglacial features are scattered across the whole forefield and include stone stripes (fig. 5.7), sorted circles (fig. 5.7), gelifluction lobes and cryoplanation terraces (fig. 5.7). Glacial deposits such as marginal moraines and glaciofluvial features such as engorged eskers (fig. 5.8) are also present. The lower section of the forefield, where the till is slightly ticker, is dominated by earth hummocks (tufur) and small isolated ponds in frost mounds are found in the tufur fields (see fig. 5.9). The foreland is generally sparsely vegetated by lichens, mosses, small bushes, plants and grass.

Figure 5.6 The glacial foreland, seen from Namnlauselva with the glacier and the moraine in the top-centre. Photo: Sofie Jordheim

Figure 5.7 Stone stripes (left), sorted circles (middle) and cryoplanation terraces (right). Photos by: Sofie Jordheim

Figure 5.8 Glaciofluvial deposit suggested to be an engorged esker in the lower part of the study area Photos by: Sofie Jordheim

Figure 5.9 Tufur fields and small isolated ponds in frost mounds. Photos by: Sofie Jordheim

5.2 Quaternary geological maps

The quaternary geological mapping of the ice-cored moraine (fig. 5.10) shows how tumultuous the moraine topography is and indicates which areas are the most affected by subsidence. It is worth noting that the size of the snow patch marked on the map varies from season to season and throughout the summer, with it entirely disappearing some years (based on analysis of aerial imagery, see section 3.3). The flutes identified next to the lake, between the marginal ice-cored moraine and the glacier can be seen as an indication of the glacier having changed its thermal regime from polythermal to temperate. In a polythermal glacier regime the sole in the ablation zone is frozen to the bed, while in a temperate glacier regime it is sliding along the bed and may produce fluted basal till (Irvine-Fynn *et al.* 2011).
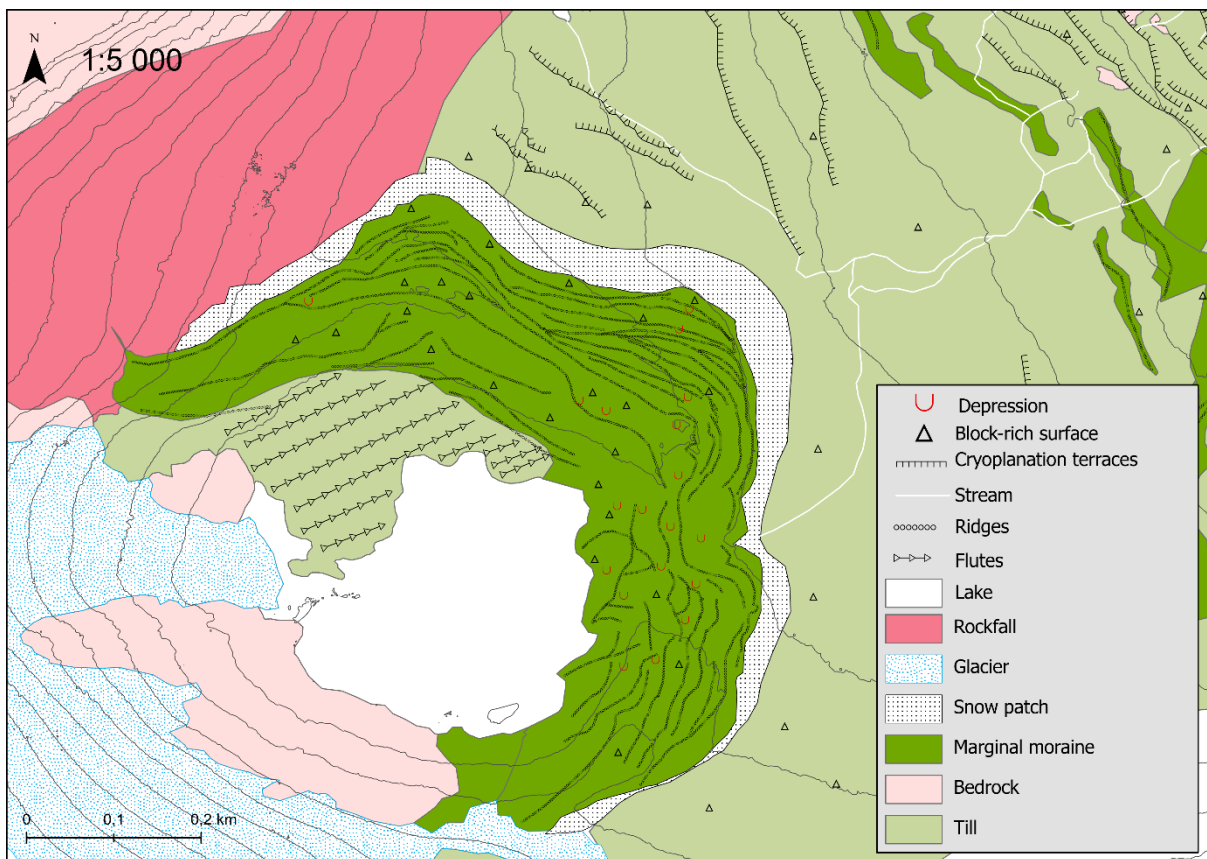
Figure 5.10 Quaternary map of the ice-cored moraine, nomenclature and colours based on the standard by the Norwegian Geological survey (NGU). Note the fluted basal till inside the marginal moraine.

The quaternary mapping of the study area highlights the presence of periglacial features and shows how a slow reworking of the landscape is happening in a previously glaciated terrain (see fig. 5.11). Note that only main water pathways are marked on the map and does not show all the small streams present in the foreland. Fig. 5.11 shows how this small glacial system has been a part of a former much larger and older glacier system in the Saltfjellet area with demarcated lateral meltwater channels formed by marginal glacial meltwater drainage along the sides of the valley.
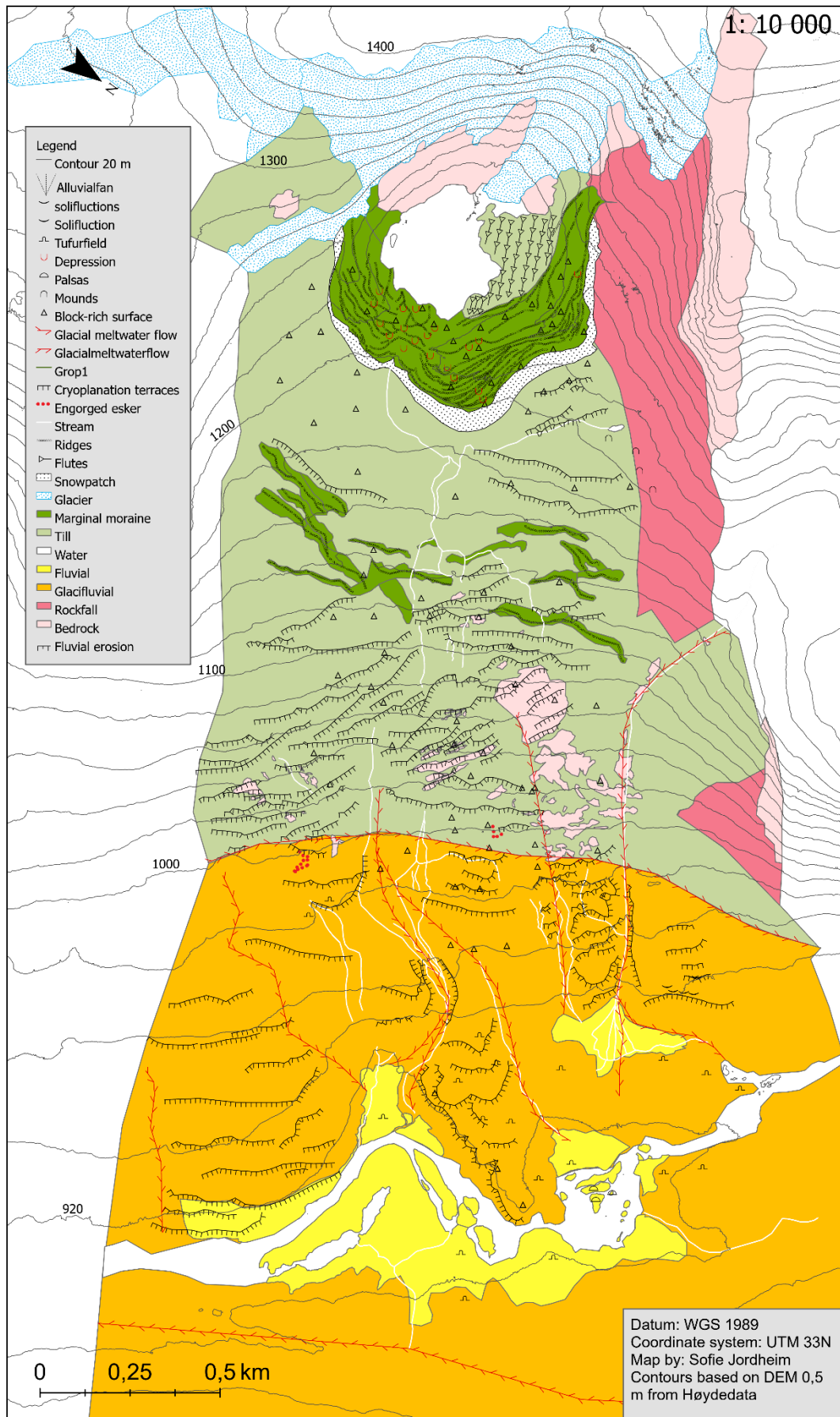
Figure 5.11 Quaternary map of the study area, nomenclature and colours based on the standard by the Norwegian Geological survey (NGU).

5.3 Hydrology

5.3.1 Lake level fluctuations summer 2021

Monitoring of the lake throughout the summer season showed that the lake level increased rapidly at the beginning of the summer, reaching a maximum lake level around mid-July, before it gradually decreased in the second half of the season, with smaller incidents of increase following periods of increases in air temperature (see fig. 5.12 and 5.13). The logger was moved a few meters closer to shore in the evening of July 25th, as the lake level had increased so much that I feared it would continue to increase above the place we fastened the logger. Data was also retrieved from the logger on August 3rd. The water level of the graph (fig. 5.14) has been adjusted to account for the movement of the logger to a new position on these two dates. No sudden changes in temperature were recorded when the logger was moved to a different position, thus the temperature graph has not been adjusted.

On fig. 5.14, one may see that the lake level was very steady from the start of the logging, (26.06. - 01.07.21), which might be connected to a threshold being reached in terms of drainage capacity. The lake level then increased steadily from July 1st to July 8th, from a water

Figure 5.12 Selected photos from the time lapse camera between 26.06.21 – 02.09.21. The selection shows the seasonal changes with the lake being almost fully ice covered at the end of June, to peak lake level around mid-July, and decreases in the lake level towards the end of the summer season.

column above the logger of about 170 cm to about 345 cm. This period coincides with an increase in air temperature, as registered by the barometric logger on the shore of the lake (fig. 5.14). Looking at the photos from the time lapse camera (see fig. 5.12), the extent of the glacier diminished drastically in this period; indicating that the increase in lake level may be attributed to the melting of glacier ice and surrounding snow following increases in air temperature. A close study of the timelapse photos showed that the lake was ice free 12.07.21 (second photo

from the top on fig. 5.12), and the lake level continued to increase until 16th of July, though at a considerably lower rate following a drop in air temperature. The water level reaches its highest level on July 16th, with a water column of 370 cm above the water logger. The water level thus increased by around 200 cm from the start of the logging on June 26th. From 15th to 25th of July there is a period with temperatures below 10 degrees, and in this period the lake level decreased with about 70 cm (see fig.5.14). From 25th – 31st of July there is another warm period, with air temperatures between 10°C and 25°C and the water level gradually increased until 31st of July, with a water column of ca. 320 cm. Thus, the water level rose with almost 20 cm in this warm period. From 30th of July, there is again a drop in air temperature, and from the 31st of July the lake level is steadily decreasing. Between the 31st of July and 7th of August, the water column decreased to ca. 260 cm, lake level thus decreased about 59 cm in this period. Following a warmer period from 6th to 8th of July, the lake level increased until the 12th of August with about 36 cm. From the 12th of August until 7th of September, the trend shows that the lake level is decreasing. There are a few small increases in lake level in this period, namely from 19th – 21st of August, and on the 25th of August. Photos from the time lapse camera (bottom of fig. 12) shows that there was a snowfall at the beginning of September, and the increase in lake level from the 7th of September may be attributed to the melting of this snow, as the air temperature rose again. Variations in the lake temperature correlate fairly well with changes in air temperature, though with a slight lag time. The lake temperature fluctuated from around 0 °C to about 10,5 °C in the warmest part of the summer (see fig.5.14). The average daily precipitation (see fig. 5.15), recorded at the closest weather station indicate that the precipitation has little influence on the lake level this summer. The precipitation is generally very low, with most days having 0 – 5 mm precipitation, a few days over 20 mm and one day having over 35 mm. Only slight increases in lake level can be seen on the days with any significant precipitation but increases in air temperature leading to melting of snow and ice on the glacier seems to be a larger driver of lake level fluctuations in the summer of 2021.

Figure 5.13 Lake level 26.06.21 (first from the left), 25.07.21 (second), 15.09.21 (third and fourth). Photos by: Sofie Jordheim
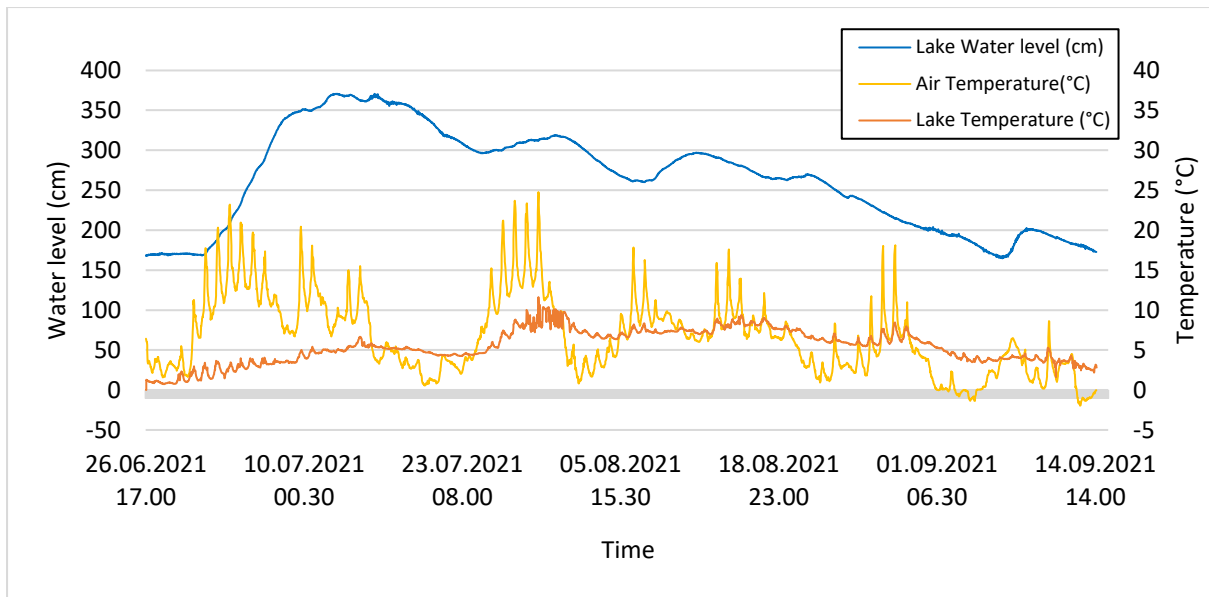
Figure 5.14 Lake level fluctuations, air, and water temperature every 30 min between 26.06.21 – 14.09.21. The water level and temperature were recorded by a diver logger placed in the lake, while the air temperature was recorded by a barometer placed on the shore of the lake.
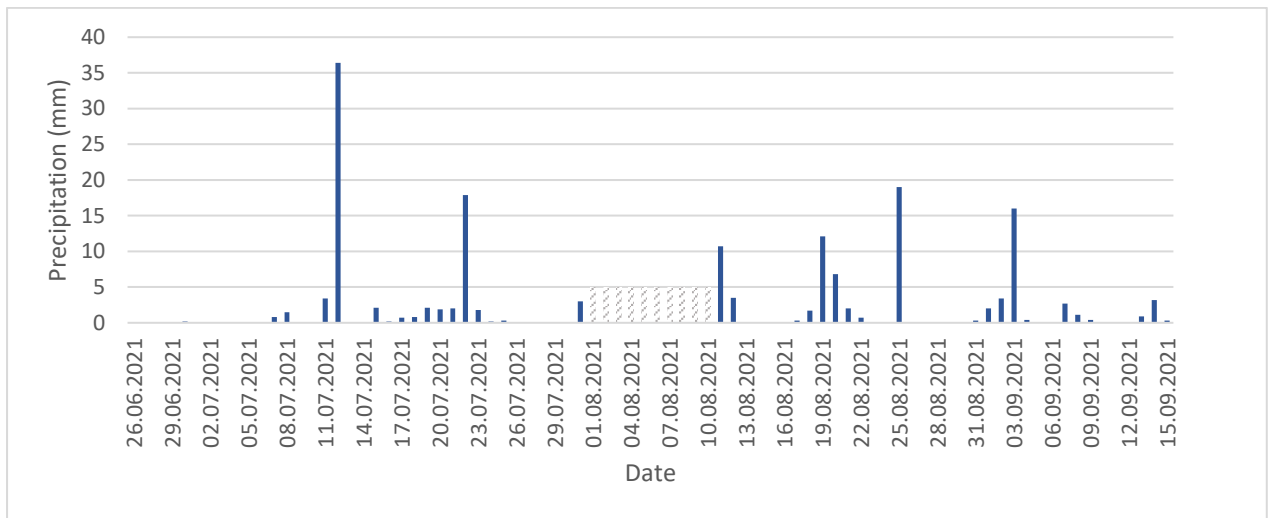
Figure 5.15 Average precipitation (mm) per day recorded at Lønsdal weather station at 520/510 m a.s.l., weather data retrieved from seklima.no 28.09.21, MET (2021). No data (marked in grey) from 01.08.21 – 10.08.21.

5.3.2 Water level fluctuations of streams in front of the moraine summer 2021

When comparing the water level curve of stream LS and the lake, one sees that the curve of the water level for this stream resembles the lake level fluctuations (fig.17). Thus, stream LS has been identified as the main drainage passage from the lake. In addition, the water level of the lake and stream LS had a strong correlation with an r^2 of 0,848. At the end of June, the water level of stream LS started rising before the water level of the lake, which might be connected to the stream also being supplied by local snowmelt in addition to water from the lake (see fig.5.16).

Figure 5.16 Stream LS in front of the moraine, snow patch visible. Photo by: Sofie Jordheim 26.06.21
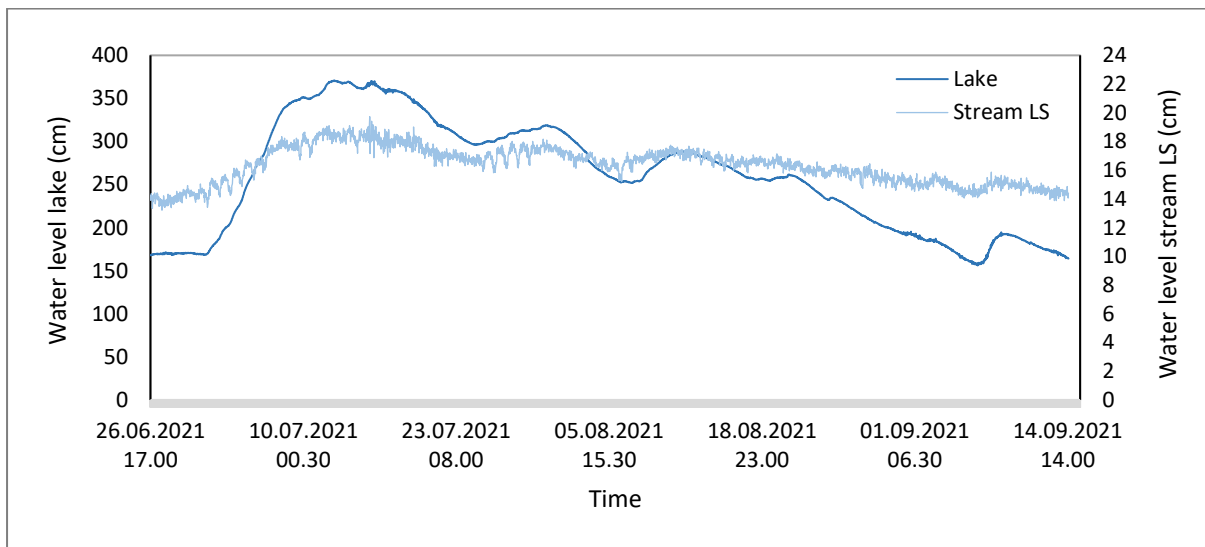
Figure 5.17 Water level of the lake and stream LS every 30 min between 26.06.21 – 14.09.21. The water level was recorded by diver loggers placed in the lake and stream LS. The water level for both the lake and stream LS has been adjusted to account for slight changes in position when data was retrieved from the loggers.

Further looking at the water level of the streams exiting the moraine between 26.06-03.08.21 (fig. 18), the water level by the logger positions LL and LS are in fact part of the same stream, with the position of LS being right below the moraine, and the position of LL being about 50 meters downstream, but with the position of LL also having some minor influx of water stemming from another stream (see fig.4.3 in section 4.2.1). The water level at the logger positions LS and LL both have a slightly increasing trend from the start of the lake level recordings at the end of June until it stabilizes around the middle of July, following the

fluctuations of the lake fairly well. LL starts with a water level of about 11,5 cm, reaching a maximum depth around 15 cm, while LS begins around 13,4 cm and reaches a max level of about 16,9 cm. Both logger positions (LL and LS) had an increase of about 3,5 cm from the end of June until mid-July. From mid-July the trend is slightly decreasing to ca. 14,7 cm for LS and 12,6 cm for LL. A decrease of about 2,2 cm for LS and 2,4 for LL.

The water level at position LN1 fluctuates more and seems to be more prone to changes in air temperature than the other streams, but with a decreasing trend throughout the summer season, running dry by August 3rd, when the logger also was moved to a nearby stream. The fluctuations at LN1 might be seen as indications of the source of the stream being ice or snow melt from the snow patch around the moraine. That the stream became dry might be attributed to a change in the route of the stream, possibly due to the retreat of the snow patch as the summer progressed. It is worth noting that the waterflow in front of the moraine was not restricted to just a few defined channels, but that it was a network of shallow streams of water over a wider area which gradually expanded and changed pathways throughout the summer season.
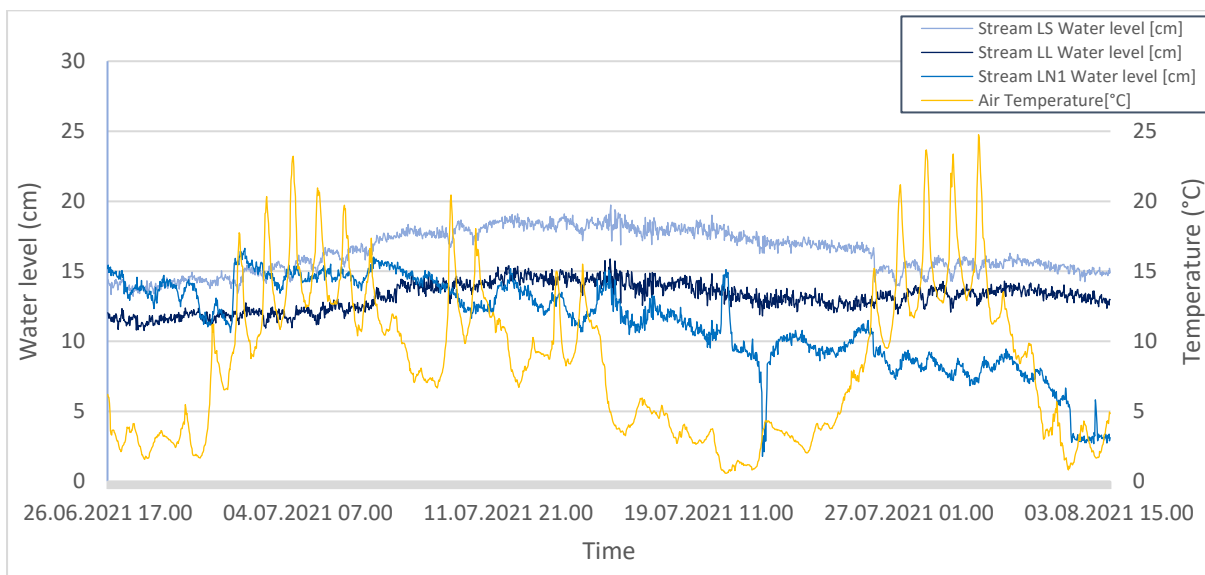
Figure 5.18 Overview of water level of three streams and temperature 26.06.2021 – 03.08.21 at 30 min intervals. Mark that LL is the same stream as LS, about 50 m downstream.
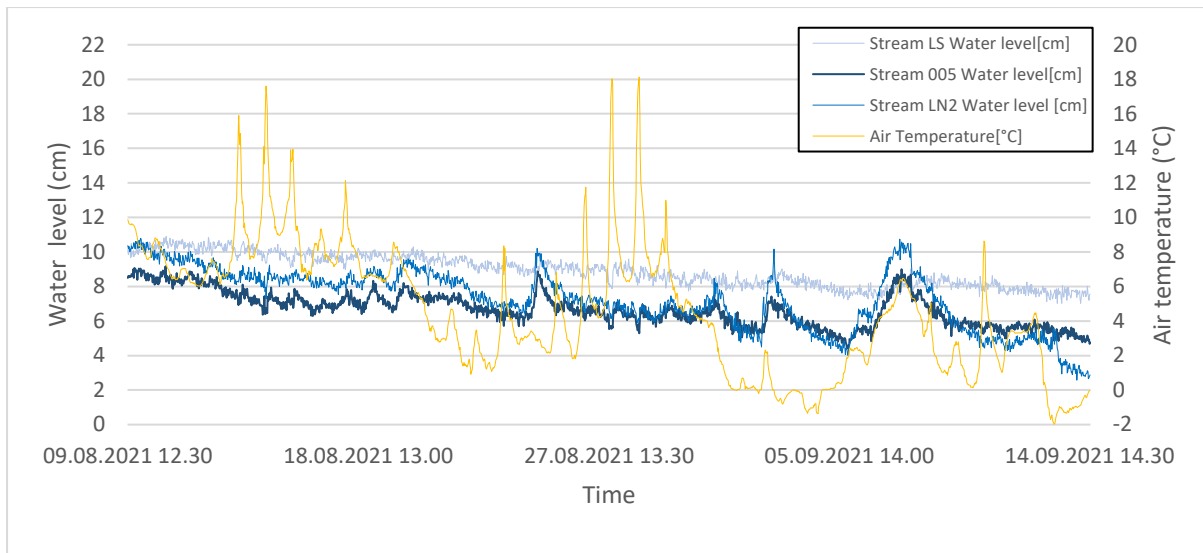
Figure 5.19 Overview of water level of three streams 09.08.2021 – 14.09.21 at 30 min intervals, mark that loggers LN2 and LL (fig. 5.18) has been moved to a different stream, LN2 and 005 respectively.

Some of the loggers, (LN1 and LL) were moved to different streams for the latter part of the summer, the new positions, namely LN2 and 005 can be seen on (fig 4.3 in section 4.2.1). From the 9th of August to the 14th of September, the general trend is a decrease in water level for all streams, though with more fluctuations following the changes in temperature and precipitation (see fig. 5.15 and fig.5.19) for positions LN2 and 005. The water level of position LS has a slightly decreasing trend in this period, from right above 10 cm in water depth to less than 8 cm when the logger was retrieved. The water level at position LN2 also has a decreasing trend going from above 10 cm to a depth of ca. 2-3 cm. Similarly, position 005 has a decreasing trend from close to 9 cm depth to just below 5 cm. While the water level of position LS is fairly stable throughout this period, the water level of 005 and LN2 corresponds with increases in precipitation and temperature. This can be an indication of the sources of streams for positions 005 and LN2 being snow or ice melting when the temperature increases, leading to an influx of meltwater, while the stream with position LS is seen as the main drainage pathway of the lake, having a steady flow of subsurface flow from the lake.

5.3.3 Temperature of lake and streams summer 2021

The water temperature at all the logging positions during the first part of the summer (26.06.21 - 03.08.21) were influenced by changes in air temperature to some degree, as peaks in air temperature also can be visually identified to follow the peaks of the water temperature on fig. 5.20. The water temperature at LN1 corresponds the most with the changes in air temperature, reaching temperatures over 20 °C at the highest and around 0 °C at the lowest. This might be linked to the location of the logger being located further away from the moraine (see fig. 4.3 in section 4.2.1 for location). However, a statistical analysis of correlation gives an $r^2 = 0,117$ between the water temperature at LN1 and the air temperature, this is likely due to the time lag associated with the changes in water temperature, and the low water level in the stream towards the end of this period (see fig. 5.18 in section 5.3.2). The water temperature of the lake and other streams seem to be less affected by variations in air temperature (see fig 5.20). The water temperature at LS and LL follows the variations in the lake temperature fairly well (see fig. 5.20), though the curve for temperature of stream LS is slightly smoother, indicating that the water temperature at position LS is less affected by air temperature variations compared to the water temperature in the lake and at LL. A statistically significant relationship (p=0) and a strong correlation with $r^2 = 0,837$ was found between the lake temperature and temperature of LS. Giving further weight to the interpretation of stream LS being the main drainage pathway of the lake. The water temperature at LL had the highest correlation to air temperature, with $r^2 = 0,241$. This might be linked to the position of LL being the furthest away from the moraine. The fluctuations in water temperature at LN1 compared to the other monitored streams indicate that stream LN1 has a different source, which might be attributed to melting of the snow patch or ice within the moraine.

For the second part of the summer, 09.08.21 - 14.09.21, all streams, except stream 005 seems to some degree to be affected by the fluctuations in air temperature. The water temperature at 005 is very stable, ranging between 0,85 – 1,8°C throughout this period (fig. 5.21). Logger position 005 was very close to the snow patch and in a deeper hole between two rocks, which might be part of explaining the small changes in water temperature. Stream LN2 also had relatively small fluctuations in water temperature, ranging between 0,01 and 4,63 °C. The water temperature of the lake and stream LS continues to follow each other between 09.08 – 14.09.2, though the water temperature at LS is slightly more stable than that of the lake. The lake temperature ranged between 0,74 and 11,6 °C in this period, while the minimum water temperature at LS was 2,62°C and the maximum temperature was 7,57 °C. The r^2 between the

water temperature of stream LS and the lake was $r^2=0,851$, indicating a strong correlation and making it a significant relationship (P=0). The lower temperatures of stream LN2 and 005 compared to stream LS and the lake, as seen on fig. 5.20, might indicate that these streams have a different source than stream LS.
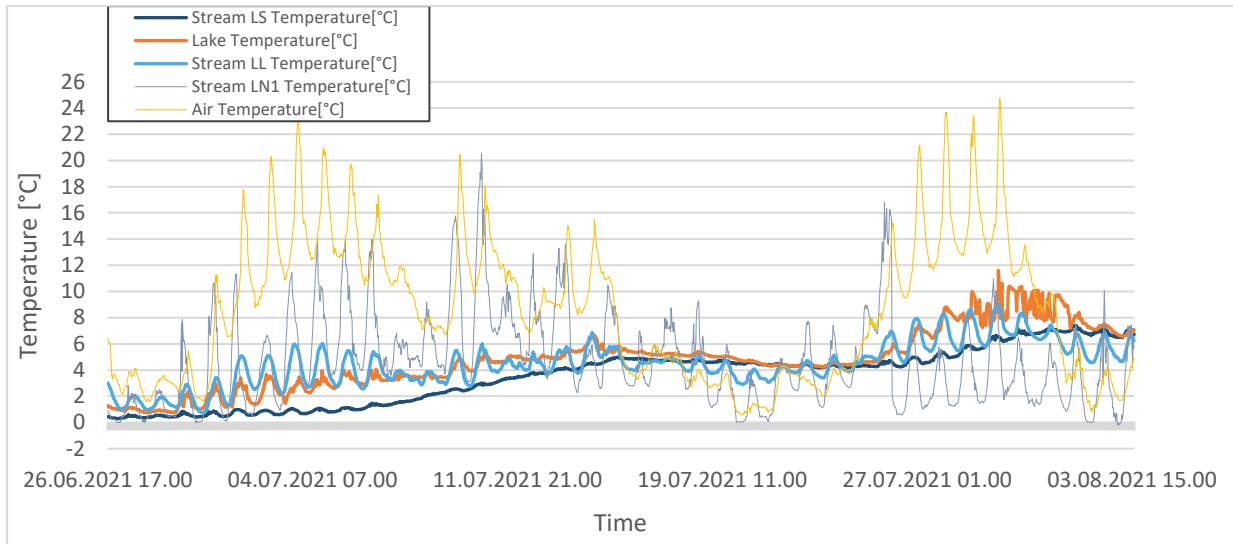
Figure 5.20 Logger data of water temperature from the lake, streams, and air temperature from 26.06.21 – 03.08.21 recorded at 30 min intervals.
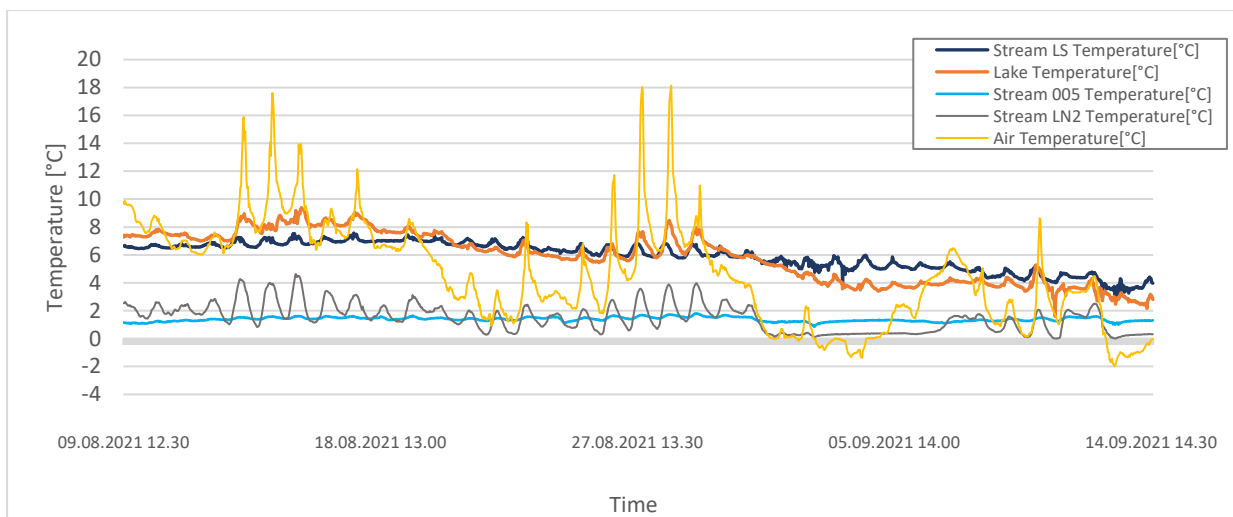
Figure 5.21 Logger data of water temperature from selected streams, the lake and the air temperature from 09.08.21 – 14.09.21, recorded at 30 min intervals.

5.3.4 Residence time

In order to find the residence time of the water in the moraine for the main drainage pathway, break points for temperature change in the lake and stream LS were identified on fig. 5.22: These breakpoints were used as markers in an attempt to see how fast the water is flowing through the moraine, and perhaps deduce something in terms of the environment of the subsurface flowpath. The water is flowing beneath the till cover of the moraine for ca. 150 m, before it surfaces on the distal side of the moraine. Figure 5.22 shows the daily average of water temperature measurements from the lake and stream LS, in addition to air temperature, portraying the timelag associated with changes in temperature for the lake and when this same change in temperature may be picked up in stream LS. Interestingly, the water seems to be flowing slower at the beginning of the season, as the temperature change in the lake on 28.06.21 may be spotted one week later in stream LS - 05.07.21. Later on in the summer, the water seems to be flowing faster, as the timelag in the temperature change can be identified two days after (see for example 30.07.21-01.08.21). However, in the latter part of the season, when the water level is decreasing, it is harder to distinguish between the different break points in temperature, and exactly when the break points are happening are more open for interpretation.

A close investigation of the temperature profiles of stream LS and the lake (see fig. 5.22) shows that the water temperature of stream LS remains a couple degrees lower than the lake temperature until 21.08.21, with the exceptions of the two periods when the air temperature was lower than the lake temperature (around 20.07.21 and 02.08.21). This may be read as a sign of the water temperature being lowered in the subsurface environment that it runs through.
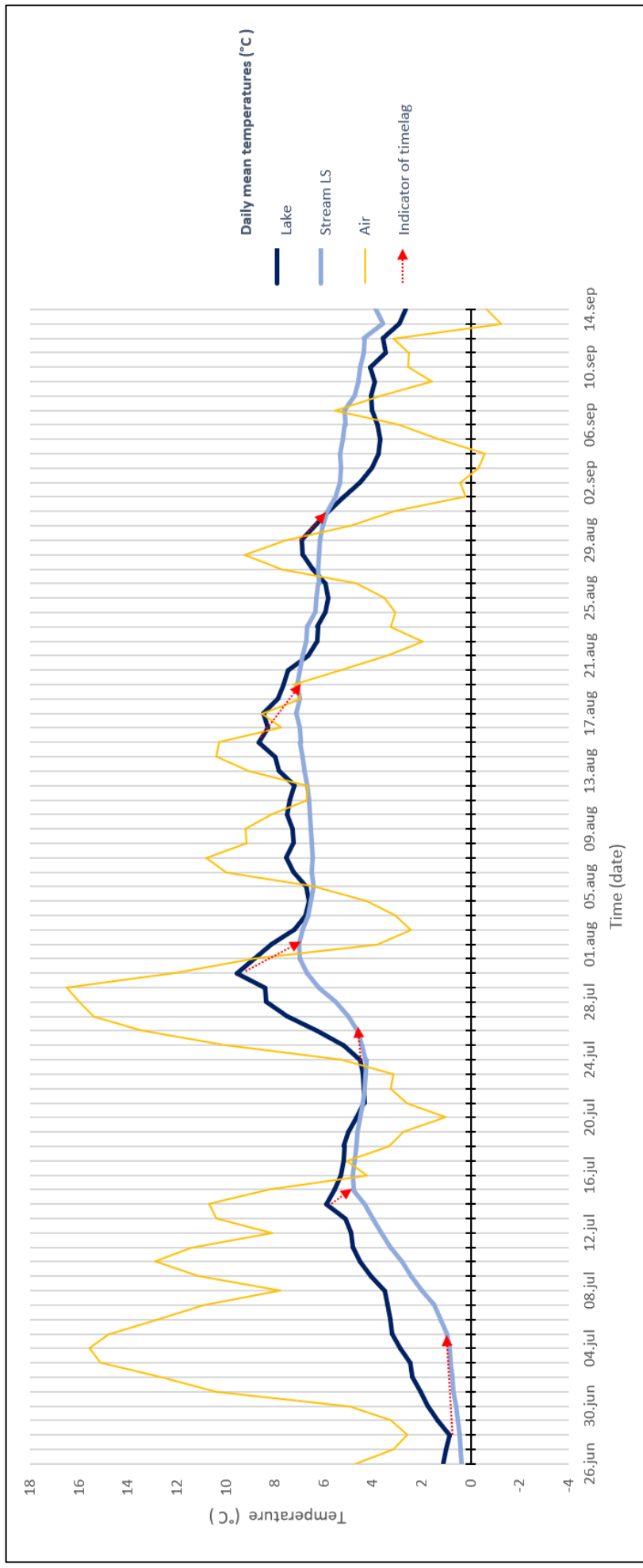
Figure 5.22 Daily averaged logger data of water temperature from the lake and stream LS, in addition to air temperature, from the whole period 26.06.21 – 14.09.21. Red arrows indicate the timelag associated with changes in water temperature as an indication of changes to the residence time of the water running through the moraine.

5.3.5 Temperature and conductivity of lake and streams

The spatial distribution of mean stream temperature and conductivity based on in-situ measurements between 26.06 – 05.08.21 are displayed on fig. 5.23. and shows indications of the streams having different sources and/or are going through different environments in the moraine. It is worth noting that the number of streams in the forefield of the moraine increased and broadened throughout the summer. This might be an indication of different parts of the hydrological system in the area becoming active at various times and could possibly be seen in association with increases in air temperature throughout the season. The streams exiting the central-eastern part of the moraine have similar mean temperatures (around 5-6 °C) and conductivity (10 – 11 µS/cm) as the lake, indicating that these streams have the same source, and go through a similar subsurface environment. The relatively low electric conductivities might reflect the relatively higher discharge of these streams (based on field observations), being associated with the main drainage pathway of the lake, and the sloping of the terrain. At the beginning of August, the snow patch along the margin of the moraine had retreated so much in the central eastern section of the moraine, that it was evident that these streams were not just a result of the melting of the snow patch. The average conductivity of the streams coming out of the northern part of the moraine are between 0,1 - 3°C and conductivities are around 2-3 µS/cm. The low temperatures and conductivities of these streams are likely to be attributed to the source being from the melting of the snow patch. The snow patch retreated by several meters during the summer, but it was still present around the northern and north-eastern section of the moraine towards the end of the summer. Higher conductivities are generally found in the north-eastern section of the moraine between 13 and 21 µS/cm, and temperatures ranging between 1 – 3 °C. The streams located a bit further away from the moraine generally has higher average temperatures, indicating that they are more sensitive to variations in air temperature and incoming solar radiation. Streams exiting the southern part of the moraine have a lower mean conductivity between 4 – 6,5 µS/cm and average temperatures around 3 °C.
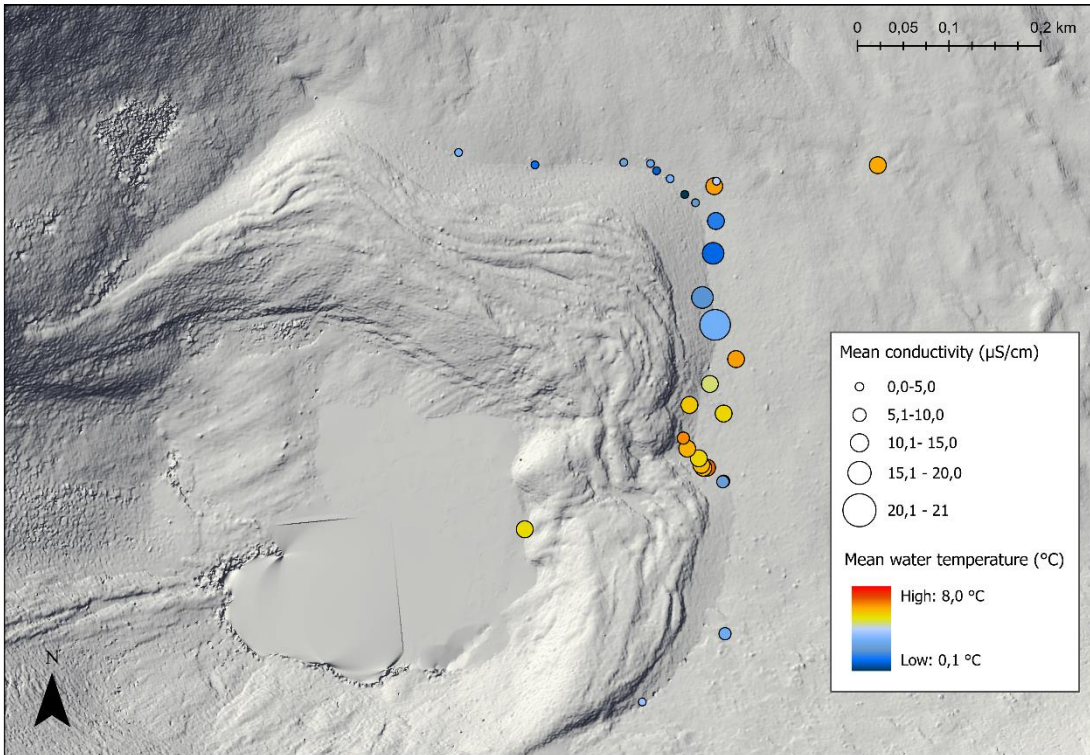
Figure 5.23 In-situ water temperature and conductivity measurements from the lake and streams 26.06 – 05.08.21. The colours indicate average water temperature, and conductivity is indicated by the size of the circles. Hillshade based on DEM 1 m from Høydedata. Datum: ETRS/WGS 1989, Coordinate system: UTM 33N.

5.3.6 Stable water isotopes

The analysis of stable water isotopes showed variations between the isotopic composition of the sampled snow and water. The values for $\delta^{18}O$ ranged from -13,85 ‰ to -9,53 ‰ (see fig.5.24) with an uncertainty of 0,06 ‰ for the measurements. The mean for $\delta^{18}O$ was -12,44 ‰, with a relatively small standard deviation of 0,69 ‰. For δD the results ranged from -98,9‰ to -65,5 ‰, with an uncertainty of 0,4 to 0,5 ‰ (see fig.5.24). The average for δD was -85,69 ‰, with a standard deviation of 5,01 ‰. A least squares linear regression line is plotted for all the samples composition, for which other samples may be compared. The trend line has a slope of 7,03 with an r^2 value of 0,934. Meteoric samples represent the highest and lowest compositions in the dataset (Dansgaard, 1964), with the lowest $\delta^{18}O$ and δD stemming from snow samples. The snow samples, highlighted in yellow on fig 5.24, have the least deviation from the GMWL, with d-excess values between 9,6 and 10,7 ‰ (fig. 5.25). All of the water samples plot above the global meteoric water line (GMWL) (fig. 5.24), as also can be seen by the positive d-excess values; with d-excess ranging from 11,6 to 17,6 ‰ (fig.5.25).
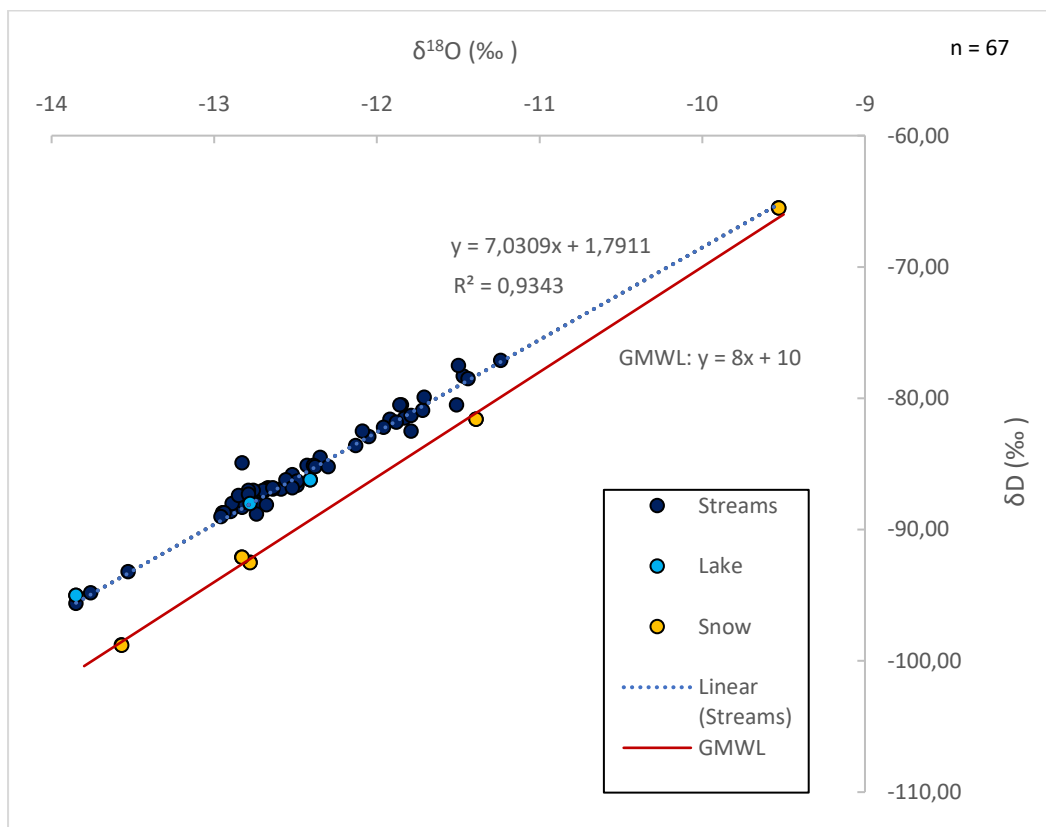
Figure 5.24 Relationship between $\delta^{18}O$ and δD from Semskfjellet in relation to the global meteoric water line (red). Samples collected from 26.06 – 05.08.21
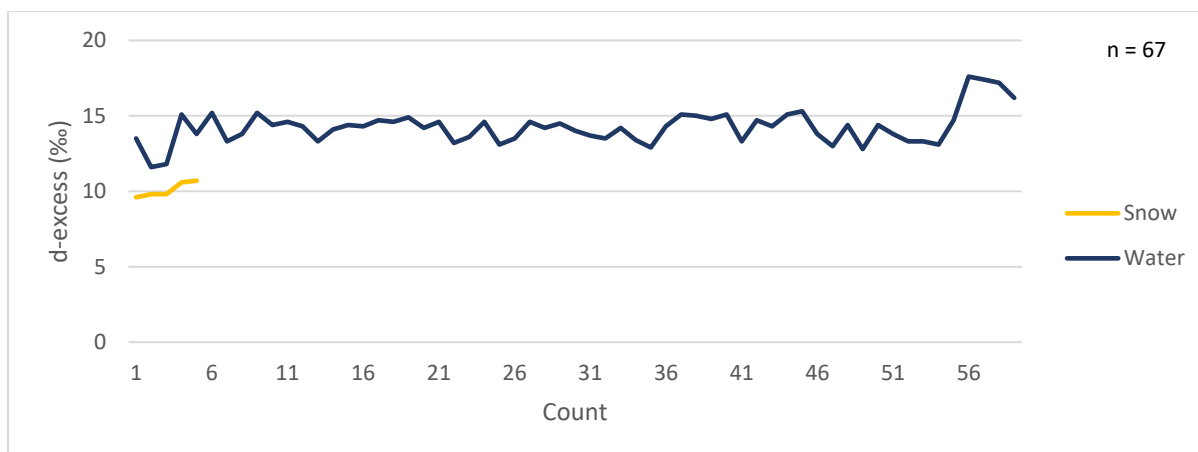
Figure 5.25 Shows d-excess (‰) values for all samples from Semskfjellet. Samples collected from 26.06 – 05.08.21.

The small deviations from the GMWL of the snow samples (fig-Xgraph) might be indicating no or negligible secondary fractionation effects during the deposition and melting processes before the time of sampling. The snow was sampled early in the melt season and at high elevations and may therefore be representative of the snowpack of 2021. That the isotopic composition of the snow samples aligned along the GMWL (fig. X 5.24), might also indicate that the winter precipitation has a similar geographic origin compared to what one may find in other seasons (Penna *et al.* 2017).

The spatial and temporal distribution of the isotopic composition of $\delta^{18}O$ throughout the summer can be seen on (figs.5.26, 5.27, 5.28 and 5.29), exhibiting that the isotopic composition of the snow patch, lake and streams change throughout the summer. Due to the collinearity between the δD and $\delta^{18}O$ (see fig.5.24) and the higher precision of $\delta^{18}O$, only results from $\delta^{18}O$ are shown on figs.5.26, 5.27, 5.28 and 5.29. It is worth noting that the increase in the number of samples from each sampling frame is attributed to the emergence of new streams as the season progressed.

The water samples from 26.06.21 (see fig.5.26), showed small variations, with $\delta^{18}O$ values of the lake and streams ranging from -13,53 ‰ to -13,85 ‰. The snow samples had slightly higher $\delta^{18}O$ values ranging from -11,39 ‰ to -13,57 ‰, indicating that the snowpack was more enriched in $\delta^{18}O$ than the meltwater at the same point (Theakstone 2003). The snow sampled at an elevation of 1240 m a.s.l., at a depth of 25 cm had a lower value of $\delta^{18}O$ (-13,57 ‰) than the sample from the same location at a depth of 6 cm (-12,78 ‰). The snow sample from the

side of the lake show indications of having been more influenced by fractionation with a higher $\delta^{18}O$ value than the other snow samples (Fig. 5.26).

The water samples taken at the end of July (25.-29.07.21), show more spatial variation in $\delta^{18}O$, ranging from -12,95 ‰ to -11,72 ‰ (see fig. 5.27), and the $\delta^{18}O$ value of the water samples are considerably lower than the one snow sample taken from the snow patch (-9,53 ‰). Hence, the isotopic composition of the snow patch is isotopically heavier (enriched in ^{18}O) compared to the meltwater (Theakstone, 2003). There are differences in the spatial distribution of $\delta^{18}O$ values along the margin of the moraine, but no clear trend can be recognised. Two streams in the northern section of the moraine (white circles), show slightly lower values of $\delta^{18}O$, which might indicate that they have a different source, or that the snow melt has not come as far in this section of the moraine. It is also worth noting the variability in $\delta^{18}O$ of the streams in the vicinity of the main drainage pathway in the central eastern part of the moraine. This might be an indication of the streams emerging just south of the main drainage pathway having a different source than the main drainage pathway, possibly stemming from or mixing with snowmelt. Comparing the samples from the end of July to the samples from the end of June, both the water in the lake and streams in addition to the snow is becoming more isotopically enriched in heavier isotopes, as the lighter isotopes are preferentially evaporated (Clark & Fritz, 1997; Theakstone, 2003).

The samples taken in a transect further down in the proglacial area 29.07.21 (see fig.5.28) had $\delta^{18}O$ values ranging from -11,5 to -13,26 ‰, with the central samples having lower $\delta^{18}O$ values, than the north-western samples. The north-western samples are not attributed to the water coming from the main study area, but rather from another small system north-west of the study area. Compared to the samples close to the margin of the moraine, the samples in this "reference transect" further down in the glacial foreland (fig.5.28) have lower values of $\delta^{18}O$, which might be connected to mixing of water from different sources (Yde & Knudsen, 2004). The upper point of the main river, Namnlauselva, was sampled 30.07.21, giving a $\delta^{18}O$ value of -11,79 ‰ and the lower point of the river was sampled 05.08.21, giving a $\delta^{18}O$ value of -11,51 ‰, only showing a slight change in the isotopic composition of the water in the river in this period.

The water samples from 04.-05.08.21 (fig.5.29) display a concentration of lower values of $\delta^{18}O$ in the vicinity of the main drainage pathway, compared to the water sampled further north and south along the margin of the moraine. The lake was sampled on the evening of 04.08.21, while the rest of the samples displayed on fig.5.29 were taken 05.08.21, thus the difference

between the $\delta^{18}O$ values of the lake and the main drainage pathway might be attributed to diurnal variations (Yde & Knudsen, 2004). The $\delta^{18}O$ value of the lake is also slightly higher in August compared to July (From -12,78 ‰ 25.07.21 to -12,41 ‰ 05.08.21).

Seasonal dynamics of isotope fractionation is apparent for the sampled streams, with the meltwater becoming more enriched in ^{18}O from the end of June to the end of July (see figs. 5.26, 5.27, 5.30). The timeseries of $\delta^{18}O$ (fig. 5.30) displays a trend of increasing $\delta^{18}O$ values from June to July, but there are more variations from July to August. The streams in the vicinity of the main drainage pathway can be identified to be the deviations to the trend from the end of July to the beginning of August (see fig. 5.29), as these streams then show to have lower values of $\delta^{18}O$ again. The timeseries of d-excess (fig.5.30), shows a stark decrease in d-excess from the end of June to the end of July for the water samples, but there is less of a clear trend for the sampled snow. From the end of July to the beginning of August, there is also less of a clear trend for the water samples.
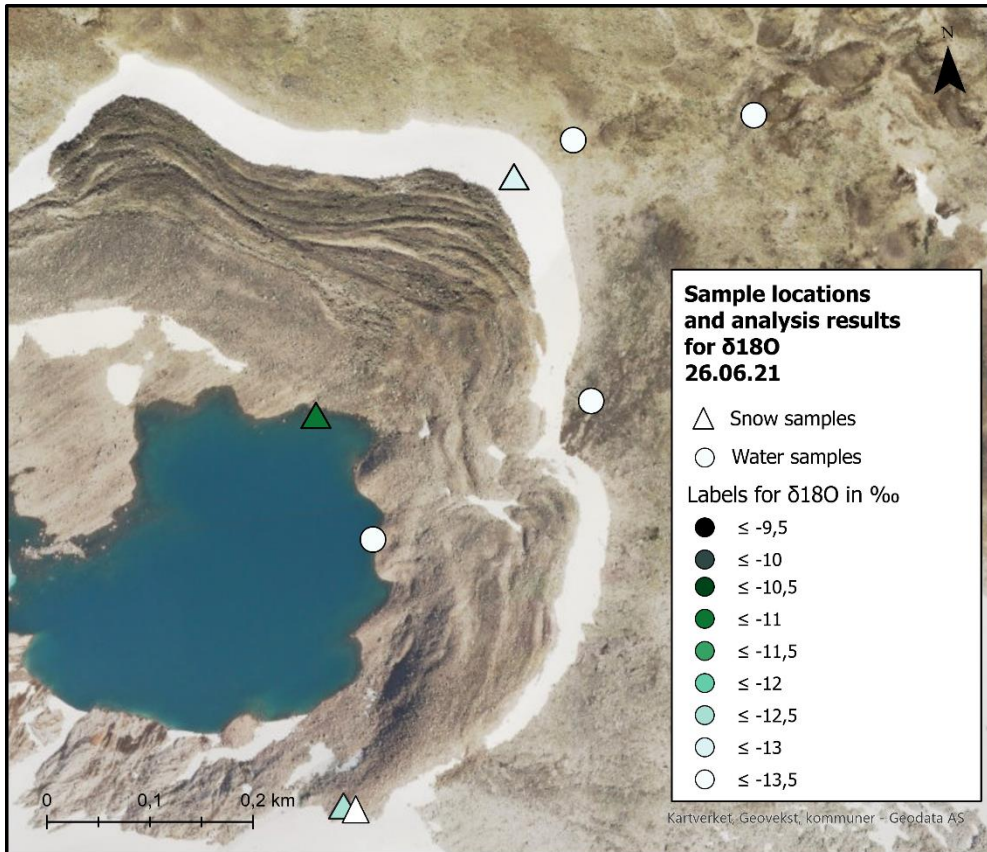
Figure 5.26 Spatial distribution of water and snow samples of $\delta^{18}O$ 26.06.2021.
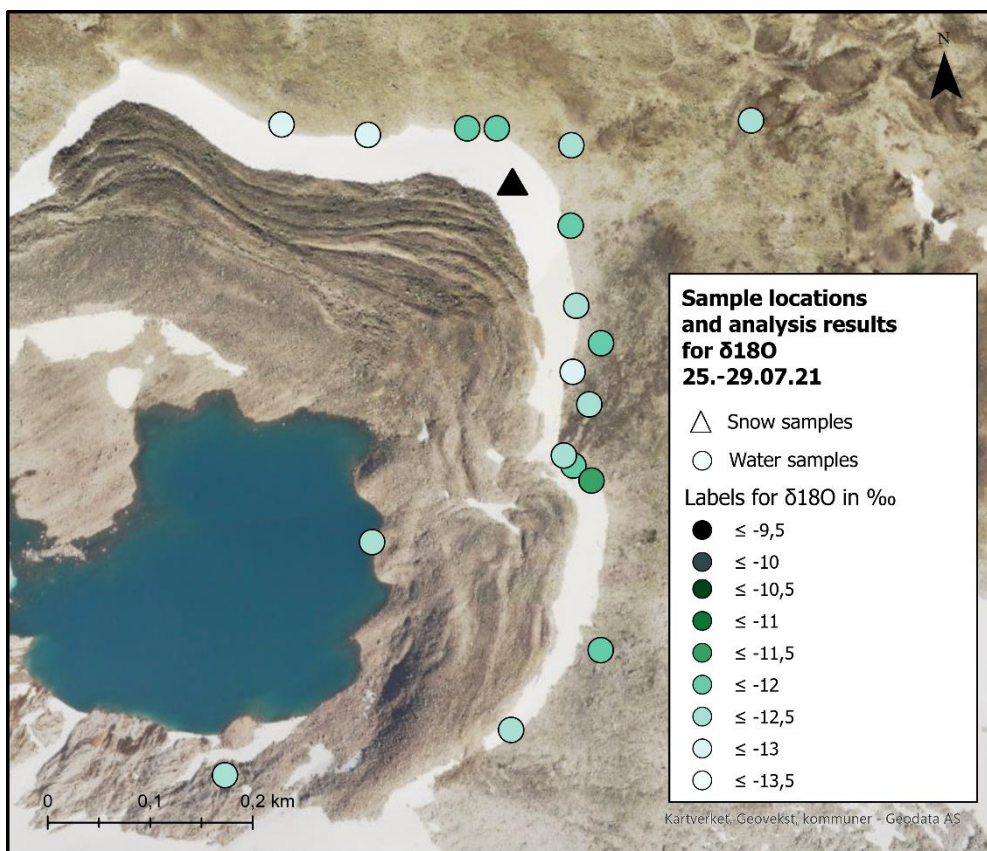
Figure 5.27 Spatial distribution of water and snow samples of $\delta^{18}O$ sampled 25.-26.07.21 and 28.-29.07.2021.
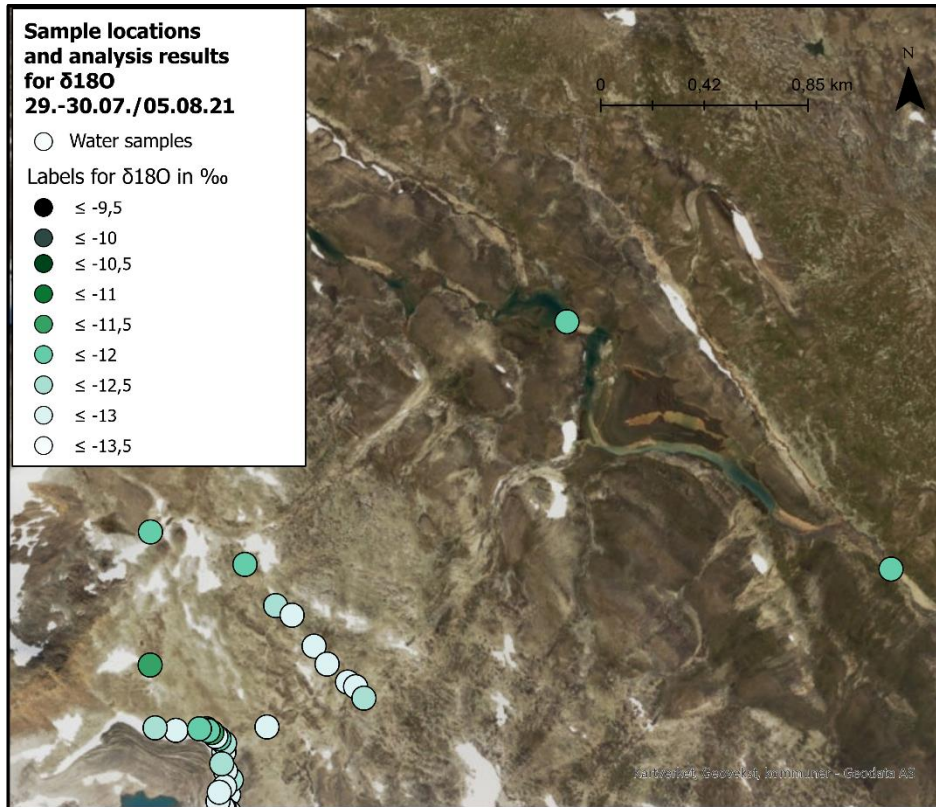
Spatial distribution of water samples of $\delta^{18}O$ sampled 29.07.21 (lower transect), 30.07.21 (northern point of Namnlauselva), 05.08.21 (southern point of Namnlauselva).
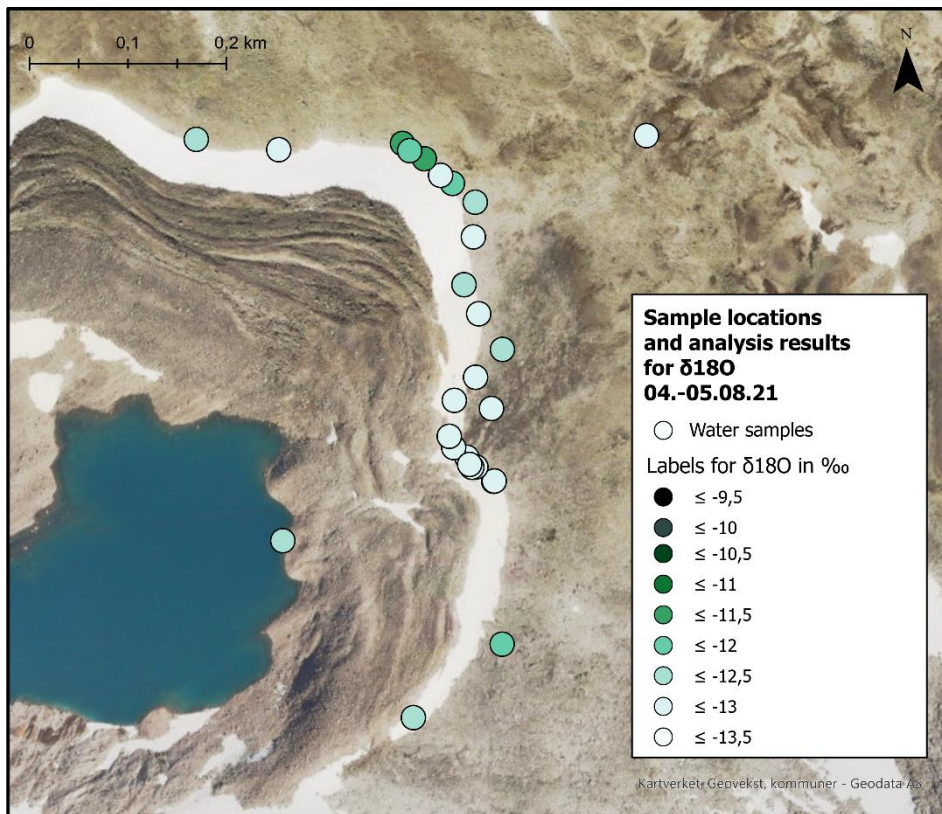
Figure 5.29. Spatial distribution of water samples of $\delta^{18}O$ sampled 04.08.21 (the lake) and 05.08.2021 (streams).
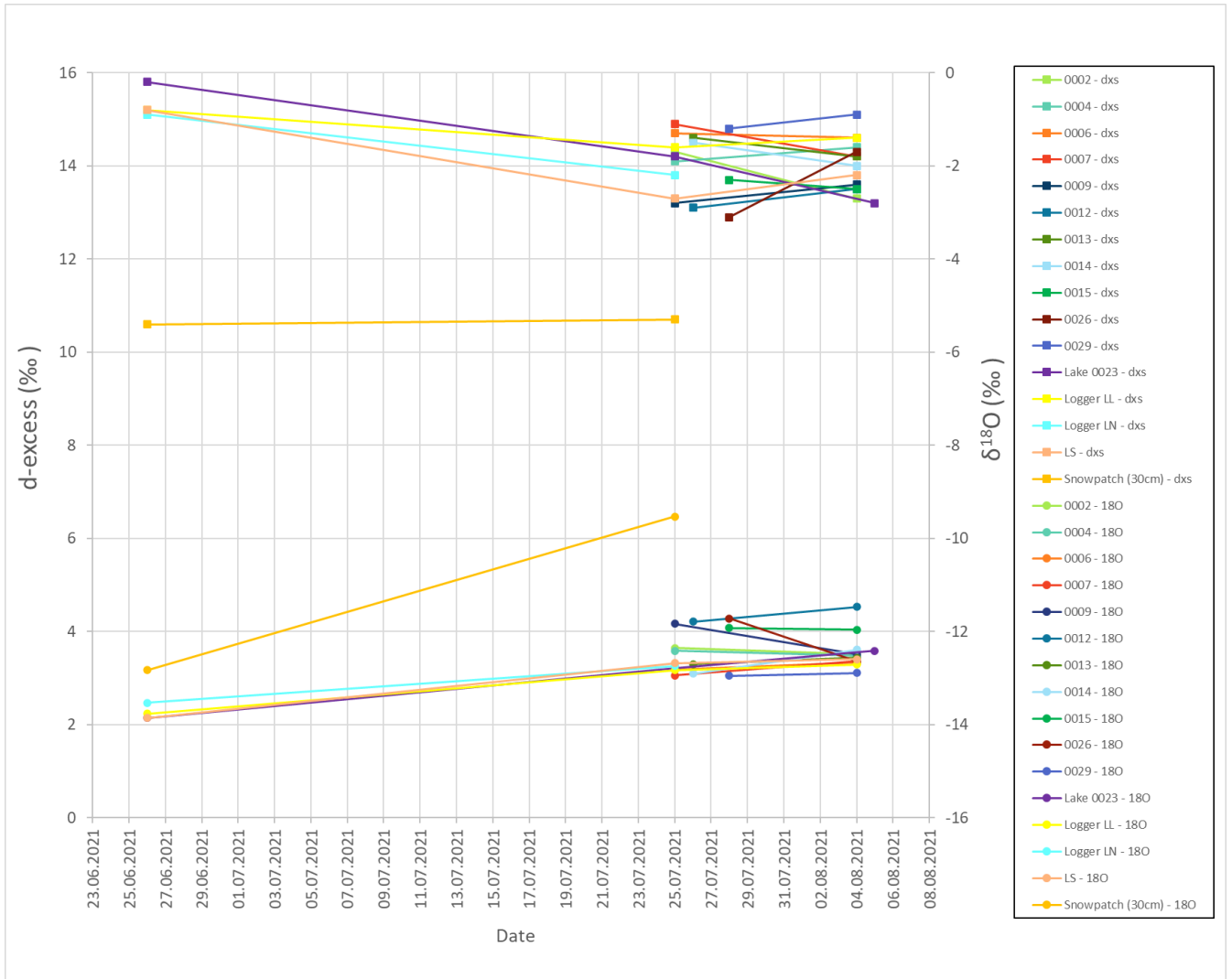
Figure 5.30. Timeseries for samples of δ¹⁸O (circles) and d-excess (squares) in (‰) at 16 different locations, showing the changes in isotopic composition throughout the summer for samples from the lake, the snow patch, and streams.

5.3.7 Summary of hydrological results

Changes in air temperature and incoming solar radiation are the main drivers of fluctuations in lake level and water level of streams, as they affect the melting of ice and snow from the glacier, and surrounding area. Thus, in periods when there are lower air temperatures, the rate of ablation is lower, and the lake level decreases. A twofold season has been identified, where the lake level increases rapidly in the first part of the summer season as the lake is becoming ice free, followed by input of meltwater from surface melt of snow and ice from the glacier, in addition to basal melt, when the air temperature rises. Thus, as the temperature and incoming solar radiation becomes weaker towards the end of the summer season, the lake level decreases.

Stream LS has been identified as the main drainage pathway for the lake, going through a subsurface pathway surfacing in the central eastern section on the distal side of the moraine. Stream LS has a relatively steady outflow, following the fluctuations in lake level with a statistically significant correlation. Hence, the moraine both dams the lake, while at the same time providing a drainage pathway for it through stream LS. The waterflow through the moraine is inefficient using the main drainage pathway, but the residence time seems to change throughout the summer, indicating that there is a barrier which can be breached, as the moraine seems to become more permeable throughout the summer. This is highlighted by the increasing number of streams in the vicinity of stream LS throughout the summer season, making the main hydrological drainage pathway(s) broader. The spatial distribution of temperature and conductivity of streams, in addition to the temporal and spatial development in stable water isotopes during the summer suggest that the northern and southern part of the moraine are not associated with the drainage from the lake, and might still have an ice core producing some meltwater, or that the streams in this area are attributed to the melting of the snow patch around the margin of the moraine which will be further discussed in section 6.2.

5.4   Deformation

5.4.1   Observations in the field

Observations in the field showed several signs of ground subsidence, as portrayed in a few photos on fig.5.31. The terrain on the moraine was in general highly unstable with a mix of all sorts of grain sizes from silty sand to boulders of several meters in diameters. A typical feature observed was the disappearance of finer material between rocks. There were also examples of several meter deep holes going down into the moraine (as can be seen on the top photos of fig. 5.31). No observations of ground ice were observed in any sections of the moraine, nor in the holes. Some snow patches were observed between the ridges at the field visit at the end of June but had disappeared by the next field visit at the end of July. The disappearance of finer materials might be linked to the melting of these snow patches and the finer materials being transported with the meltwater percolating through the moraine and possibly being deposited

Figure 5.31 Field observations of ground subsidence on the moraine. Photos by Sofie Jordheim

lower down in the moraine or being transported out by subsurface waterflow in the moraine. Another possible explanation might be heavy precipitation events in the summer/autumn. The ground subsidence and disappearance of finer materials may also be indications of the former presence of ice, as the melting of ice might create space for the finer material to be transported deeper into the moraine. The field observations indicate that it is an unstable landform undergoing a slow transition of disintegration.

5.4.2   Deformation over time

Fig.5.32 highlights the surface elevation change of the glacier between August 1968 and August 2019. The glacier has thinned and retreated (see fig.3.6 in section 3.3) substantially the last fifty years, with the middle, south-eastern and top section thinning the most. Fig. 5.32 shows that large sections of ice have thinned by 20 - 35 meters. The maximum change in surface elevation at the southern top section of the glacier was estimated to about 41 meters. The mean surface elevation change was 8,97 m.
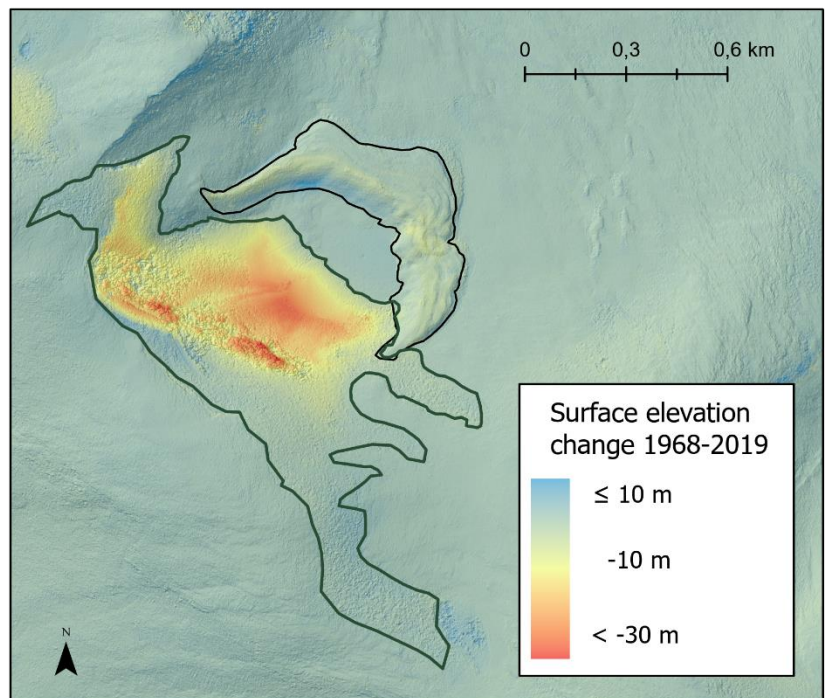
Figure 5.32. Surface elevation change, in meters, from 1968 – 2019 (green outline marks the extent of the glacier in 1968, outline of the moraine in black).

Fig.5.33 shows the estimated surface elevation change on the moraine from August 1968 to August 2019. In general, there has been a negative surface elevation change almost all over the moraine, with a mean change in surface elevation of 2,01 m with the highest rate of change along the proximal ridges and in the central eastern section above the main drainage pathway, with a mean surface elevation change of 5,96 m. The least subsidence is to be found in the north-eastern section of the moraine, where the moraine ridges are the most pronounced. The central section of the moraine, where the main subsurface drainage pathway has been identified

is the area for which the largest lowering of the surface has occurred, with a surface lowering of around 12 meters at the most and a mean surface elevation change of around 6 m. On the highest south-eastern ridges, the decrease of the surface is about 4-7 meters. The surface elevation changes on the ridges most proximal to the lake on the northern section of the moraine might be a combination of surface
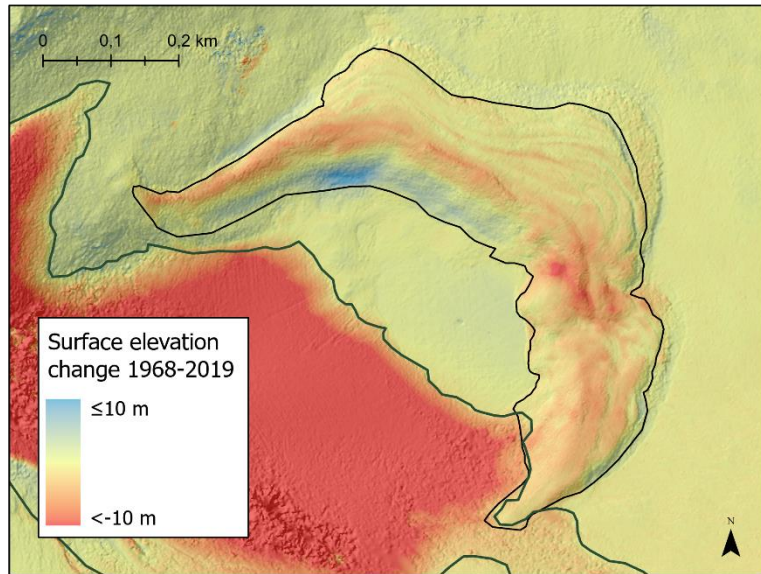
Figure 5.33. Surface elevation change, in meters, from 1968 – 2019, focused on the moraine (outline of the moraine in black, green outline marks the extent of the glacier in 1968).

lowering and mass wasting, as there are areas of accumulation below the ridges with a positive surface elevation change of up to 10 m, seen in blue on fig.5.33. Upon inspection of the aerial imagery from 2019 of which the DEM is based on, the blue areas showing an increase in surface elevation might be due to snow.

For the glacier, the average change in surface elevation per year, based on the outline of the 1968 glacier, was 0,17 m, while mean change exceeded 0,7 m per year in the central section of the glacier (fig. 5.34). The mean surface elevation change per year for the moraine over the last 51 years can be seen on fig.5.35. Mean yearly change for the whole moraine is 0,039 m, and between 0,1 - 0,25 m per year for
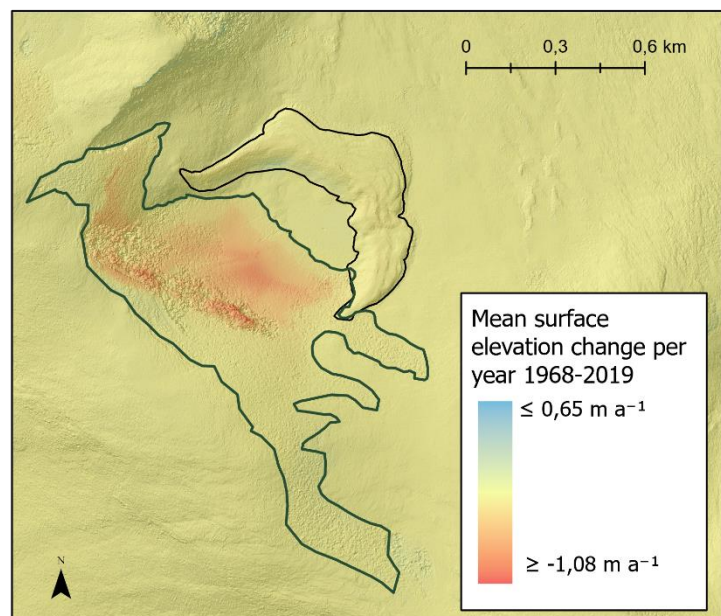
Figure 5.34. Mean surface elevation change of the glacier, per year, in meters, from 1968 – 2019 (glacier extent in 1968 marked by green line, outline of the moraine in black).

the sections of the moraine with the highest rates of change. the central section of the moraine over the main drainage pathway, in addition to the southern ridges and the most proximal moraine ridges. This indicates a rather slow rate of change on the moraine, but it is unlikely that the mean surface elevation change per year has been constant over the last 51 years.
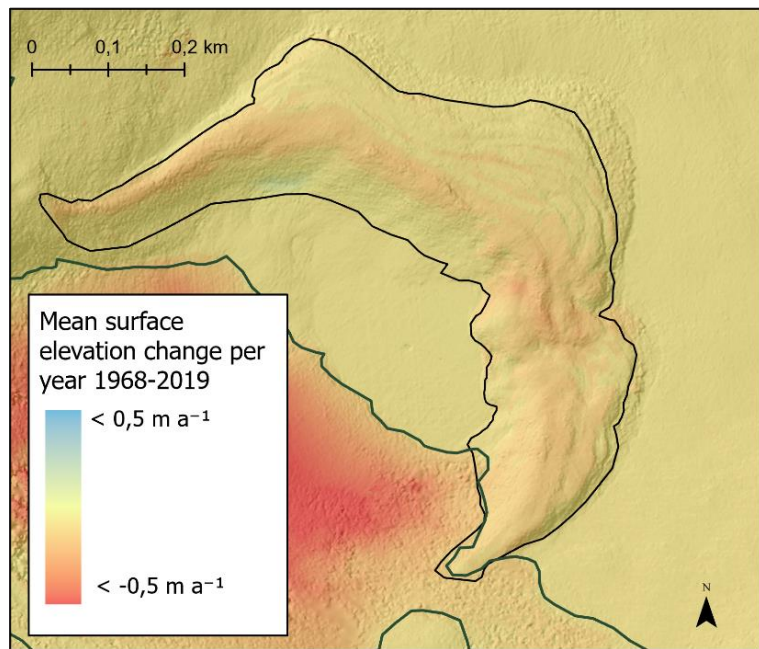
Figure 5.35 Mean surface elevation change per year, focused on the moraine, in meters, from 1968 – 2019 (outline of the moraine in black, green outline marks the extent of the glacier in 1968).

Coupled with the observations in the field of ground subsidence and disappearance of finer materials into the moraine (see fig. 5.31); the results from the estimated surface elevation change from 1968-2019 (fig. 5.33 and 5.35), indicate that at least sections of the moraine have been ice-cored, and it may be inferred that at least the northern section of the moraine might still be partly ice-cored, as the rate of subsistence is significantly smaller than in the other sections. It is worth noting that the results only show total surface elevation change and does not indicate the rate of change over time. Due to the changes in climate over the last fifty years, it is likely that the change has not been linear.

5.4.3 Velocity of displacement in recent years

Looking at InSAR data showing the velocity of deformation from 2015-2020, based on data from ascending and descending Sentinel 1 satellites, there are evidence of significant surface subsidence over the last five years with a mean velocity of – 34,09 mm per year for the chosen point (white circle on the map, red dots in the graph) over the five-year period (fig.5.36). This rate is very similar to the average yearly surface lowering of the moraine since 1968, though it's lower than the average for this specific section (see section 5.4.2). The InSAR data indicates that deformation has occurred on the moraine in recent years and might still occur.
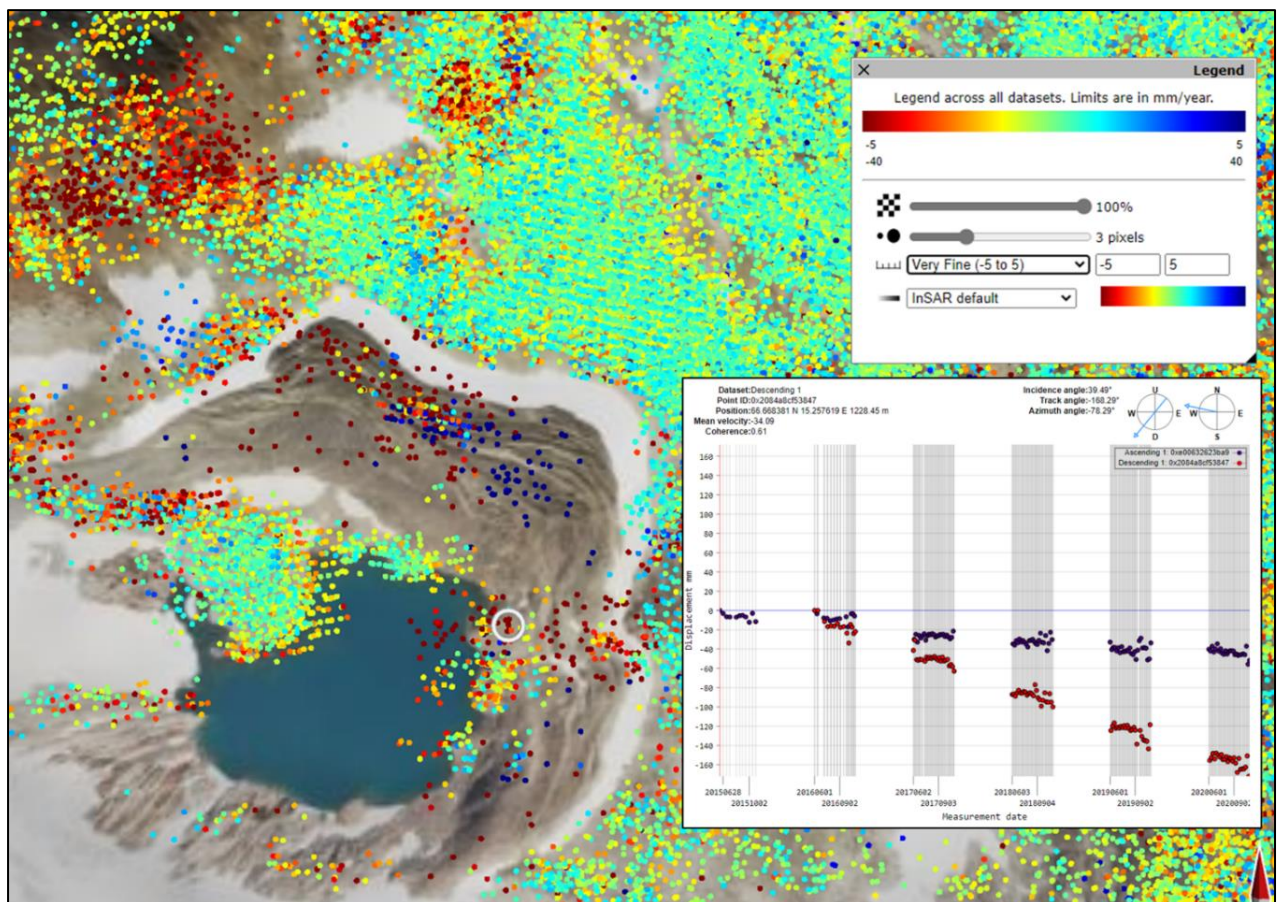
Figure 5.36 InSAR data indicating the displacement of each point in mm, and the mean rate of change of a chosen point in the central section. Source: InSAR Norway (ngu.no) retrieved 24.02.22

5.4.4 Incoming solar radiation

An analysis of incoming solar radiation for the period 01.06.21 – 01.10.21, shows that the southern facing slopes, and in particular the northern proximal flank of the moraine, are subject to the highest rates of incoming solar radiation (see fig. 5.37). Comparing to the areas on fig.5.33, that have undergone the largest changes in surface elevation over the last 51 years, it might be that incoming solar radiation is a contributing factor. The analysis was done in ArcGIS pro, using the Solar radiation toolset on a 1 meter DEM from Høydedata, 2019.
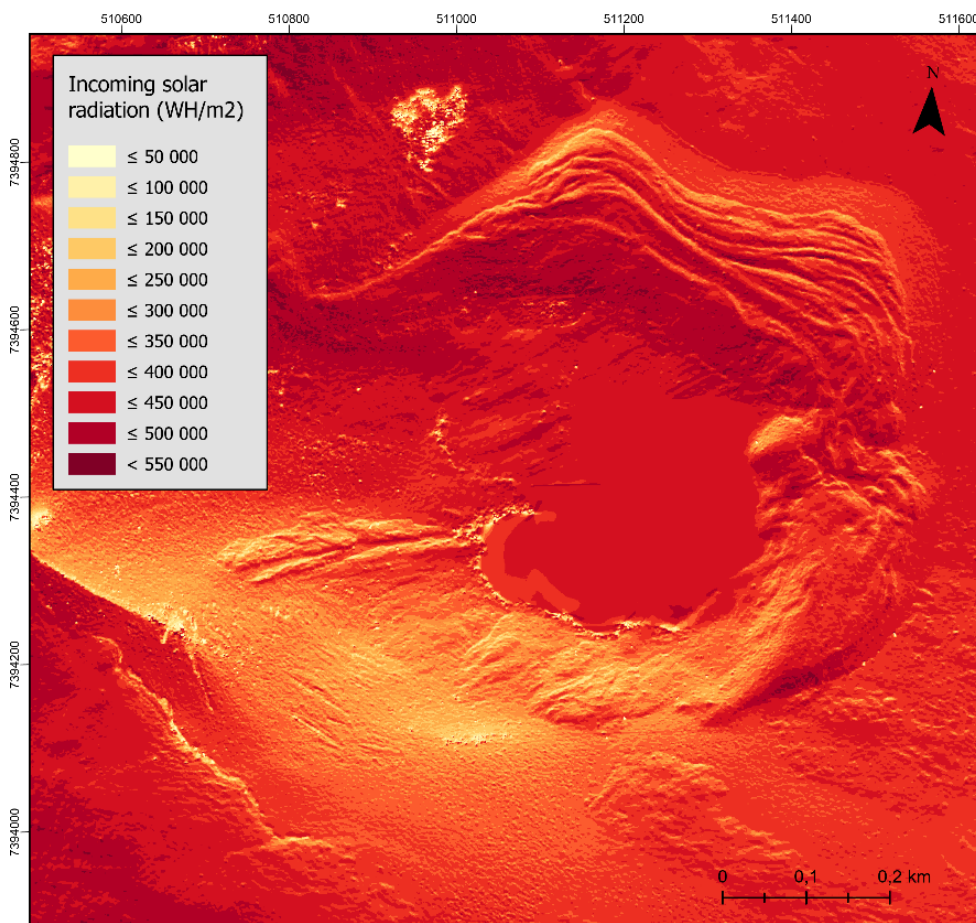
Figure 5.37 Incoming solar radiation (diffuse and direct) from 01.06.21 – 01.10.21 in WH/m². Coordinate system: ETRS 1989 UTM 33N. Calculated based on 1 m DEM from Høydedata. Parameters: Skysize 200, 14 days time interval, 0,5 h time interval for sky sector, 32 azimuth directions for calculating viewshed for the complex topography, 8 zenith divisions for the sky sector in the skymap.

5.5   Age chronology of moraine ridge

The chronology of the moraine ridges on the north-eastern section of the moraine estimated by lichenometric dating on fig 5.38. shows no clear trend when seen all together. However, the most central transect indicate that the proximal ridges are the youngest and that the ridges are becoming progressively older towards the distal side. The oldest estimated lichenometric measurement based on the average of five lichen at each site on the ridges is 1333 AD, while the lichen on the most proximal ridges mostly date from around the 1930s. Giving a deviation of around 600 years between the estimated oldest and youngest ridges in this section. The most central and highest ridges of the north-eastern section mostly date back to the middle of the 18th century.

The measurements performed on the ridges on the southern end of the moraine do not show any clear trend in terms of chronology, but dates range between 1899 and 1953. There are fewer measurements on these ridges in the southern section, as there were fewer clearly observable ridges in this area. The age estimates for the most proximal ridges in the southern section matches fairly well with the estimates from the proximal ridge in the north-eastern section, stemming from around the 1930s.

The standard deviation for each site for lichen measurements ranged from 1,55 to 48,2 cm – depending on the size of lichen thalli found. Furthermore, the standard deviation for each sampling location in years ranged from 5 – 568 years, with an average standard deviation of 88 years for all sampling locations, reflecting the ununiform size distribution of lichen for the various sampling sites.
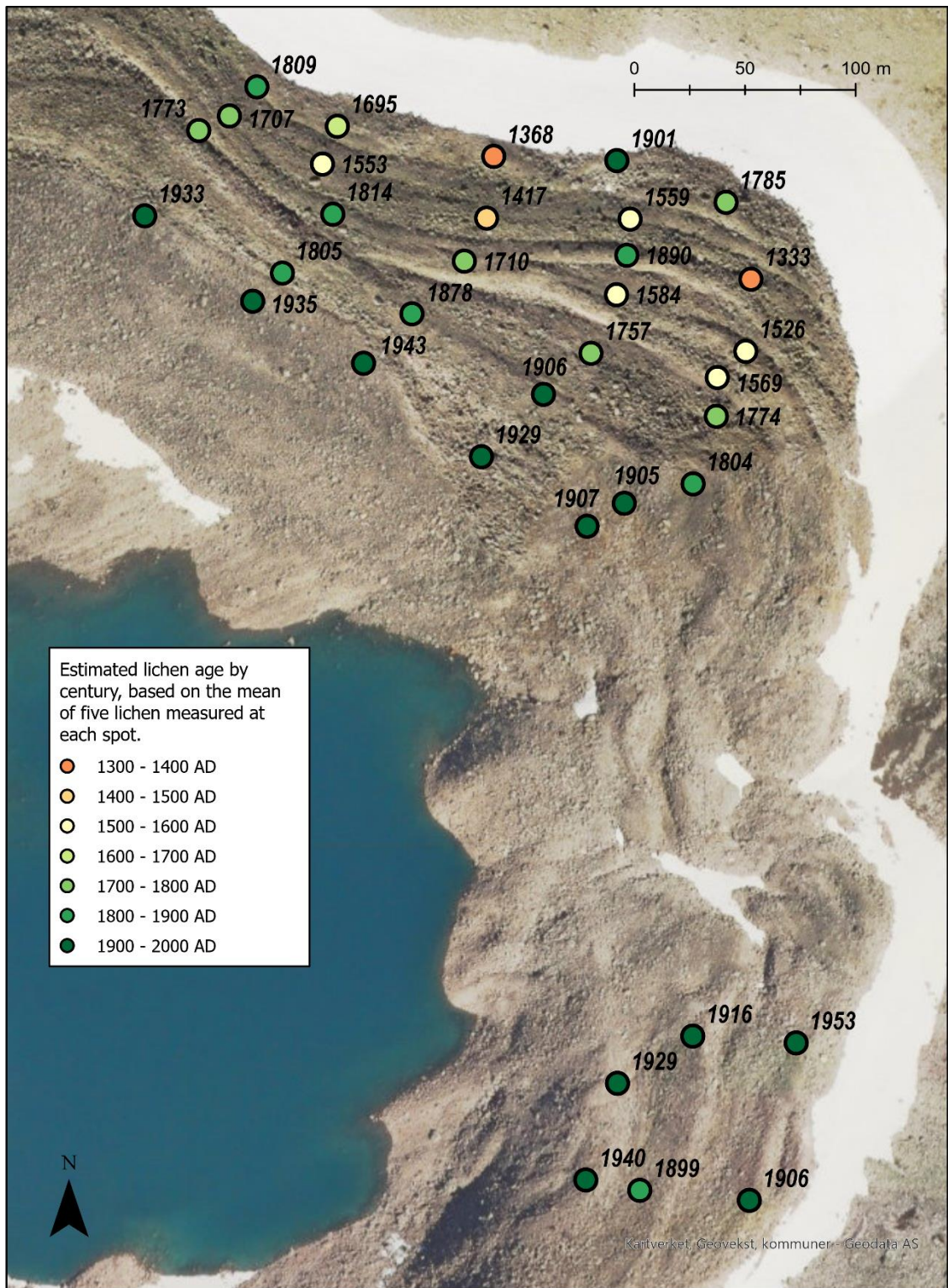
Figure 5.38 Dating of moraine ridges based on the mean size of 5 lichen and date estimates based on an indirect lichenometric dating curve: log (y + 150) = 0.003 3 + 2.2343, by Winkler (2003) for Øvre Beiarnbre (ca. 38 km west).

6 Discussion

6.1 Evaluation of methods and results

6.1.1 Quaternary geological mapping

The terrain in the study area was rather treacherous, which made it challenging to cover the whole area and all parts of the moraine on foot. The geomorphological mapping therefore also relied on remote sensing analysis. Combining these two techniques are favourable for accuracy, though too much reliance on remote sensing might lead to smaller details in the land system being overlooked and certain landforms that look similar might also be harder to identify using remote sensing techniques. The active periglacial processes in the study area might also have altered the signature of glacial landforms, which therefore might make the landform descriptions less accurate, especially for less experienced mappers. More detailed field notes and logs could also have been made for the various sites, though stratigraphic profiles proved to be challenging in the moraine due to the number of large rocks and boulders in the moraine. It is also important to remember that the quaternary mapping is a simplified interpretation of the field area, and thus the full complexity associated with smaller details might not be fully captured in such a representation. Drone surveys using an unmanned aerial vehicle and generation of a digital elevation model of the field area might be a good tool to assist and increase the accuracy of the quaternary mapping of the field site (James *et al.* 2017).

6.1.2 Hydrological investigations

The hydrological investigations provide a one-season snapshot of the hydrological connections in the system, a multiannual study could reveal more about how the system is working and developing from season to season. One season might be significantly different from other seasons, and this study might therefore not allow for an interpretation of long-term fluctuations. The monitoring of water level and temperature of the proglacial lake and streams gave a good indication of the fluctuations throughout the summer. However, the imagery from the time lapse camera was challenging to analyse in terms of lake level fluctuations and positioning the camera by the shore of the lake instead of on top of a ridge could have given a better indication of smaller fluctuations in lake level. A shorter interval

between the times the photos were taken would also have provided a more detailed overview of the lake level fluctuations. Even so, having both the loggers and the time lapse camera proved useful in terms of having a backup if one of the systems failed, though the loggers provided more detailed data than the time lapse camera. The changing flow paths of the smaller streams throughout the summer made it necessary to move the loggers. Even if it led to less of a full season insight into the fluctuations of each stream, it provided insight into the melt dynamics of the perennial snow patch. The placing of the barometric logger under a larger rock, lead to it not being exposed to incoming solar radiation, resulting in a possible underestimation of the air temperature in the study area. This is apparent when looking at the records from stream LN1 which ran dry, and one sees that the temperature recorded by logger LN1 exceeded the temperature recorded by the barometric logger (see fig. 5.20 in section 5.3.3). The analysis of lag time of the logged water temperature of the lake and stream LS was performed by manual identification of break points in the graph. A statistical change point analysis as outlined by for example Irvine-Fynn *et al.* (2005), based on moving averages and cross-correlation for a 24h period, might give a more reliable identification of break points in the graph than the manual interpretation.

The methodology of the in-situ sampling of water temperature and conductivity for all the streams along the margin of the lake has some flaws in terms of reproductivity of the study, as the number of streams along the margin of the moraine fluctuated during the summer. This led to some streams being sampled several times, while other streams were only sampled once. The timing of the sampling did not happen at the same time of the day and diurnal variations might therefore have affected the results (Taylor *et al.* 2001). A time series of the seasonal evolution might also have provided a more accurate depiction of the data than averaging the samples. Daily sampling, or sampling at a set day-interval, and at the same time of the day, could have been better for making a time series of the evolution of the streams throughout the summer and for comparing results from the various streams.

A drawback of the methodology for the sampling of stable water isotopes was the limited amount of snow samples from different times of the season, in addition to no samples of glacier ice or precipitation. No samples of glacier ice were taken, as the risk of sampling seemed too high. Precipitation samples would have been needed to construct a local meteoric

water line (LMWL). Sampling was carried out at various times of the day, but for comparisons of the seasonal fluctuations it would have been better to sample at the same time of the day (e.g. Penna *et al.* 2017). Theakstone (2003) highlights that the values of $\delta^{18}O$ within and between precipitation events may cause deviations of $\delta^{18}O$ values compared to the more regular pattern of stream values, and as samples were generally collected during no-rain periods, the contribution of precipitation to the isotopic composition and electrical conductivity was probably underestimated.

The monitoring of water level and water temperature, in addition to the in-situ measurements of water temperature and electrical conductivity was a cheap and efficient methodology which gave a snapshot of spatial and temporal variations of the lake and streams in the field site. Measurements of conductivity and water temperature might be favourable for provenance studies in smaller catchments that are dominated by snowmelt, as it is a cheap and efficient way of sampling. The method gave similar results to the stable water isotopes, which is a more costly alternative. Combining this with analysis of other trace elements might be favourable (e.g. Theakstone, 2003).

In general, the hydrological measurements could only infer the subsurface environment of the streams surfacing on the distal side of the moraine. As the melting of the snow patch is likely to be faster than the melting of ice in the moraine, a possible signal from melting of ice inside the moraine might be diluted by the amount of meltwater from the snow patch. An alternative method would be to measure discharge and suspended sediment concentrations of the streams, in addition to water sampling for analysis of various trace elements. This might give a better indication of the differences between the various streams. A principal component analysis of the various trace elements could further assist with this (see for example Irvine-Fynn *et al.* 2005). Ground penetrating radar (GPR) and electrical resistivity imaging (ERI) could also be performed to gain insight into the internal structure of ice-cored moraine (see for example Langston *et al.* 2011).

6.1.3   Photogrammetry for studying deformation over time

Photogrammetry is a relatively easy to use, cheap and fast way of gaining valuable data of changes in surface elevation over time. Sources of error in the analysis of surface elevation change from photogrammetry is often associated with the quality of the images used. Old scanned optical aerial imagery might have speckles of dust etc. which may distort the quality of the image, and the general photo quality will in addition influence how well tie points might be identified and generated between the images. The quality of the imagery from 1968 was high, which is also reflected in how good of a fit the co-registration between the generated models was. Fig. 6.1 shows how well the two DEMs used to calculate the surface elevation change aligned before and after running a linear and polynomial tilt correction. The results on fig. 6.1 gives a median accuracy of -0,02 m after running the co-registration, and -0,01 m in incremental difference for Z. Whilst other studies have found more severe linear biases (e.g. Xue *et al.* 2016), there did not seem to be any severe tilt distortions. The delineation of the manually generated shapefile for unstable terrain is another source of error, as areas regarded as "stable terrain" might not be so stable due to the active periglacial processes in the area. Differences in snow cover in 1968 and 2019 are also picked up as differences in surface elevation and might lead to an overestimation of surface elevation change in certain areas.
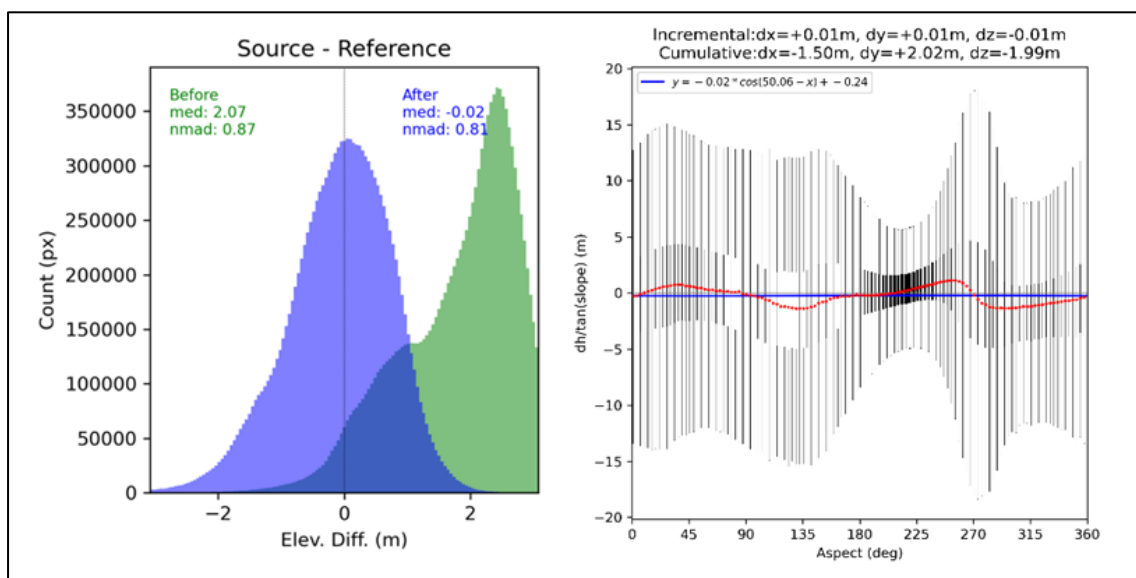
Figure 6.1. Results from the co-registration of the two DEMs, after running the linear correction and polynomial tilt correction based on "stable areas" in both DEMs.

The results of the surface elevation change from the DEM comparison from 1968 and 2019 display total surface elevation change. Due to the changes in climate over the last fifty years,

however, the mean rate of change over time may not have been constant during this period (Hock *et al.* 2019). To further improve the analysis, multi-temporal aerial imagery comparing shorter time frames may be acquired and used to construct DEMs for detecting and quantifying short term changes.

Ideally it would have been better to have comparisons of surface elevation change over shorter, and more than one time timeframe, to better estimate how the rate of change varies over time to see how it links with fluctuations in climate. Not having physical ground control points (GCPs) in the field site to georeference DEMs for newer aerial imagery posed a challenge when attempting to generate georeferenced DEMs for more recent years using AgisoftMetashape. Manually setting out GCPs in the field and recording the positions with a differential GNSS is needed to make comparisons between various time frames (Smith *et al.* 2016) and quantify the melting of the ice-cored moraine under different climate conditions. Repeated yearly drone surveys would be good to monitor the small-scale changes from year to year over smaller scales (see for example Tonkin *et al.* 2016; James *et al.* 2017).

6.1.4   InSAR for studying small scale changes over shorter time frames

This study shows that there is potential in InSAR technology for detecting small scale change for shorter time scales in periglacial environments. However, due to the acquisition geometry and near polar orbit of the Sentinel satellite, no reliable results may be achieved in terms of deformation in the north-south direction (along track), as they do not contribute to the measured LOS displacement component (Manzo *et al.* 2006). The topography, atmospheric effects, presence of snow and too rapid deformations in the area are sources of error which might influence the results. Shadowing or layover effects from steep mountain sides is another limitation associated with the geometry of the orbit and may make an area appear with no data. The results in the InSAR Norway map are based on a method which makes use of identifying coherence between small and clear ground points, such as bedrock. Thus, if the same point is not possible to detect in multiple image pairs, no data will be shown in the data, or the estimation is faulty. This might be because of too large changes in the surface or changes in the surface cover by for example snow or snowmelt. Similarly, in areas with displacement over 100 mm/year, or at non-linear velocities due to seasonal changes, it will not be registered (NGU, 2022, 25. February). The imagery from InSAR Norway is covering

the period from May to October for 2015-2020. The snow cover lasted for a long time into 2020, and this may have reduced the reliability of the results. The steep topography and possibility of rapid mass movement on the moraine adds to this uncertainty. This is emphasized by looking at the scarce distribution of points on the moraine. In addition, as the neighbouring points are displaying opposing values on the moraine, the results may be less reliable and should be interpreted with care (see fig. 5.36 in section 5.4.3).

6.1.5   Lichenometry

The results of the lichenometric dating based on *Rhizocarpon geographicum* did not give any clear indications of the chronology of the moraine ridges. The estimates for the most proximal moraine ridge seem fairly precise and may be regarded as a minimum age for when the glacier last had this extent. Lichenometry is generally vulnerable to sampling errors, and to get the most accurate information, Bickerton and Matthews (1992) highlight that it is important to identify the largest lichens at the site. As observations were used to establish the five largest lichens in each of the sites in the transects, it may have been prone to sampling error. The large standard deviation of the measured lichens might be a reflection of this. It may be debated if dating based on the "single largest lichen" or "mean of five lichen" approach is the most accurate. Bickerton & Matthews (1992) points out that the first approach is more prone to inaccuracy in measurements, while the latter approach might lead to an underestimation of the age of the lichen (*cf.* date estimates based on the approach of the "single largest lichen" might be found in the appendices, fig. A9 for comparison). In addition, the unstable and unclear terrain of the moraine opened for the possibility of rocks and boulders to have changed position over time. This implies that larger lichens might be hiding on non-visible sides of boulders and is a factor of uncertainty for the exposure time of the spotted lichens. Another source of error associated with sampling is amalgamated thalli. Two, or more lichens may be identified as one, or a lichen with a less circular shape is disregarded. In both cases, this may lead to inaccurate results when attempting to identify the largest lichen (Armstrong, 2014). Long laying snow cover on different parts of the moraine, which there were several indications of in the field, is another factor of uncertainty. Snowbanks that do not melt during the growth season may inhibit lichen growth, and the lichen size might thus not give an accurate estimate for age (Koerner, 1980; Benedict, 1993).

It is recommended to map lichen on the proximal side of a moraine ridge (Bickerton and Matthews, 1992), but due to the unclear terrain and the presence of long laying snowbanks on and/or between the moraine ridges the approach of this study was to sample in sections covering the top and/or on the proximal side of the ridges. Furthermore, the methodological approach of doing transects across the ridges was influenced by the fact that it was hard to distinguish the various moraine ridges from each other when in the field as the ridges would merge into each other at various points. A better approach would be to walk along each moraine ridge, as each line then would be representative of that ridge.

Various environmental and biological factors connected to lichen growth adds to the uncertainty associated with this dating method. There are some aspects of lichen growth which there are limited information of, especially regarding the early stages of lichen growth. This includes lag time between when an area became ice free and lichen colonisation, the issue of small lichen thalli merging at an early stage and lichen mortality at an early stage of the colonisation (Loso and Doak, 2006). Uncertainty is also connected to how climatic factors influence lichen growth over time and thus the shape of the growth-curve. Lichen growth tend to slow down and become fairly constant at older age, and climatic conditions also influence the growth rate. Higher elevations, cold and dry conditions and a shorter growing season may lead to a slower growth rate (Bradley, 2014; p. 117). As the climate in Norway has become warmer and wetter (Hock *et al.* 2019) since Winkler (2003) developed a regional lichenometric growth curve, one might infer that the growth rate of the lichen might have increased in this period. In addition, possible local climatic variations between my study area and the site for which the lichenometric dating curve was established by Winkler (2003), with for example higher annual precipitation 2000 - 4000 mm (see fig. 3.3 in section 3.2), the transferability of this lichenometric dating curve for this study site may be less precise. Despite these setbacks and inaccuracies, lichenometry can still be considered an easy, cheap and relatively accurate method for dating surfaces. In Arctic and Alpine environments, surfaces, and deposits up to thousands of years old may be dated, but it is regarded as most useful for dating going back around 500 years. Thus, covering a period which is less accurate with for example radiocarbon dating (Armstrong, 2014). Hence, the dating of the smaller lichen going back less than 500 years might be deemed more precise than the older ones. Additional dating methods and dating outside the main ridge are encouraged for comparison.

6.2   Discussion of results

The results of the lichenometric dating of the moraine ridges will be discussed and considered in association with the timing of formation of the ice-cored moraine and proglacial lake and its possible link to the amelioration of the climate at the beginning of the 20th century. The discussion then moves on to the present, first discussing what the hydrological investigation of this study may reveal about the spatial distribution, origin and subsurface environment of the streams running along the margin of the moraine. Then, the role of the internal structure of the ice-cored moraine and impacts of seasonal fluctuations in water temperature and lake level for controlling lake drainage will be discussed. Thereafter, the role of hydrology for the deterioration of the moraine and further development of the ice-cored moraine in a changing climate will be evaluated. Finally, a conceptual model for the life cycle of this ice-cored moraine system will be presented.

6.2.1   Age estimates for the formation of the ice-cored moraine and timing of the development of the proglacial lake in relation to climate fluctuations

Lichenometric dating was performed to date the moraine system to better inform the processes of formation in relation to the climate at the time. The results of the lichenometric dating of the moraine ridges displayed large variations in lichen size, but no clear conclusions may be drawn in terms of the age, nor of the age chronology of the moraine ridges (see fig.5.38 in section 5.5). However, the lichenometric dating of the highest and most central ridges of the northern section of the moraine points to this possibly being a Little Ice Age moraine, dating back to the 18th and 19th century, which coincides with other studies estimating the Little Ice Age glacier maximum around Svartisen to around the middle of the 18th century (see for example Winkler, 2003; Jansen *et al.* 2018). A few larger lichens, dating back to the 14th century were also found (see fig. 5.38 in section 5.5), which might suggest that the moraine has an older origin.

The age of the ridge most proximal to the lake had the least variance in the age estimates, dating back to 1931 if considering the mean age of the ridge (see section 5.5). In northern Norway, a temperature rise of ~1°C was recorded between 1910 and 1930 (Nordli, 2009 in Theakstone, 2013), and the temperatures were noted to be especially high in the 1930s

(Theakstone, 1990). This coincides with the early 20th century warming of the Arctic, which started in the 1920s and peaked around the 1930 – 1940s. This amelioration of the climate has been associated with strong westerly winds between northern Norway and Svalbard, influencing the extent of the sea ice (Bengtsson *et al.* 2004). In addition, a sharp decline in snow depths were recorded for the 1920s, which can be associated with a weak winter North Atlantic Oscillation (NAO) (Theakstone, 2013). It may thus be deduced that the winter accumulation on the glacier was low in the period preceding the increased warming, and it is likely that the glacier experienced an increased rate of ablation at the beginning of the 20th century, and then possibly a sharp decline in mass balance from the 1930s. The increases in air temperature at the beginning of the 20th century, in addition to the damming of the meltwater by the moraine may thus have contributed to a change in the thermal regime of the glacier, from polythermal to temperate.

6.2.2 Spatial distribution and source of streams

The hydrological investigations carried out during the summer of 2021 showed that multiple surface streams emerged on the distal side of the moraine in the summer season, with most streams emerging along the northern and central-eastern section of the moraine, forming a braided network of streams. The results from the hydrological investigations may only infer the origin and environment of the flow path of these streams. When it comes to the origin of these streams, no surface outlets were identified from the lake, and no inlets were identified on the surface of the moraine. The sources of the streams are stipulated to either be water coming from the subsurface drainage of the lake, ice melting from an ice core, thawing of ground ice, surface and subsurface melt of the snow patch along the margin of the moraine, water from infiltrating of precipitation or melting of snow accumulated on top of the moraine.

The hydrological investigations revealed one main subsurface drainage pathway from the lake, stream LS, which surfaces on the distal side of the central section of the moraine (see fig. 4.3 in section 4.2.1). This stream was identified as the main drainage pathway as the water level, temperature fluctuations, electrical conductivities, and isotopic composition of the water in the lake and this stream had a high correlation throughout the summer season (see section 5.3). The outflow of stream LS was also present the whole summer, and as the snow patch retreated in this section throughout the summer, it became evident that the

outflow was a subsurface pathway from the lake going through the moraine. Stream LS had the highest water level and discharge of the streams emerging on the distal side of the moraine, adding weight to the interpretation of this stream being the main drainage pathway. The slope of the terrain around the ice-cored moraine also contribute to a natural gravity driven drainage of the lake towards the central section of the moraine (see fig.5.10 and 5.11 in section 5.2). This stream may also be identified on aerial imagery running back to 1968 (see fig. 3.6 in section 3.3), showcasing that it is a well-established drainage pathway.

Considering the drainage pathway of stream LS through the ice-cored moraine, the water flow is not efficient enough to be channelised (see section 5.3.4), through an old englacial meltwater channel, like Moorman (2005) identified in an ice-cored moraine at Stagnation Glacier, Bylot Island, Canada. In this site, old meltwater channels had remained linked to the glacier system and still served as pathways for water transport during the summer. It is possible that such channels existed at an earlier stage at Semskfjellet. However, the downwasting of the ice-cored moraine are likely to have led to collapses, and that the channels have thus been blocked by overlaying morainic material with time (c.f. Moorman, 2005; Krüger & Kjær, 2000; Gulley *et al.* 2009). A broadening of the flow path of the main drainage pathway was also observed throughout the summer, with several new streams emerging. The composition of mean temperature and electrical conductivity of these streams (fig.5.23 in section 5.3.5), in addition to the isotopic composition of the streams at the beginning of August (fig. 5.29 in 5.3.6), further suggests that the shape of the main underground flow path(s) for drainage is not channelised.

An abundance of other streams also surfaced along the margin of the ice-cored moraine as the summer progressed (see section 5.3). Looking at the spatial differences in water temperature and electrical conductivity of the streams (fig. 5.23 in section 5.3.5), the streams on the northern side of the moraine have very low water temperatures and electrical conductivities, which might reflect melting of the snow patch. The streams in the north-eastern section also have lower water temperatures, but considerably higher electrical conductivities (fig. 5.23 in section 5.3.5). There were also pro-nival ridges emerging in this section towards the end of the summer as the snow patch retreated (see fig.5.5 in section 5.1.2). Finer sediments in the pro-nival ridges might have contributed to a higher number of solutes mixing with the snowmelt in this area. The logging of water temperature for the second half of the summer

showed very consistent results in terms of water temperature of stream 005 and LN2 (see fig. 5.21 in section 5.3.3), even if the water level fluctuated (see fig.5.19 in section 5.3.2). It is particularly interesting to see how stable the low temperature of 005 is. This might be attributed to the logger recording the water temperature being placed closer to the moraine and in a deeper hole, thus being less affected by incoming solar radiation, compared to the position of the logger in stream LN2. The very stable temperature could possibly be an indicator of the source of the stream being from the ice core melting inside the moraine, or from the melting of the snow patch. However, as the water level of stream 005 fluctuate in accordance with changes in the air temperature (see fig. 5.19 in section 5.3.2), it may be more likely to be attributed to snow melt. It is still worth noting that the electrical conductivity measured in the north-eastern section of the moraine is considerably higher than for the other streams along the margin of the moraine (see section 5.3.5). This could possibly be associated with the origin of the meltwater being deeper inside the moraine, or that fine-grained sediments exist in and/or beneath the snow patch in this area. In general, the high incoming solar radiation in the summer leads to a quicker melting of the snow patch compared to the ice core which is insulated by the debris cover (Østrem, 1959). Thus, the amount of water coming from the melting of an ice core will probably be quite small compared to the amount of meltwater from the snow patch. Hence, the signal from the melting of the ice core is thus likely to be overshadowed by the signal from the melting of the snow patch. The presence of the snowbank running along the margin of the moraine thus makes it difficult to distinguish between various sources of origin for the streams not associated with the main drainage of the lake.

In general, the electrical conductivity was very low for the streams in this catchment. Other studies from northern, central and western Norway have shown comparably low values of electrical conductivity (e.g. Theakstone & Knudsen, 1989; Beylich & Laute, 2012; Miesen, 2019). This could be explained by a lack of mineralisation at the base of the glacier due to the high melt rates, and that the sampling occurred under periods of high discharge (Etzelmüller & Hagen, 2005; Beylich & Laute, 2012), or possibly due to the high input of meltwater from the snow patch. It might also be an indication of the water not having a long residence time in the moraine.

The spatial and temporal variations in the stable water isotopes of the snowpack and meltwater may be associated with seasonal dynamics of isotope fractionation. The snowpack became more enriched in ^{18}O throughout the ablation season. A slight trend of the meltwater becoming isotopically heavier was also observed from June to July, but this trend was not observed for all of the water samples from July to August (see section 5.3.6). Similar studies (c.f. Theakstone & Knudsen, 1996; Theakstone, 2003; Yde *et al.* 2016; Penna *et al.* 2017; Zuecco *et al.* 2019), have also found trends of glacier ice, snowpacks and associated meltwater becoming isotopically enriched during the ablation season. However, variability also occurs for the meltwater in all studies mentioned above. The spatial and temporal variations might reflect seasonal melting of various layers of the glacier ice and snowpack (Taylor *et al.* 2001). Other factors causing the variability of results might be due to diurnal variations at the time of sampling, differential melting rates for various sections of the snow patch, mixing with other water sources or precipitation events (Taylor *et al.* 2001; Theakstone, 2003; Yde & Knudsen, 2004; Zuecco *et al.* 2019). Comparing these samples to those of Theakstone & Knudsen (1996) from Austre Okstindbreen, northern Norway, the range of the δ^{18}O were smaller, but displayed similar values to the meltwater of snow and ice. The isotopic composition of the samples collected at this field site were generally isotopically lighter than samples from similar studies further south, for example in the Italian Alps (Penna *et al.* 2014). This is to be expected considering that isotopes in precipitation becomes lighter towards the poles and with increasing continentality and altitude (Dansgaard, 1964). Penna *et al.* (2014) traced stable water isotopes and electrical conductivity of run-off sources and seasonal variations in the Italian Alps. In their study from 2011 – 2013, snowmelt dominated in the late spring, a mix of melt from snow and glacial ice during the summer, and glacial melt during the fall. A similar pattern of the melting of snow and glacier ice could possibly be linked to the variations seen at Semskfjellet too.

6.2.3 The influence of the internal structure of the moraine on lake drainage, related to thresholds associated with fluctuations in temperature and lake level

The internal structure of the moraine influences the ability of the moraine to work as a barrier damming the proglacial lake. The fluctuations in the water level of the proglacial lake (see section 5.3.2), indicate that there is a threshold associated with the internal structure of the moraine and the environment of the subsurface drainage pathways. The threshold connected

to the internal structure of the moraine may be associated with a core of buried glacier ice and/or ground ice, densely packed glacial till, bedrock, or a combination of the above. For a threshold of densely packed glacial till or bedrock, increases in the water level may breach the threshold, while a threshold associated with an ice core and/or ground ice is connected to the temperature of the lake and the ground, in addition to water level. Increases in air temperature, and to some extent precipitation, are the main drivers for breaching any of these thresholds, as they are determining for increases in lake level by influencing the rate of glacial ablation and/or increases in water temperature. If the internal structure is associated with ice, the ground temperature of the moraine and factors affecting this also plays an important role, as it influences the depth of the active layer (Frey & McClelland, 2009; Langston *et al.* 2011; Miesen, 2019). Figure 6.2 indicate how the different types of thresholds may be influenced by increases in water level and water temperature.

Figure 6.2 a) shows how the subsurface flow path for lake drainage might work with a threshold consisting of a core of buried glacier ice. The ice core is an impermeable layer at the beginning of the season, which the water cannot run through. If the lake level is high enough, the water may still find its way through established drainage pathways above the ice core in unsaturated finer sediments, or in the pore space between larger rocks. Rising air temperatures, high rates of incoming solar radiation, and precipitation events may contribute to melting of the ice core. However, as the thick debris layer and influence of Balch ventilation (Thompson, 1962), in addition to the seasonal snow cover on the moraine, have an insulating effect on the ice core, the influence of incoming solar radiation for melting the ice core might be limited. The effect of increases in lake level and the water temperature of the lake are therefore important for warming the ground and contribute to melting of the ice core. When the water temperature and lake level increases, the water warms up the ground of the moraine, instigating top melt of the ice core, having the water flow on top of the ice core. This further enhances melting of the ice core, leading to a lowering throughout the season. Increases in lake level, due to increases in ablation of the glacier and seasonal snow melt, also leads to an increase in the hydrostatic pressure. This, in combination with the increasing water temperature of the lake might assist with opening old fractures/channels in the buried glacier ice, making a flow path through the ice. This might either be existing flow paths, or new drainage pathways (Moorman, 2005). As the water melts the ice, it may lead to a redistribution of overlaying rocks and sediments, which can then block the waterflow, leading the water to other and more permeable sections of the

moraine. The pathways associated with the ice core, refreezes in the winter when the temperature drops, and may be opened again when the temperature rises (Williams & Smith, 1989; Waller *et al.* 2012). Hence, these pathways reflect a cyclical drainage pattern associated with seasonality (Bowling et al. 2000; Miesen, 2019). Moreover, this threshold is likely to exist in combination with permafrost dynamics, where the dept of the active layer also influences the spatial and temporal extent of the threshold.

Figure 6.2 b) portrays how the presence of ground ice inhibits the water from percolating through the moraine early in the season, because of an ice-saturated frozen active layer. When the air temperature increases, the thickness of the active layer may also increase, and the ground ice thaws, increasing the permeability of the sediments. Similarly, to the scenario described for figure 6.2 a, atmospheric processes with rising air temperatures, strong incoming solar radiation and precipitation events contributes to the thawing of ground ice. The insulating effects from the debris cover, Balch ventilation (Thompson, 1962), and seasonal snow cover on the moraine influences to what extent changes in the air temperature and incoming solar radiation affects the thawing of ground ice. Hence, increases in lake level and water temperature are regarded as important for warming the ground, and in particular for the deeper sections of the moraine. An increase in water temperature thus contributes to thawing of ground ice, making the frost saturated finer grained sediments more permeable, and contributes to melting of interstitial ground ice in the larger pore spaces between the rocks. The depth of the active layer will still be determining for the waterflow, and the water will most likely flow on top of the active layer (Pecher, 1994; Cooper *et al*. 2011). As the water melts the ice below the sediments, it may lead to a redistribution of overlaying rocks and sediments, which can then block the waterflow, leading the water to other and more permeable sections of the moraine. In addition, when the lake level increases, new flow paths through less dense material might be found. The lake level also increases the hydrostatic pressure which might make it possible to percolate through more dense matrices of ice and sediment. This combination of increasing water level and temperature leads to the water finding new ways through the moraine in the ice, in addition to expanding the existing flow path(s). The subsurface flow routes associated with ground ice close in the winter season when the temperature decreases, and new ground ice is formed. Next summer, these routes may be reopened, or new pathways established as the ice thaws. This depends on the distribution of ground ice (Williams & Smith, 1989; Waller *et al.* 2012). A cyclical drainage

pattern associated with seasonality is thus created (Bowling et al. 2000; Miesen, 2019). This scenario might exist in combination with any of the other outlined thresholds as well.

On figure 6.2 c) an internal structure with a threshold of dense glacial till is displayed. Increases in water level, and associated increase in the hydrostatic pressure is the most important mechanism in this scenario. Here, the increase in water level leads to the water finding new flow paths through the higher sections of the moraine, and the flow path will be established above the dense glacial till in more permeable sections of the moraine. As the hydrostatic pressure increases the water might be able to penetrate and percolate through the denser glacial till.

Figure 6.2 d) shows how a threshold of bedrock within the moraine may be breached by an increasing water level. As the water level rises, it is allowed to flow through the more permeable morainic material, finding ways through the coarser material above the impermeable bedrock. It might be possible that the water also finds a way through old existing fractures in the bedrock (McClymont *et al.* 2011).

The fluctuations in water level throughout the summer makes a threshold of bedrock or dense glacial till less likely. Looking at fig. 5.14 in section 5.3.1, the lake reached its highest water level on 16.07.21, and the lake temperature was ca. 5 °C at this point. The lake also became ice free right before this, and it is likely that most of the seasonal snow on top of the moraine had melted by mid-July. After this point in time, the lake level started to decrease – pointing to a threshold in the moraine being breached, which increased the hydraulic conductivity of the moraine. As the lake level then gradually decreased throughout the latter part of the summer, a threshold of bedrock or dense glacial till seems unlikely as the number of streams on the distal side of the moraine kept increasing even while the lake level was decreasing in the latter part of the summer. However, the matrix of material in the moraine is complex and it is possible that layers of dense glacial till exist as patches, and not as a uniform bottom layer. Thus, it is possible that a patch of dense glacial till might block the waterflow, which fluctuations in lake level may overcome, leading the water to more permeable sections of coarser material.
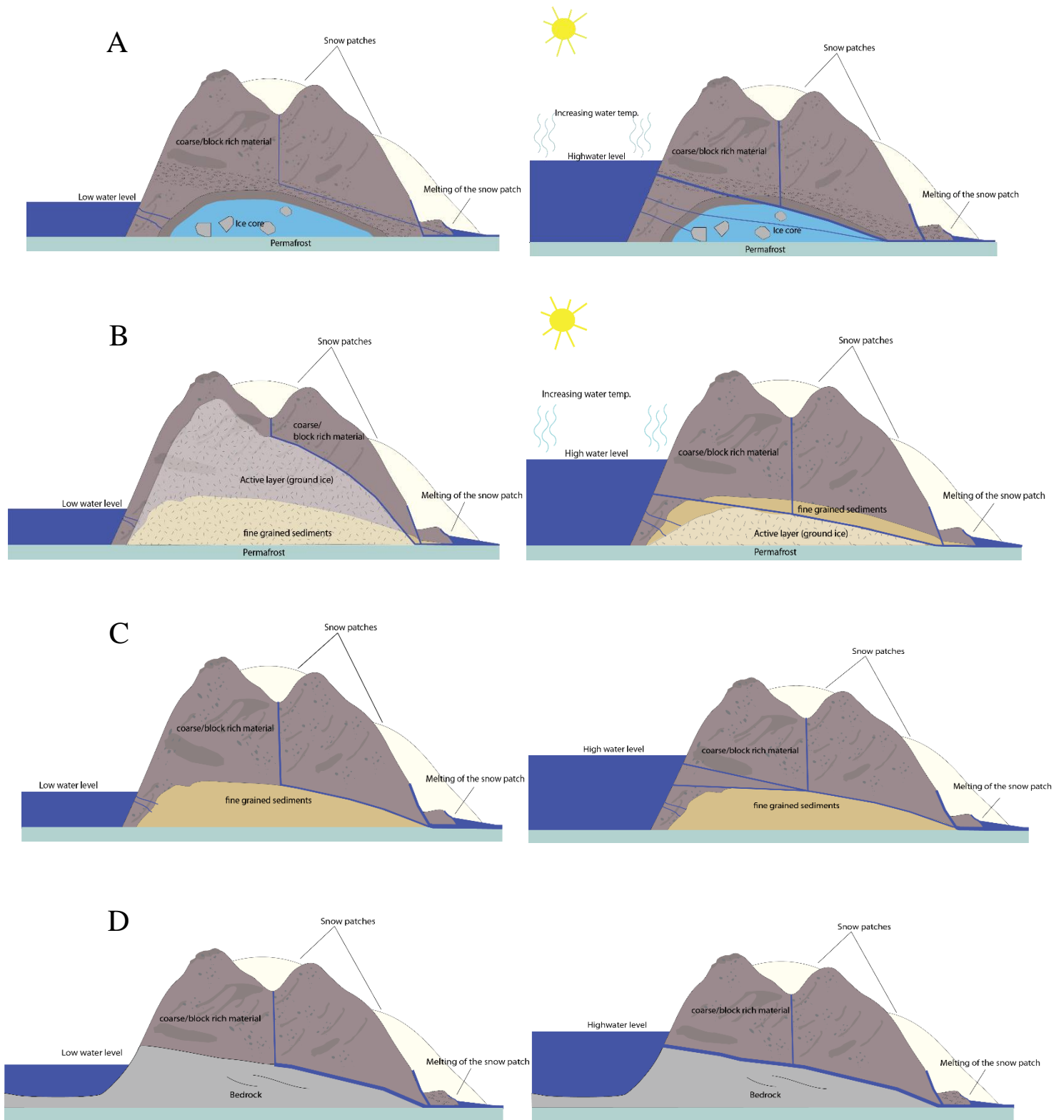
Figure 6.2 Four different scenarios of how the subsurface waterflow may be influenced by increases in water temperature and increases in water level due to increased glacial ablation throughout the summer season. A) Threshold with a core of buried ice, B) Threshold of ground ice, C) Threshold of densely packed fine sediments, D) Threshold of bedrock.

Based on the results of the hydrological investigations and remote sensing analysis (section 5.3 and 5.4), it is likely that the subsurface waterflow is affected by seasonal permafrost dynamics and atmospheric processes controlling the ground temperature of the moraine and the rate of ablation of the glacier. Hence, these factors together with the temperature of the lake are suggested to control the timing of lake drainage. The expansion of the flow path, as outlined in 5.3, with an abundance of new streams surfacing on the distal side of the moraine, might be associated with the increases in lake level and thawing of ground ice and possibly thawing of an ice core (as outlined on fig. 6.2 a and b). This could also lead to the water being able to flow through a higher section of the moraine where the pore spaces between the morainic material may be larger and there is higher interconnectivity between the pores. The field observations also showed that fine grained material had been transported further down into the moraine (see section 5.4.1), where it may be deposited or transported out. It is likely that this is associated with the infiltration of rain, melting of snow on the top of the ridges, or melting of interstitial ice in the moraine.

The water in the main drainage pathway is not moving along an efficient flow path, and the decrease in the time it takes for the water to flow through the moraine might be associated with thawing of ground ice, linked to the changes in lake and air temperature. When the water temperature of the lake reaches a certain level, the water contributes to warming of the ground in the moraine. This leads to melting of ice and thus expansion of existing pathways and opening of new routes for the water to pass through in the moraine. The ice which melts inside the moraine may either be debris covered glacier ice (Kjær & Kruger, 2001; Langston *et al.* 2011), ground ice from the incorporation of snowbank ice (Østrem, 1964; 1971), or it could be perennially frozen ground in the active layer of the permafrost (Williams *et al.* 2006; Miesen, 2021). During the winter season the active layer refreezes, and the pathways are again closed as the air temperature drops (Bowling *et al.* 2000; Miesen, 2021). The decreasing difference in the water temperature of the lake and stream LS throughout the summer (fig. 5.22 in section 5.3.4), interpreted as a change in the residence time of the water running through the moraine (section 5.3.4), indicates that the subsurface environment changes throughout the summer, which is likely to be caused by increased melting of ground ice and/or an ice core. This leads to an expansion of the existing flow path, in addition to the opening of new drainage pathways, and thus reducing the time it takes for the water to flow through the moraine from around one week to a couple of days (as highlighted on fig. 5.22 in

section 5.3.4). At the beginning of the season, there might still be ice present, functioning as a barrier to the water flowing through the moraine. Hence, the discharge is lower at the beginning of the season as the water is flowing slower and there will be less water coming through the system. Interstitial ice content may reduce the connectivity among pore spaces within the moraine, creating a barrier to the flow of subsurface water. Studies of rock glaciers, which resemble ice-cored moraines, have shown that the ice content may range between 40 to 70 % (Haeberli *et al.* 2006; Hausmann *et al.* 2007). The hummocky nature of the terrain over the main drainage pathway may indicate that there are heterogenous melting rates, and possibly blocks of dead ice under the surface, which have an influence on the flow path of the main drainage pathway.

Looking at the temperature profiles of stream LS and the lake at the beginning of the season, (see fig. 5.22 in section 5.3.4), the temperature of the water is getting colder as it flows through the subsurface environment of the moraine. This might be another indication of ice being present along the flow path at the beginning of the season, which might indicate that ground ice is the main factor here. Another possible explanation is that the variation of the water temperature might also stem from the lack of incoming solar radiation in the subsurface pathway. On the other hand, the lowering of the water temperature may also be caused by snow melt from the snow patch laying above and around the outlet of stream LS from the moraine (see fig. 5.16 in section 5.3.2). The temperature of stream LS is occasionally higher than the lake temperature later in the summer. This might be due to the lack of input of meltwater from the snow patch. On the other hand, the water temperature of stream LS might just seem higher due to the associated lag time of the water travelling through the moraine. Thus, the presence of an ice core in the subsurface environment of the main drainage pathway is still uncertain, but a cyclical seasonal pattern associated with the seasonal dynamics of the active layer being thawed by the lake seems to be present.

In comparison, Langston *et al.* (2011) studied a partially ice-cored moraine in the Lake O'Hara watershed in the Canadian Rockies. The internal structure of the moraine was found to have a strong influence of the flow and storage of water, reflected by different degrees of hydrological connections between the lake and tarns (ponds) on the surface of the moraine. Langstone *et al.* (2011) found that the lake level and several of the ponds on the moraine responded differently

to precipitation, snowmelt, and glacier melt, and that these features and the groundwater flow in the moraine thus had different degrees of hydrological connections. The location and geometry of the buried ice, and the bedrock topography were identified as factors influencing the hydrological connectivity in the moraine. Surveys with ground penetrating radar (GPR) and electrical resistivity imaging (ERI) showed that regions of perched groundwater and focused infiltration seemingly were controlled by buried ice. Furthermore, a relatively thin layer (<5 m) of saturated sediments and/or fractured bedrock were thought to supply a big flow system in the moraine. The distribution and extent of ice, and variations in the compaction and grain sizes of till are believed to play a similar role in the ice-cored moraine system of Semskfjellet.

6.2.4 The role of hydrology for the decay of the ice-cored moraine and further development of the land system

6.2.4.1 The role of hydrological processes in the decay of the ice-cored moraine

The decay of the moraine appears to be spatially and temporally heterogenous, with the section underlain by the main drainage pathways having the largest rates of subsidence (see section 5.4). Hydrological processes, with external input of water plays an important role in controlling the rate of melting in the ice-cored moraine. Water draining from the lake, snowmelt from seasonal and perennial snow patches and precipitation events in the summer play an important role in controlling the rate of melting in the ice-cored moraine. However, other topography specific effects may also be influential.

The main subsurface drainage pathway seems to play a very important role in the decay of the moraine in this area. Looking at deformation over time, the analysis of changes in surface elevation between 1968 and 2019 shows that the surface has lowered up to around 12 meters in this area, and with an average lowering for this section of around 6 meters (see fig. 5.32 in section 5.4.2). Fig 6.3. highlights the delineation of the area of the moraine affected by the subsurface waterflow associated with the main drainage pathway. The slope of the terrain where the ice-cored moraine is located and the rather flat section on the northern side of the proglacial lake contribute to a natural channelling of the drainage of the lake towards the central section of the moraine (see figs. 5.10 and 5.11 in section 5.2). Hence, the northern and southern sections of the moraine do not seem to be influenced by subsurface waterflow in the

same way. The terrain of the central section of the ice-cored moraine is more hummocky than the northern and southern sections of the moraine which are higher with more demarcated ridges (see fig.5.4 in section 5.1.2, and fig. 6.3). Comparing the surface elevation change of the central section to the other sections of the moraine where no subsurface drainage is evident in the same way (see section 5.4), the moraine seems to be more intact in the northern and southern sections (see fig. 5.33 in section 5.4.2.). The subsurface water flow is thus likely to be an important factor in the deterioration of the ice-cored moraine in the areas where it is present, and it may therefore be inferred that there is still interstitial ground ice and/or a larger ice core present in the northern and southern sections of the moraine.
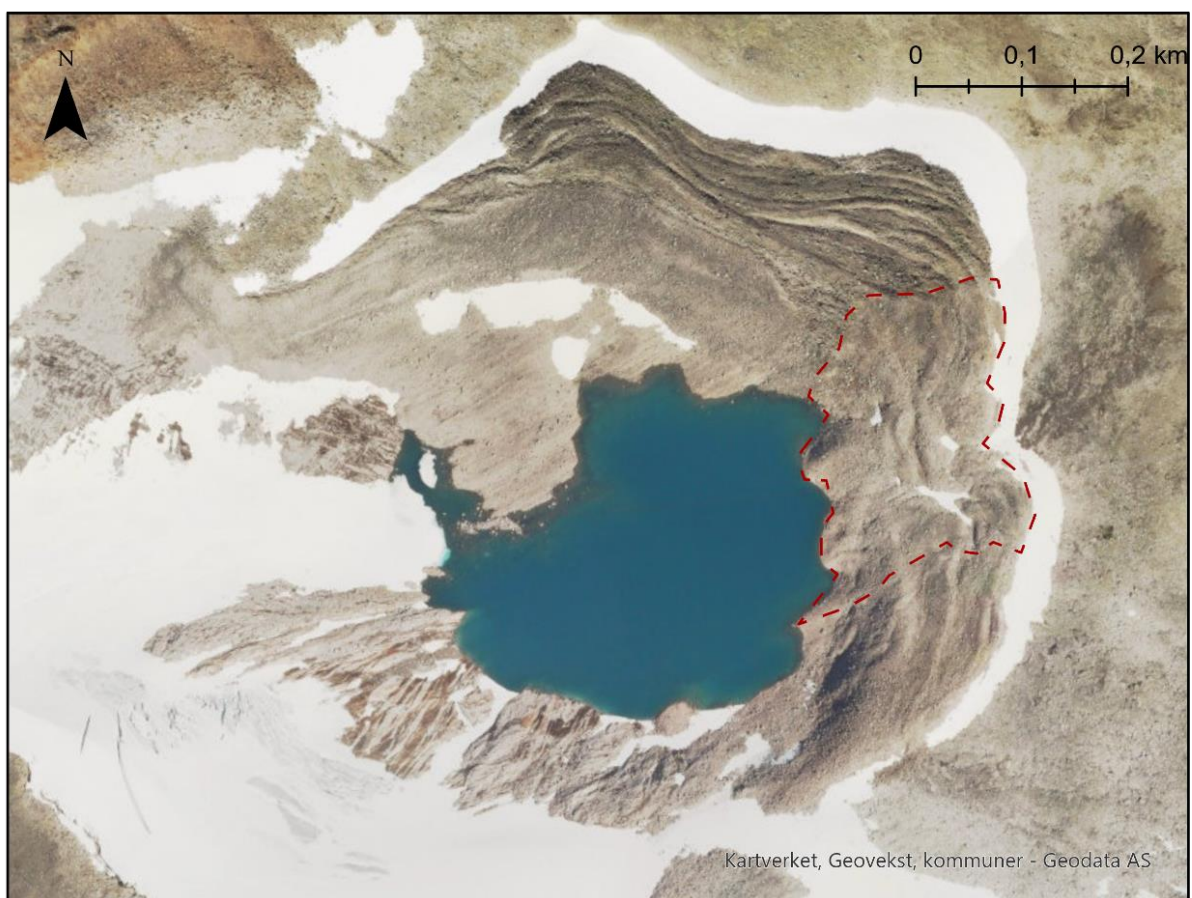
Figure 6.3. Delineation of the area of the moraine affected by the subsurface waterflow of the main drainage pathway and associated signs of downwasting and backwasting on the surface.

The remote sensing analysis highlighted that there has been surface lowering happening all over the moraine, and for the northern section of the moraine, which is not in direct contact with the lake, it is suggested that incoming solar radiation plays a larger role in the de-icing than subsurface waterflow. Kjær & Krüger (2001) highlight that topography is an important

factor for the rate of de-icing, and that south-facing slopes of ice-cored moraines may retreat faster than north-facing slopes, due to higher input of incoming solar radiation. In the northern section, the surface lowering is mostly focused on the south-facing proximal flank (fig. 5.33 in section 5.4.2). The analysis of incoming solar radiation (fig. 5.37 in section 5.4.4) also showed that the glacier proximal south-facing slope of the northern ridge, had a higher input of incoming solar radiation compared to the surrounding terrain. The DEM comparison between 1968 and 2019 highlights that this slope has a larger change in surface elevation than the surrounding areas of the ridge. The pattern of change in surface elevation on (fig. 5.33 in section 5.4.2) further shows a decrease in the higher sections of the flank and an increase in the lower sections. Mass wasting processes associated with backwasting are likely to have occurred. Field observations and the steepness of the slope further supports the other findings (see fig. A10 in the appendices). The InSAR results further indicate that the distal side of the northern section of the moraine is experiencing higher rates of surface elevation change. Higher air temperatures in the summer and incoming solar radiation might play a role here. Moreover, snowmelt from perennial snow patches on top of and between the ridges, as well as precipitation events may also introduce water into the system (Kjær & Kruger, 2001). When the snow melts, the water may percolate down into the system in the larger voids between the boulders, and in the pore space between the finer sediments. This also contributes to the transport of finer material deeper into the system. Introducing water from the surface into the system may impact the thawing of interstitial ground ice or melting of the ice core. Which again leads to surface lowering and destabilisation of the overlaying sections of the morainic material, initiating downwasting and backwasting processes. Inside the moraine, the water stemming from snowmelt and or precipitation might refreeze, due to the lower temperature existing inside the moraine and the presence of balch ventilation (Thompson, 1962). During intense events of precipitation during the summer and autumn, water and transport of finer materials are likely to occur (Kjær & Kruger, 2001). For the southern section of the moraine, surface or basal melt from the glacier might be introducing some meltwater into the system. This can perhaps be another contributing factor to the higher rates of surface lowering in the higher parts of the southern ridges.

Schomacker (2008), looked at how different factors influence the rate of backwasting of dead-ice areas, from climate to topographic and mass wasting processes, at fourteen different sites around the world, stretching from Yukon in Canada, to Antarctica, Svalbard, Iceland,

the Himalayas and New Zealand. The climatic factors mean annual air temperature, average summer air temperature, mean annual precipitation, mean summer precipitation and the annual sum of positive degree days were correlated with backwasting rates at ice cliffs in the dead-ice areas of these sites. Changes in the mean annual air temperature were found to correlate the most with rates of backwasting. However, the correlation between melt rates and climate parameters were found to be rather low. The lowest rates of backwasting were found in cool, dry climates, and the highest rates in humid, temperate climates. Schomacker (2008) thus stresses that topography and processes such as mass movements by gravity and liquefaction are important for the melt rate and associated backwasting, as it contributes to reduce the shear strength of the debris-cover. The same might be said for this field site, where the role of hydrological processes seem to be a dominating factor for the deterioration of the moraine.

6.2.4.2 Rate of degradation and future development

Comparing the annual rate of change for the period from 1968 to 2019 from the DEM comparison of surface elevation change with the annual rate of change from the InSAR data from 2015 – 2020 (see section 5.4), the heterogeneity of the surface lowering is evident. This supports the assumption that there still might be a more intact ice core present in the southern and northern sections of the moraine. For the southern section, topographic shading may play a role in the lower rates of surface elevation change (see for example Tonkin *et al.* 2016). In the central section, where the main drainage pathway is located, the rate of change over the last five years for the chosen point ($-34{,}09$ mm m a^{-1}) is very similar to the average rate of change between 1968 – 2019 (-39 mm m a^{-1}) for the moraine, though slightly lower. This might be an indication of the general surface lowering being gradual. However, the InSAR data does not specify the direction of change for each point (NGU, 2022, 25. February), as of such the two approaches for studying rate of change are not directly comparable. There have been several studies looking at the rate of surface elevation change of ice-cored moraines on Svalbard: Schomacker and Kjær (2008) found that the rate of mean vertical change was $-0{,}9$ m a^{-1} on Holmströmbreen between 1985 – 2004, Ewertowski and Tomczyk (2015) recorded between $0{,}3$ m a^{-1} (passive down-wasting) and $-1{,}8$ m a^{-1} (active mass movements) at Ragnarbreen between 2012 and 2014, and Midgley *et al.* (2018) recorded a mean change of $-0{,}64$ m a^{-1} between 2003 and 2014. Midgley *et al.* (2018) highlighted the heterogeneity in the

pattern of surface change across different sections of the moraine, with the largest changes being detected on the medial moraine ridge crest and in areas next to standing water – with change exceeding -14 m in 11 years. The change in surface elevation also depended upon site-specific characteristic controls, such as the ratio of ice to debris, the topographic context, and the influence of meltwater, which also seems to be the case at Semskfjellet. The mean annual rate of change seems somewhat lower at Semskfjellet in comparison, which is likely linked to the continental climate of the study area.

In terms of the future development of the ice-cored moraine, one may question to what extent the rate of disintegration will decrease, increase or be more gradual. Brook and Paine (2012) studied ablation on an ice-cored moraine at Fox glacier, New Zealand, and suggested that as the downwasting of the ice core progresses with time, the ablation rate is likely to decrease. This is due to the simultaneous melt-out of englacial material with downwasting, hence leading to a gradually thicker debris cover over time. This highlights the importance of the debris cover in reducing the influence of temperature on the rate of ablation, and it is likely that this might also be the case here for the southern and northern sections which are not directly influenced by subsurface waterflow. However, with expected increases in prolonged periods of extremes (e.g. prolonged periods of dry conditions, cold events, heat waves etc), broken up by extreme weather events, such as intense rainfall (Seneviratne *et al.* 2021). The moraine might be decaying at a faster pace than what is seen today, as the hydrological processes seem to be playing a larger role in the degradation of the moraine than atmospheric processes. Infiltration of water from intense rainfall events accompanied by associated transport of fine-grained material into the moraine might contribute to an increased instability of the top of the moraine and faster deterioration of the ice core. Furthermore, intense heat waves in the summer might contribute to increased melting. An amelioration of the climate is likely to lead to the disappearance of the snow patch along the margin of the moraine, which further decreases the insulating effect for the ice core on the more distal ridges, and higher rates of surface lowering might therefore occur in these sections in the years to come. As the debris cover is unequally distributed, the melt out of the moraine will probably continue to be spatially and temporally heterogeneous and will with time lead to a general lowering of the surface and more irregular topography in the transitional phase and a stepwise flattening of the top topography may be seen as a long-term result. However, this will depend on if downwasting or backwasting processes will be dominant in the future (Kjær & Kruger,

2001). The scale for this might be long and possibly associated with the longevity of the glacier, and the related presence and influence of the proglacial lake.

6.2.5 A conceptual model for the life cycle of the ice-cored moraine system

A conceptual model for the life cycle of the ice-cored moraine system at Semskfjellet has been developed (fig. 6.4). The model is based on theories of formation and glacier-permafrost interactions from Østrem (1959), (1964), (1971), Blatter and Hutter (1991), Etzelmüller and Hagen (2005), Irvine-Fynn *et al.* (2011), Lilleøren and Etzelmüller (2011) and Monz *et al.* (2022). The model further shows how the interplay with hydro-geomorphological processes influence the thermal regime of the glacier, inspired by models of switching of thermal regime of polythermal glaciers by Irvine-Fynn *et al.* (2011). The role of water in the process of degradation are inspired by Langston *et al.* (2011), Midgley (2018), Miesen (2019) and Miesen *et al.* (2021). It further suggest how this system might develop in the future, given the predicted impacts of climate change as indicated in works by Kjær and Kruger (2001), Schomacker and Kjær (2008) and Brook and Paine (2012). The conceptual model applies to the development of the central section of the moraine.

Figure 6.4a) shows how an ice-cored moraine may form at the front of a polythermal glacier in a permafrost environment. The snout of the glacier (the ablation zone) is believed to be cold based and frozen to the bed and is underlain by permafrost. Temperate ice exists as a function of ice thickness and geothermal heat flux in the higher section of the glacier. Due to the temperate regime, it is uncertain if this section is underlain by permafrost. The polythermal regime of the glacier leads to different velocities in the various parts of the glacier, which may contribute to crevasse formation in the higher sections of the glacier and to the creation of shear planes in the temperate to cold ice transition zone (TCZ). A source of material is further needed for the formation of an ice-cored moraine. The steep headwalls of Semskfjellet may contribute to supraglacial material through active slope processes. Another source of material stems from basal ad-freezing of subglacial and glaciofluvial material beneath the temperate ice. This material is then transported supraglacial, englacial and/or sub-glacial towards the margin of the glacier (as outlined in fig 6.4a). Sediments that have been transported sub- and englacially may be transported towards the glacier surface at the front of the glacier along shear planes in the temperate to cold ice transition zone, and due to

longitudinal compression, before it is revealed by surface thinning (Østrem, 1959; 1964; 1971; Blatter & Hutter, 1991; Etzelmüller & Hagen, 2005; Irvine-Fynn *et al.* 2011; Lilleøren & Etzelmüller, 2011; Monz *et al.* 2022). Folding near the margin and/or thrusting of fast flowing ice over the stagnant marginal ice are other mechanisms that may be contributing to the uplift of material and formation of moraine ridges (Moore *et al.* 2013). This results in a thick continuous debris cover being established at the frontal part of the glacier, insulating the underlaying ice from atmospheric processes and preserving the ice below (Østrem, 1959; Mattson & Gardner, 1991). The high occurrence of large rocks and boulders in the morainic material and the snowbank along the margin of the moraine makes the presence of Balch ventilation with entrapment of cold air in voids between rocks and boulders likely (Thompson, 1962). Hence, Balch ventilation is another mechanism contributing to the preservation of ice within the moraine. The assumption by Østrem (1964) that ice-cored moraines in Scandinavia consist of a combination of glacial ice and incorporated snowbank ice with associated material is suggested to be the case for this moraine. The field observations of pro-nival ridges emerging from the snowbank along the margin of the glacier, and the instability of the moraine and traces of high occurrences of rockfall and/or rock sliding supports this.

Figure 6.4b) shows how an increase in air temperature leads to the retreat of the non-debris covered parts of the glacier due to the influence of differential melting rates in the ablation season because of the heterogeneity in the spatial extent and thickness of the debris cover (Østrem, 1959; Mattson & Gardner, 1991). The thick debris cover contributes to insulate and thus preserve the ice within the moraine, and comes in addition to Balch ventilation, while the parts of the glacier not covered by debris are thinning and/or retreating. The thickness of the debris cover is likely to have exceeded the depth of the active layer of the permafrost at this point and may thus be considered a part of the local permafrost (Berthling, 2011; Kellerer-Pirklbauer, 2017). The ice-cored moraine is thus assumed to be impermeable at this stage. Surface- and basal melt further occurs on the glacier due to the increase in air temperature, contributing to form the fluted moraine on the northern side of the lake, indicating that the glacier has changed from a polythermal to a temperate regime. The ice-cored moraine functions as a barrier to the meltwater, due to its impermeable nature, which initiates the formation of the proglacial lake.

Figure 6.4c) portrays how the emergence of the proglacial lake dammed by the moraine is likely to have had a large impact in terms of increasing the retreat rate of the glacier, contributing to for example calving (Purdie & Fitzharris, 1999). These calving events might also possibly have led to glacier lake outburst floods (GLOFs) (Falátková, 2016), which may have breached the moraine at certain points. Undercutting and thinning from below seems to be likely mechanisms also contributing to glacial retreat at this stage. The rise in air temperature might contribute to an increase in the depth of the active layer of the permafrost, which might initiate some melting of the ice core in the moraine, or interstitial ground ice between the sediments are making the moraine more permeable for water to flow through. As the water pressure and temperature increases due to the accumulation of meltwater and change to summer season, the water might start to find ways to go through the moraine. This could either be due to the water being able to melt through and reopen old preserved glacial meltwater channels in the preserved glacier ice (Moorman, 2005), or find new ways to percolate through the sediment in the moraine. The introduction of meltwater into the ice-cored moraine system initiates and increases the rate of degradation of the ice-cored moraine. The water contributes to the melting of the ice core, and transport of finer material as suspended sediment. This again leads to downwasting and backwasting and thus a reworking of the sediment cover. Backwasting of ice-cored slopes may lead to more ice being exposed, and thus a self-propagating process of degradation (Kjær & Krüger, 2001; Schomacker & Kjær, 2008). The downwasting of material may further block existing subsurface water pathways in the moraine, and thus a rerouting of the pathway may follow, increasing the rate of deacy in other areas of the ice-cored moraine.

Figure 6.4d) As the debris cover is unequally distributed, and water is not present in all sections of the moraine, the melting of the ice core will continue to be spatially and temporally heterogeneous. As the depth of the active layer increases due to a general warming of the climate, and an increase in heavy precipitation events, the ice core may completely disintegrate in the end. The topography of the moraine will have a general surface lowering, and it may develop into a combination of a more hummocky terrain, or a stepwise levelling, depending on if backwasting or downwasting processes will dominate in the future (Kjær & Krüger, 2001). The scale for this may be long as the melt out is slow due to the thickness of the debris cover and may be associated with the longevity of the glacier and proglacial lake.
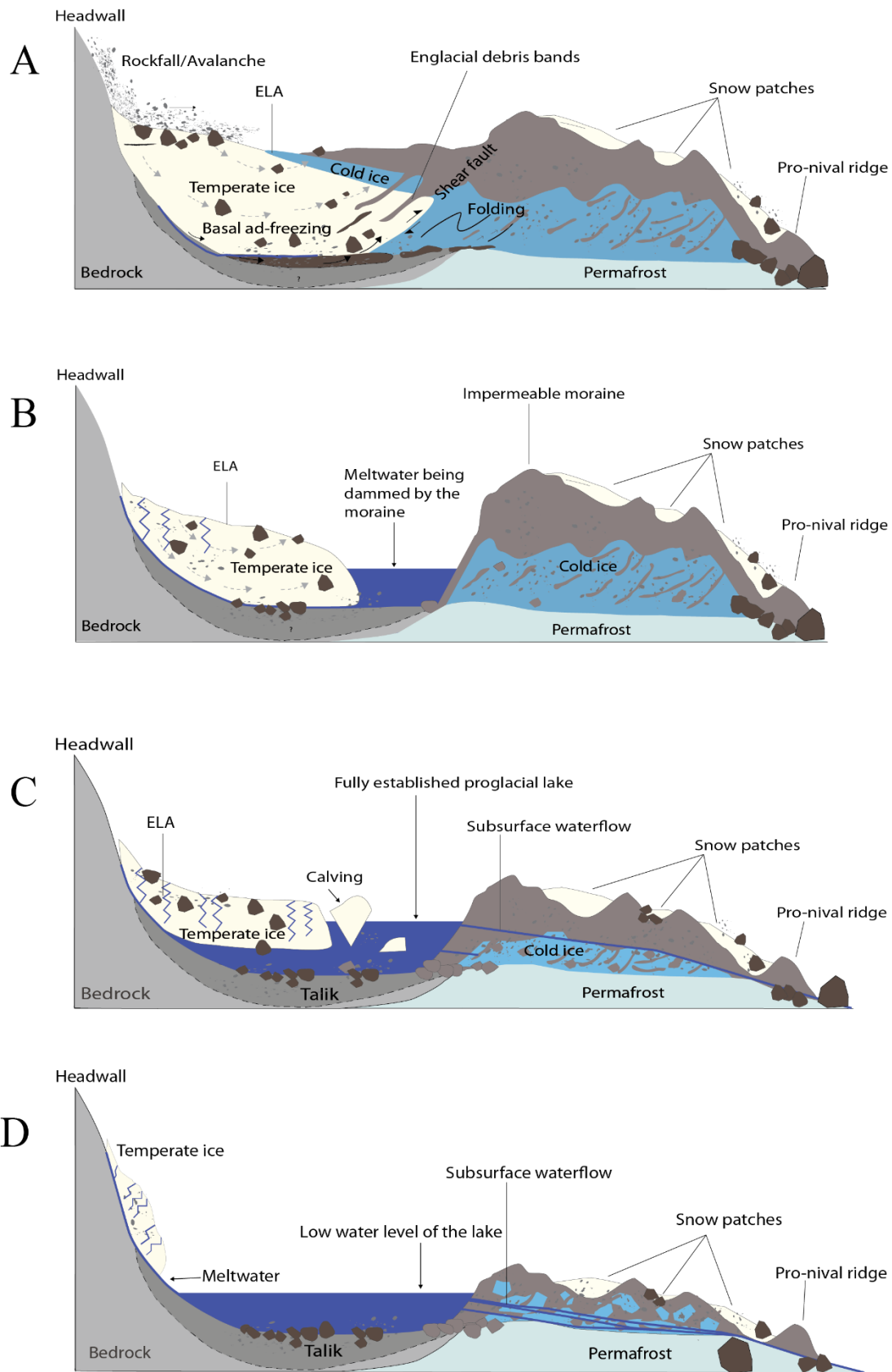
Figure 6.4 Life cycle of the ice-cored moraine at Semskfjellet. A) Formation of the ice-cored moraine, B) The moraine is impermeable, and the proglacial lake starts forming in a warming climate, C) Fully established proglacial lake, subsurface waterflow initiates degradation D) Decaying moraine, hummocky terrain starting to form.

7 Conclusion

The aim of this thesis was to study the role of hydrological processes in the degradation of an ice-cored moraine in a changing high mountain environment. To gain a holistic understanding of the formation and development of a small glacier-permafrost system and to better understand how it may develop in the future under the current climatic forcing, a multifaceted methodology combining hydrological investigations with geomorphological mapping, lichenometric dating and remote sensing techniques were applied.

The results of the lichenometric dating of the moraine ridges suggest that this is a rather young system, with the timing of formation of the ice-cored moraine possibly being linked to a minimum age of formation during the Little Ice Age and the occurrence of the proglacial lake might be connected to the warming of the climate in the 1930s.

The hydrological investigations looking into the spatial distribution, subsurface environment and origin of the streams found that an abundance of surface streams emerged along the distal side of the moraine throughout the summer. One main subsurface drainage pathway from the proglacial lake through the central section of the moraine was identified. Due to the inefficiency of the drainage pathway and the broadening of the stream throughout the summer, the subsurface pathway is suggested to not be channelised. The origin of the streams in the northern and southern section of the moraine might stem from melting of ice inside the moraine or from the melting of the snow patch. However, the hydrological investigations were so diluted with meltwater from the snow patch that a possible signal from melting of ice inside the moraine could not be distinguished.

The hydrological investigations found that the internal structure of the moraine seemed to influence the efficiency of the main drainage pathway and thus to what extent the moraine functions as a barrier to the pro-glacial lake. A threshold connected to an internal structure affected by seasonal permafrost dynamics with the presence of ground ice and/or buried inactive glacier ice seems plausible. A seasonal drainage pattern of the pro-glacial lake was

observed and seemed to be influenced by changes in air temperature, glacial ablation, and water temperature. The remote sensing analysis showed that the central section of the moraine has experienced the highest rates of changes in surface elevation, and it is uncertain if an ice core is still present here. The northern and southern sections of the moraine might still have an ice core, as they have experienced the least changes in surface elevation.

In general, hydrological processes seems to play an important role in the decay of the moraine. The main drainage pathway was identified to have been instrumental in initiating downwasting and backwasting processes contributing to the deterioration of the moraine. The northern and southern sections of the moraine have experienced less surface lowering and appear more intact, possibly due to the thickness of the debris layer and lack of influence from subsurface waterflow from the lake, hence other factors, such as aspect and topography also seemed influential.

This study has highlighted the interplay of glacier-permafrost interactions in the formation and role of the proglacial lake and subsurface waterflow as active agents in the development and deterioration of this system. As a result, a conceptual model for the life cycle of this ice-cored moraine system in connection to glacier-permafrost interactions and hydro-geomorphological processes has been proposed.

In the future, with an expected increase in heavy and prolonged precipitation events and heat waves, due to anthropogenic induced climate change, it is likely that the rate of degradation might increase. The rate of disintegration is not expected to be homogeneous for the different parts of the moraine, due to the varying influence of subsurface waterflow and variations in thickness of the debris cover. Furthermore, the scale for the disintegration of the ice-cored moraine might be long, possibly associated with the longevity of the glacier and proglacial lake.

8 Further research

Further research is needed to better understand the internal structure of ice-cored moraines, and how they may develop in the future. GPR, ERI and seismic refraction surveys might give a clearer image of the internal structure and hydrological pathways of these systems than hydrological investigations alone and are thus encouraged to better assess the mechanisms associated with lake drainage and future development of the ice-cored moraine. Supplementary dating techniques are needed for a more precise age estimate of the ice-cored moraine system. Repeat drone surveys and DEM generations for shorter time frames are further encouraged to monitor the rate of change for these systems, as they might have implications for the water supply and risk of geohazards in the near future.

9 References

Ambach, W., Dansgaard, W., Eisner, H., & Møller, J. (1968). The altitude effect on the isotopic composition of precipitation and glacier ice in the Alps. *Tellus, 20*(4), 595–600. https://doi.org/10.3402/tellusa.v20i4.10040

Andreassen, L., Elvehøy, H., Kjøllmoen, B., & Belart, J. M. C. (2020). Glacier change in Norway since the 1960s – an overview of mass balance, area, length and surface elevation changes. *Journal of Glaciology, 66*(256), 313–328. https://doi.org/10.1017/jog.2020.10

Appleby, J. R., Brook, M. S., Horton, T. W., Fuller, I. C., Holt, K. A., & Quincey, D. J. (2017). Stable isotope (δD–δ18O) relationships of ice facies and glaciological structures within the mid-latitude maritime Fox Glacier, New Zealand. *Annals of Glaciology*, *58*(75), 155–165. https://doi.org/10.1017/aog.2017.11

Armstrong, R.A. (2014). Lichen Growth and Lichenometry. In *Recent Advances in Lichenology* (pp. 213–227). Springer India. https://doi.org/10.1007/978-81-322-2181-4_10

Benedict, J.B. (1993). A 2000-year lichen-snowkill chronology for the Colorado Front Range, USA. *Holocene (Sevenoaks), 3*(1), 27–33. https://doi.org/10.1177/095968369300300103

Bengtsson, L., Semenov, V.A., & Johannessen, O.M. (2004). The Early Twentieth-Century Warming in the Arctic—A Possible Mechanism. *Journal of Climate, 17*(20), 4045–4057. https://doi.org/10.1175/1520-0442(2004)0172.0.CO;2

Beniston, M. Farinotti, D., Stoffel, M., Andreassen, L. M., Coppola, E., Eckert, N., Fantini, A., Giacona, F., Hauck, C., Huss, M., Huwald, H., Lehning, M., López-Moreno, J.-I., Magnusson, J., Marty, C., Morán-Tejéda, E., Morin, S., Naaim, M., Provenzale, A., … Vincent, C. (2018). The European mountain cryosphere: a review of its current state, trends, and future challenges. *The Cryosphere, 12*(2), 759–794. https://doi.org/10.5194/tc-12-759-2018

Benn, D. & Evans, D. J. A. (2010). *Glaciers and Glaciation, 2nd edition.* Routledge. https://doi.org/10.4324/9780203785010

Berthling, I. (2011). Beyond confusion: Rock glaciers as cryo-conditioned landforms. *Geomorphology (Amsterdam, Netherlands), 131*(3), 98–106.

https://doi.org/10.1016/j.geomorph.2011.05.002

Beschel, R. E. (1961). Dating rock Surfaces by lichen growth and its application to glaciology and physiography (lichenometry). In *Geology of the Arctic (Second. Edition)* [Raasch, G. O. eds]. University of Toronto Press, Toronto, 1044-1062.

Beylich, A.A. & Laute, K. (2012). Seasonal and annual variations of surface water chemistry, solute fluxes and chemical denudation in a steep and glacier-fed mountain catchment in western Norway (Erdalen, Nordfjord). *Catena (Giessen), 96*, 12–27.

https://doi.org/10.1016/j.catena.2012.04.004

Bickerton, R.W. & Matthews, J. A. (1992). On the accuracy of lichenometric dates: an assessment based on the 'Little Ice Age' moraine sequence of Nigardsbreen, southern Norway. *Holocene (Sevenoaks), 2*(3), 227–237. https://doi.org/10.1177/095968369200200304

Blatter, H. (1987). On the thermal regime of an Arctic valley glacier: a study of White Glacier, Axel Heiberg Island, N.W.T., Canada. *Journal of Glaciology, 33*(114), 200–211. https://doi.org/10.1017/S0022143000008704

Blatter, H. & Hutter, K. (1991). Polythermal conditions in Arctic glaciers. *Journal of Glaciology, 37*(126), 261–269. https://doi.org/10.1017/S0022143000007279

Bowling, L. C., Lettenmaier, D. P., & Matheussen, B. V. (2000). Hydroclimatology of the Arctic drainage basin. In *The freshwater budget of the Arctic Ocean* (p. 57-90). Springer, Dordrecht.

Bradley, R. S. (2014*). Paleoclimatology: reconstructing climates of the quaternary (Third edition.)*. Elsevier. 116-190.

Brook, M.S. & Paine, S. (2012). Ablation of ice-cored moraine in a humid, maritime climate: fox glacier, new zealand. *Geografiska Annaler. Series A, Physical Geography, 94*(3), 339–349. https://doi.org/10.1111/j.1468-0459.2011.00442.x

Brown, J., Harper, J., & Bradford, J. (2009). A radar transparent layer in a temperate valley glacier: Bench Glacier, Alaska. *Earth Surface Processes and Landforms, 34*(11), 1497–1506. https://doi.org/10.1002/esp.1835

Carrivick, J.L. & Tweed, F. S. (2013). Proglacial lakes: character, behaviour and geological importance. *Quaternary Science Reviews, 78,* 34–52.

https://doi.org/10.1016/j.quascirev.2013.07.028

Caballero, Y., Jomelli, V., Chevallier, P., & Ribstein, P. (2002). Hydrological characteristics of slope deposits in high tropical mountains (Cordillera Real, Bolivia). *Catena (Giessen), 47*(2), 101-116. https://doi.org/10.1016/S0341-8162(01)00179-5

Chandler, J. (1999). Effective application of automated digital photogrammetry for geomorphological research. *Earth Surface Processes and Landforms, 24*(1), 51–63. https://doi.org/10.1002/(SICI)1096-9837(199901)24:13.0.CO;2-H

Clague, J.J. & Evans, S. G. (2000). A review of catastrophic drainage of moraine-dammed lakes in British Columbia. *Quaternary Science Reviews, 19*(17), 1763–1783. https://doi.org/10.1016/S0277-3791(00)00090-1

Clark, I. D. & Fritz, P. (1997). *Environmental isotopes in hydrogeology.* Lewis Publishers.

Cooper, R., Hodgkins, R., Wadham, J., & Tranter, M. (2011). The hydrology of the proglacial zone of a high-Arctic glacier (Finsterwalderbreen, Svalbard): Sub-surface water fluxes and complete water budget. *Journal of Hydrology (Amsterdam), 406*(1), 88–96. https://doi.org/10.1016/j.jhydrol.2011.06.008

Cuffey, Conway, H., Hallet, B., Gades, A. M., & Raymond, C. F. (1999). Interfacial water in polar glaciers and glacier sliding at $-17°C$. *Geophysical Research Letters, 26*(6), 751–754. https://doi.org/10.1029/1999GL900096

Dansgaard, W. (1964). Stable isotopes in precipitation. *Tellus, 16*(4), 436–468. https://doi.org/10.1111/j.2153-3490.1964.tb00181.x

Driscoll, F.G. (1980). Wastage of the Klutlan ice-cored moraines, Yukon Territory, Canada. *Quaternary Research, 14*(1), 31–49. https://doi.org/10.1016/0033-5894(80)90005-8

Etzelmüller, B. & Hagen, J. O. (2005). Glacier-permafrost interaction in Arctic and alpine mountain environments with examples from southern Norway and Svalbard. *Cryospheric Systems: Glaciers and Permafrost, 242*(1), 11–19.

https://doi.org/10.1144/GSL.SP.2005.242.01.02

Evans, D. (2014) Introduction to glacial landsystems. In Evans, D. & Gooster, L (eds), *Glacial landsystems*. Routledge, London.

Ewertowski, M. (2014). Recent transformations in the high-arctic glacier landsystem, ragnarbreen, svalbard. *Geografiska Annaler. Series A, Physical Geography, 96*(3), 265–285. https://doi.org/10.1111/geoa.12049

Ewertowski, M.W. & Tomczyk, A. M. (2015). Quantification of the ice-cored moraines' short-term dynamics in the high-Arctic glaciers Ebbabreen and Ragnarbreen, Petuniabukta, Svalbard. *Geomorphology (Amsterdam, Netherlands), 234*, 211–227.

https://doi.org/10.1016/j.geomorph.2015.01.023

Falátková, K. (2016). Temporal analysis of GLOFs in high-mountain regions of Asia and assessment of their causes. Acta Universitatis Carolinae. *Geographica, 51*(2), 145–154. https://doi.org/10.14712/23361980.2016.12

Fisher, D. A. (1990). A Zonally-Averaged Stable-Isotope Model Coupled to a Regional Variable-Elevation Stable-Isotope Model. *Annals of Glaciology, 14*, 65–71. https://doi.org/10.3189/S0260305500008284

Flett, V., Maurice, L., Finlayson, A., Black, A. R., MacDonald, A. M., Everest, J., & Kirkbride, M. P. (2017). Meltwater flow through a rapidly deglaciating glacier and foreland catchment system: Virkisjökull, SE Iceland. *Hydrology Research, 48*(6), 1666–1681. https://doi.org/10.2166/nh.2017.205

Frey, K. E. & McClelland, J. W. (2009). Impacts of permafrost degradation on arctic river biogeochemistry. *Hydrological Processes, 23*(1), 169–182. https://doi.org/10.1002/hyp.7196

Fritz, P., & Fontes, J. C. (1980). *Handbook of environmental isotope geochemistry : 1 : The terrestrial environment.* A (1). Elsevier. XII – 545. https://doi.org/10.1016/B978-0-444-41780-0.50006-7

Gisnås, K., Etzelmüller, B., Lussana, C., Hjort, J., Sannel, A. B. K., Isaksen, K., Westermann, S., Kuhry, P., Christiansen, H. H., Frampton, A., & Åkerman, J. (2017). Permafrost Map for Norway, Sweden and Finland. *Permafrost and Periglacial Processes, 28*(2), 359–378.

https://doi.org/10.1002/ppp.1922

Gruber, S., Fleiner, R., Guegan, E., Panday, P., Schmid, M.-O., Stumm, D., Wester, P., Zhang, Y., & Zhao, L. (2017). Review article: Inferring permafrost and permafrost thaw in the mountains of the Hindu Kush Himalaya region. *The Cryosphere, 11*(1), 81–99.

https://doi.org/10.5194/tc-11-81-2017

Gulley, J.D., Benn, D.I., Müller, D. & Luckman, A. (2009). A cut-and-closure origin for englacial conduits in uncrevassed regions of polythermal glaciers. *Journal of Glaciology, 55*(189), 66–80. https://doi.org/10.3189/002214309788608930

Haeberli, W. (2005). Investigating glacier-permafrost relationships in high-mountain areas: historical background, selected examples and research needs. *Cryospheric Systems: Glaciers and Permafrost, 242*(1), 29–37. https://doi.org/10.1144/GSL.SP.2005.242.01.03

Haeberli, W., Hallet, B., Arenson, L., Elconin, R., Humlum, O., Kääb, A., Kaufmann, V., Ladanyi, B., Matsuoka, N., Springman, S., & Mühll, D. V. (2006). Permafrost creep and rock glacier dynamics. *Permafrost and Periglacial Processes, 17*(3), 189–214.

https://doi.org/10.1002/ppp.561

Haeberli, W., Noetzli, J., Arenson, L., Delaloye, R., Gärtner-Roer, I., Gruber, S., Isaksen, K., Kneisel, C., Krautblatter, M., & Phillips, M. (2010). Mountain permafrost: development and challenges of a young research field. *Journal of Glaciology, 56*(200), 1043–1058.

https://doi.org/10.3189/002214311796406121

Haeberli, W., Schaub, Y., & Huggel, C. (2017). Increasing risks related to landslides from degrading permafrost into new lakes in de-glaciating mountain ranges. *Geomorphology (Amsterdam, Netherlands), 293*, 405–417. https://doi.org/10.1016/j.geomorph.2016.02.009

Harris, C. & Murton, J. B. (2005). Interactions between glaciers and permafrost: an introduction. Cryospheric Systems: Glaciers and Permafrost, 242(1), 1–9.

https://doi.org/10.1144/GSL.SP.2005.242.01.01

Hausmann, H., Krainer, K., Brückl, E. & Mostler, W. (2007). Internal structure and ice content of Reichenkar rock glacier (Stubai Alps, Austria) assessed by geophysical investigations. *Permafrost and Periglacial Processes, 18*(4), 351–367. https://doi.org/10.1002/ppp.601

Hipp, T., Etzelmüller, B., & Westermann, S. (2014). Permafrost in Alpine Rock Faces from Jotunheimen and Hurrungane, Southern Norway. *Permafrost and Periglacial Processes, 25*(1), 1–13. https://doi.org/10.1002/ppp.1799

Hock, R., G. Rasul, C. Adler, B. Cáceres, S. Gruber, Y. Hirabayashi, M. Jackson, A. Kääb, S. Kang, S. Kutuzov, A. Milner, U. Molau, S. Morin, B. Orlove, and H. Steltzer. (2019): High Mountain Areas. In H.-O. Pörtner, D.C. Roberts, V. Masson-Delmotte, P. Zhai, M. Tignor, E. Poloczanska, K. Mintenbeck, A. Alegría, M. Nicolai, A. Okem, J. Petzold, B. Rama, N.M. Weyer (eds.): *IPCC Special Report on the Ocean and Cryosphere in a Changing Climate*. In press.

Humlum, O. (1997). Active layer thermal regime at three rock glaciers in Greenland. *Permafrost and Periglacial Processes, 8*(4), 383–408.

https://doi.org/10.1002/(SICI)1099-1530(199710/12)8:43.3.CO;2-M

Hutter, K. (1982). A mathematical model of polythermal glaciers and ice sheets. *Geophysical & Astrophysical Fluid Dynamics, 21*(3-4), 201-224.

https://doi.org/10.1080/03091928208209013

IAEA/WMO (2021). *Global Network of Isotopes in Precipitation. The GNIP Database.* Accessible at: http://www.iaea.org/water

Irvine-Fynn, T.D.L., Moorman, B. J., Willis, I. C., Sjogren, D. B., Hodson, A. J., Mumford, P. N., Walter, F. S. A., & Williams, J. L. M. (2005). Geocryological processes linked to High Arctic proglacial stream suspended sediment dynamics: examples from Bylot Island, Nunavut, and Spitsbergen, Svalbard. *Hydrological Processes, 19*(1), 115–135.

https://doi.org/10.1002/hyp.5759

Irvine-Fynn, T.D.L., Moorman, B. J., Williams, J. L. M., & Walter, F. S. A. (2006). Seasonal changes in ground-penetrating radar signature observed at a polythermal glacier, Bylot Island, Canada. *Earth Surface Processes and Landforms, 31*(7), 892–909.

https://doi.org/10.1002/esp.1299

Irvine-Fynn, T.D.L., Hodson, A. J., Moorman, B. J., Vatne, G., & Hubbard, A. L. (2011). POLYTHERMAL GLACIER HYDROLOGY: A REVIEW. *Reviews of Geophysics., 49*(4). https://doi.org/10.1029/2010RG000350

James, M.R., Robson, S., d'Oleire-Oltmanns, S., & Niethammer, U. (2017). Optimising UAV topographic surveys processed with structure-from-motion: Ground control quality, quantity and bundle adjustment. *Geomorphology (Amsterdam, Netherlands), 280,* 51–66.

https://doi.org/10.1016/j.geomorph.2016.11.021

Jania, J., Macheret, Y. Y., Navarro, F.J., Glazovsky, A.F., Vasilenko, E.V., Lapazaran, J., Glowacki, P., Migala, K., Balut, A., & Piwowar, B.A. (2005). Temporal changes in the radiophysical properties of a polythermal glacier in Spitsbergen. *Annals of Glaciology, 42*(1), 125–134. https://doi.org/10.3189/172756405781812754

Jansen, H.L., Dahl, S.O. & Nielsen, P.R. (2018) An inverse approach to the course of the 'Little Ice Age' glacier advance and the following deglaciation at Austerdalsisen, eastern Svartisen, northern Norway. *Holocene (Sevenoaks), 28*(7), 1041-1056.

https://doi.org/10.1177/0959683618761539

Johnson, P.G. (1971). Ice-cored Moraine Formation and Degradation, Donjek Glacier, Yukon Territory, Canada. *Geografiska Annaler. Series A, Physical Geography, 53*(3/4), 198.

https://doi.org/10.2307/520789

Jones, D.B., Harrison, S., Anderson, K., & Whalley, W. B. (2019). Rock glaciers and mountain hydrology: A review. *Earth-Science Reviews, 193*, 66–90.

https://doi.org/10.1016/j.earscirev.2019.04.001

Kartverket (Norges Geografiske Oppmåling): Heliogravyre 1:100 000, L15 Nasa, O.Lier, 1898 Retrieved from 20.01.22:

https://www.kartverket.no/om-kartverket/historie/historiske-kart/soketreff/mitt-kart?mapId=4770

Kellerer-Pirklbauer, A. (2017). Potential weathering by freeze-thaw action in alpine rocks in the European Alps during a nine year monitoring period. *Geomorphology (Amsterdam, Netherlands), 296*, 113–131. https://doi.org/10.1016/j.geomorph.2017.08.020

Kendall, C., Doctor, D.H., & Young, M.B. (2014). 7.9 - Environmental Isotope Applications in Hydrologic Studies. In: Holland, H. D. & Turekian, K.K. (eds) *Treatise on Geochemistry (Second Edition).* Elsevier Ltd. 273–327. https://doi.org/10.1016/B978-0-08-095975-7.00510-6

Kleman. (1994). Preservation of landforms under ice sheets and ice caps. *Geomorphology (Amsterdam, Netherlands), 9*(1), 19–32. https://doi.org/10.1016/0169-555X(94)90028-0

Koerner, R.M. (1980). The Problem of Lichen-Free Zones in Arctic Canada. *Arctic and Alpine Research, 12*(1), 87–94. https://doi.org/10.2307/1550592

Krüger, J. (1994). *Glacial processes, sediments, landforms, and stratigraphy in the terminus region of Myrdalsjökull, Iceland: two interdisciplinary case studies* (Vol. 21). CA Reitzel.

Krüger, J. & Kjær, K.H. (2000). De-icing progression of ice-cored moraines in a humid, subpolar climate, Kötlujökull, Iceland. *Holocene (Sevenoaks), 10*(6), 737–747.

https://doi.org/10.1191/09596830094980

Kjær, K.H. & Krüger, J. (2001). The final phase of dead-ice moraine development: processes and sediment architecture, Kötlujökull, Iceland. *Sedimentology, 48*(5), 935–952.

https://doi.org/10.1046/j.1365-3091.2001.00402.x

Kunz, J., Ullmann, T., & Kneisel, C. (2022). Internal structure and recent dynamics of a moraine complex in an alpine glacier forefield revealed by geophysical surveying and Sentinel-1 InSAR time series. *Geomorphology (Amsterdam, Netherlands), 398,* 108052.

https://doi.org/10.1016/j.geomorph.2021.108052

Lane, S.M., James, T. D., & Crowell, M. D. (2000). Application of Digital Photogrammetry to Complex Topography for Geomorphological Research. *Photogrammetric Record, 16*(95), 793–821. https://doi.org/10.1111/0031-868X.00152

Langston, G., Bentley, L. R., Hayashi, M., McClymont, A., & Pidlisecky, A. (2011). Internal structure and hydrological functions of an alpine proglacial moraine. *Hydrological Processes, 25*(19), 2967–2982. https://doi.org/10.1002/hyp.8144

Lee, J., Feng, X., Faiia, A. M., Posmentier, E. S., Kirchner, J. W., Osterhuber, R., & Taylor, S. (2010). Isotopic evolution of a seasonal snowcover and its melt by isotopic exchange between liquid water and ice. *Chemical Geology, 270*(1), 126–134.

https://doi.org/10.1016/j.chemgeo.2009.11.011

Lilleøren, K.S. & Etzelmüller, B. (2011). A regional inventory of rock glaciers and ice-cored moraines in Norway. *Geografiska Annaler*, *93*(3), 175–191. https://doi.org/10.1111/j.1468-0459.2011.00430.x

Lilleøren, K.S., Etzelmüller, B., Gärtner-Roer, I., Kääb, A., Westermann, S., & Guðmundsson, Águst. (2013). The Distribution, Thermal Characteristics and Dynamics of Permafrost in Tröllaskagi, Northern Iceland, as Inferred from the Distribution of Rock Glaciers and Ice-Cored Moraines. *Permafrost and Periglacial Processes*, *24*(4), 322–335.

https://doi.org/10.1002/ppp.1792

Ling, F., Wu, Q., Zhang, T., & Niu, F. (2012). Modelling Open-Talik Formation and Permafrost Lateral Thaw under a Thermokarst Lake, Beiluhe Basin, Qinghai-Tibet Plateau. *Permafrost and Periglacial Processes, 23*(4), 312–321. https://doi.org/10.1002/ppp.1754

Linell, K.A. & Tedrow, J. C. F. (1981). *Soil and permafrost surveys in the arctic* (p. viii, 279). Clarendon Press.

Loso, M.G. & Doak, D. F. (2006). The Biology behind Lichenometric Dating Curves. *Oecologia, 147*(2), 223–229. https://doi.org/10.1007/s00442-005-0265-3

Luethi, R., Phillips, M., & Lehning, M. (2017). Estimating Non-Conductive Heat Flow Leading to Intra-Permafrost Talik Formation at the Ritigraben Rock Glacier (Western Swiss Alps). *Permafrost and Periglacial Processes, 28*(1), 183–194.

https://doi.org/10.1002/ppp.1911

MacDonald, A.M., Black, A. R., Ó Dochartaigh, B. É, Everest, J., Darling, W. G., Flett, V., & Peach, D. W. (2016). Using stable isotopes and continuous meltwater river monitoring to investigate the hydrology of a rapidly retreating Icelandic outlet glacier. *Annals of Glaciology, 57*(72), 151–158. https://doi.org/10.1017/aog.2016.22

Manzo, M., Ricciardi, G.P., Casu, F., Ventura, G., Zeni, G., Borgström, S., Berardino, P., Del Gaudio, C., & Lanari, R. (2006). Surface deformation analysis in the Ischia Island (Italy) based on spaceborne radar interferometry. *Journal of Volcanology and Geothermal Research, 151*(4), 399–416. https://doi.org/10.1016/j.jvolgeores.2005.09.010

Marsh, P. & Neumann, N. N. (2001). Processes controlling the rapid drainage of two ice-rich permafrost-dammed lakes in NW Canada. *Hydrological Processes, 15*(18), 3433–3446. https://doi.org/10.1002/hyp.1035

Mathismoen, O. (2020). Galdhøpiggen og Glittertinden er normalt stivfrosne. Men nå skjer det dramatiske ting. *Aftenposten*, 30.08.2020.

Mattson, L.E. & Gardner, J. S. (1991). Mass Wasting on Valley-Side Ice-Cored Moraines, Boundary Glacier, Alberta, Canada. *Geografiska Annaler. Series A, Physical Geography, 73*(3/4), 123. https://doi.org/10.2307/521017

McClymont, A.F., Roy, J. W., Hayashi, M., Bentley, L. R., Maurer, H., & Langston, G. (2011). Investigating groundwater flow paths within proglacial moraine using multiple geophysical methods. *Journal of Hydrology (Amsterdam), 399*(1), 57–69.

https://doi.org/10.1016/j.jhydrol.2010.12.036

McNamara, J.P., Kane, D. L., & Hinzman, L. D. (1998). An analysis of streamflow hydrology in the Kuparuk River Basin, Arctic Alaska: a nested watershed approach. *Journal of Hydrology (Amsterdam), 206*(1), 39–57. https://doi.org/10.1016/S0022-1694(98)00083-3

MET (2021) *Seklima døgnnedbør*. Retrieved from 28.09.21

Norsk Klimaservicesenter (met.no).

MET (2022) *Seklima gjennomsnittlig årsnedbør*. Retrieved from 12.04.22

Norsk Klimaservicesenter (met.no).

MET, Kartverket, NVE (2022a) *SeNorge–døgnkart 30 år temperatur*.

Retrieved from: 12.04.2022 https://senorge.no/map

MET, Kartverket, NVE (2022b) *SeNorge – døgnkart 30 år nedbør*

Retrieved from 12.04.2022 https://senorge.no/map

MET, Kartverket, NVE (2022c) *SeNorge–døgnkart 30 år snødybde*.

Retrieved from 12.04.2022 https://senorge.no/map

Midgley, N.G., Tonkin, T.N., Graham, D.J., & Cook, S.J. (2018). Evolution of high-Arctic glacial landforms during deglaciation. *Geomorphology (Amsterdam, Netherlands), 311*, 63–75. https://doi.org/10.1016/j.geomorph.2018.03.027

Miesen, F. M. (2019). *Transient landform patterns and periglacial processes in a partly glaciated basin (North-Eastern Snøhetta, Dovrefjell, Norway) A discussion on glacier-permafrost interactions.* Master Thesis, University of Bonn.

Miesen, F.M., Dahl, S. O., & Schrott, L. (2021). Evidence of glacier-permafrost interactions associated with hydro-geomorphological processes and landforms at Snøhetta, Dovrefjell, Norway. *Geografiska Annaler. Series A, Physical Geography, 103*(3), 273–302.

https://doi.org/10.1080/04353676.2021.1955539

Monz, M. E., Hudleston, P. J., Cook, S. J., Zimmerman, T., & Leng, M. J. (2022). Thrust faulting in glaciers? Re-examination of debris bands near the margin of Storglaciären, Sweden. *Boreas, 51*(1), 78–99. https://doi.org/10.1111/bor.12549

Moore, P.L., Iverson, N. R., Uno, K. T., Dettinger, M. P., Brugger, K. A., & Jansson, P. (2013). Entrainment and emplacement of englacial debris bands near the margin of Storglaciären, Sweden. *Boreas, 42*(1), 71–83.

https://doi.org/10.1111/j.1502-3885.2012.00274.x

Moorman, B. J., & Michel, F. A. (2000). Glacial hydrological system characterization using ground-penetrating radar. *Hydrological Processes, 14*(15), 2645-2667.

https://doi.org/10.1002/1099-1085(20001030)14:15<2645::AID-HYP84>3.0.CO;2-2

Moorman, B.J. (2005). Glacier-permafrost hydrological interconnectivity: Stagnation Glacier, Bylot Island, Canada. *Cryospheric Systems: Glaciers and Permafrost, 242*(1), 63–74. https://doi.org/10.1144/GSL.SP.2005.242.01.06

Murray, T., Stuart, G. W., Miller, P. J., Woodward, J., Smith, A. M., Porter, P. R., & Jiskoot, H. (2000). Glacier surge propagation by thermal evolution at the bed. *Journal of Geophysical Research, 105*(B6), 13491–13507. https://doi.org/10.1029/2000JB900066

NGU (2021) *Berggrunn - Nasjonal Berggrunnsdatabase*. Retrieved from 20.09.21

http://geo.ngu.no/kart/berggrunn_mobil/

NGU (2022, 24. February) *InSAR Norway*. Retrieved from 24.02.22. InSAR Norway (ngu.no)

NGU (2022, 25. February) *Dataegenskaper og begrensninger.*

Retrieved from 28.02.22 https://www.ngu.no/emne/dataegenskaper-og-begrensninger

Nordli, Ø. (2009) Om dei meteorologiske målingane i Holandsfjorden i samband med Storglomfjordutbygginga. Norwegian Meteorological Institute, Oslo (met.no. Note 04/2009)

NovaMetrix LLC (2022) *TD-diver.*

Retrieved from 15.10.21 https://www.vanessen.com/products/data-loggers/td-diver/

Nuth, C. & Kääb, A. (2011). Co-registration and bias corrections of satellite elevation data sets for quantifying glacier thickness change. *The Cryosphere, 5*(1), 271–290.

https://doi.org/10.5194/tc-5-271-2011

Pecher, K. (1994). Hydrochemical analysis of spatial and temporal variations of solute composition in surface and subsurface waters of a high arctic catchment. *Catena (Giessen), 21*(4), 305–327. https://doi.org/10.1016/0341-8162(94)90043-4

Penna, D., Engel, M., Mao, L., Dell'Agnese, A., Bertoldi, G., & Comiti, F. (2014). Tracer-based analysis of spatial and temporal variation of water sources in a glacierized catchment. *Hydrology and Earth System Sciences Discussions*, *11*(5), 4879–4924.

https://doi.org/10.5194/hessd-11-4879-2014

Penna, D. Engel, M., Bertoldi, G., & Comiti, F. (2017). Towards a tracer-based conceptualization of meltwater dynamics and streamflow response in a glacierized catchment. *Hydrology and Earth System Sciences, 21*(1), 23–41. https://doi.org/10.5194/hess-21-23-2017

PERMOS (2016): Permafrost in Switzerland 2010/2011 to 2013/2014. In Nötzli, J., R. Luethi and B. Staub (eds.). *Glaciological Report Permafrost No. 12–15 of the Cryospheric Commission of the Swiss Academy of Sciences.*

Retrieved from 05.11.21: https://naturalsciences.ch/service/publications/82035-permafrost-in-switzerland-2010-2011-to-2013-2014

Pettersson, R., Jansson, P., & Blatter, H. (2004). Spatial variability in water content at the cold-temperate transition surface of the polythermal Storglaciären, Sweden. *Journal of Geophysical Research, 109*(F2), F02009. https://doi.org/10.1029/2003JF000110

Pickard, J. (1983). Surface Lowering of Ice-Cored Moraine by Wandering Lakes. *Journal of Glaciology, 29*(102), 338–342. https://doi.org/10.3189/S0022143000008388

Pickard, J. (1984). Retreat of ice scarps on an ice-cored moraine, Vestfold Hills, Antarctica. *Zeitschrift fur Geomorphologie, 28*(4), 443-453.

Pourrier, J., Jourde, H., Kinnard, C., Gascoin, S., & Monnier, S. (2014). Glacier meltwater flow paths and storage in a geomorphologically complex glacial foreland: The case of the Tapado glacier, dry Andes of Chile (30°S). *Journal of Hydrology (Amsterdam), 519*, 1068–1083. https://doi.org/10.1016/j.jhydrol.2014.08.023

Purdie, J. & Fitzharris, B. (1999). Processes and rates of ice loss at the terminus of Tasman Glacier, New Zealand. *Global and Planetary Change, 22*(1), 79–91.

https://doi.org/10.1016/S0921-8181(99)00027-2

Quincey, D.M., Lucas, R. M., Richardson, S. D., Glasser, N. F., Hambrey, M. J., & Reynolds, J. M. (2005). Optical remote sensing techniques in high-mountain environments: application to glacial hazards. *Progress in Physical Geography, 29*(4), 475–505.

https://doi.org/10.1191/0309133305pp456ra

Quincey, D.M., Richardson, S.D., Luckman, A., Lucas, R.M., Reynolds, J.M., Hambrey, M.J., & Glasser, N.F. (2007). Early recognition of glacial lake hazards in the Himalaya using remote sensing datasets. *Global and Planetary Change, 56*(1), 137–152.

https://doi.org/10.1016/j.gloplacha.2006.07.013

Richardson, S. D., & Reynolds, J. M. (2000). Degradation of ice-cored moraine dams: implications for hazard development. In *Debris-Covered Glaciers (Proceedings of a workshop held at Seattle, Washington, USA, September 2000).* IAHS PUBLICATION 264, 187-198.

Rowland, J.C., Travis, B. J., & Wilson, C. J. (2011). The role of advective heat transport in talik development beneath lakes and ponds in discontinuous permafrost. *Geophysical Research Letters, 38(*17), n/a–n/a. https://doi.org/10.1029/2011GL048497

Roy, J.W. & Hayashi, M. (2009). Multiple, distinct groundwater flow systems of a single moraine–talus feature in an alpine watershed. *Journal of Hydrology (Amsterdam), 373*(1-2), 139–150. https://doi.org/10.1016/j.jhydrol.2009.04.018

Rutter, N., Hodson, A., Irvine-Fynn, T., & Solås, M. K. (2011). Hydrology and hydrochemistry of a deglaciating high-Arctic catchment, Svalbard. *Journal of Hydrology (Amsterdam), 410*(1), 39–50. https://doi.org/10.1016/j.jhydrol.2011.09.001

Shakesby, R.A., Dawson, A. G., & Matthews, J. A. (1987). Rock glaciers, protalus ramparts and related phenomena, Rondane, Norway: a continuum of large-scale talus-derived landforms. *Boreas, 16*(3), 305–317. https://doi.org/10.1111/j.1502-3885.1987.tb00099.x

Schomacker, A. & Kjær, K. H. (2007). Origin and de-icing of multiple generations of ice-cored moraines at Bruarjokull, Iceland. *Boreas, 36*(4), 411–425.

https://doi.org/10.1080/03009480701213554

Schomacker, A. (2008). What controls dead-ice melting under different climate conditions? A discussion. *Earth-Science Reviews, 90*(3), 103–113.

https://doi.org/10.1016/j.earscirev.2008.08.003

Schomacker, A. & Kjær, K. H. (2008). Quantification of dead-ice melting in ice-cored moraines at the high-Arctic glacier Holmstrombreen, Svalbard. *Boreas, 37*(2), 211–225. https://doi.org/10.1111/j.1502-3885.2007.00014.x

Seneviratne, S.I., Zhang, X., Adnan, M., Badi, W., Dereczynski, C., Di Luca, A., Ghosh, S., Iskandar, I., Kossin, J., Lewis, S., Otto, F., Pinto, I., Satoh, M., Vicente-Serrano, S.M., Wehner, M. and Zhou. B. (2021). Weather and Climate Extreme Events in a Changing Climate. In Masson-Delmotte, V., Zhai, P., Pirani A., Connors, S.L., Péan, C., Berger, S., Caud, N., Chen, Y., Goldfarb, L., Gomis, M.I., Huang, M., Leitzell, K., Lonnoy, E., Matthews, J.B.R., Maycock, T.K., Waterfield, T., Yelekçi, O., Yu, R. and Zhou B. (*eds.*). *Climate Change 2021: The Physical Science Basis. Contribution of Working Group I to the Sixth Assessment Report of the Intergovernmental Panel on Climate Change* Cambridge University Press, Cambridge, United Kingdom and New York, NY, USA, 1513–1766, doi:10.1017/9781009157896.013

Seppälä, M. (1994). Snow depth controls on palsa growth. *Permafrost and Periglacial Processes, 5*, 283–288.

Smith, M. W., Carrivick, J. L., & Quincey, D. J. (2016). Structure from motion photogrammetry in physical geography. *Progress in physical geography, 40*(2), 247-275. https://doi.org/10.1177/0309133315615805

Slaymaker, O. (2009). Proglacial, periglacial or paraglacial? *Geological Society Special Publication, 320*(1), 71–84. https://doi.org/10.1144/SP320.6

Sollid, J.L. & Sørbel, L. (1998). Palsa bogs as a climate indicator - examples from Dovrefjell, Southern Norway. *Ambio, 27*(4), 287–291.

Svensson, H. (1962). Note on a Type of Patterned Ground on the Varanger Peninsula, Norway. *Geografiska Annaler, 44*(3-4), 413–413. https://doi.org/10.1080/20014422.1962.11881011

Svensson, H. (1992). Frost-Fissure Patterns in the Nordic Countries. *Geografiska Annaler. Series A, Physical Geography, 74*(2-3), 207–218. https://doi.org/10.1080/04353676.1992.11880363

Taylor, S., Feng, X., Kirchner, J. W., Osterhuber, R., Klaue, B., & Renshaw, C. E. (2001). Isotopic evolution of a seasonal snowpack and its melt. *Water Resources Research, 37*(3), 759-769. https://doi.org/10.1029/2000WR900341

Theakstone, W.H. & Knudsen, N.T. (1989). Temporal Changes of Glacier Hydrological Systems Indicated by Isotopic and Related Observations at Austre Okstindbreen, Okstindan, Norway, 1976–87. *Annals of Glaciology, 13*, 252–256. https://doi.org/10.3189/S0260305500007990

Theakstone, W.H. (1990). Twentieth-Century Glacier Change at Svartisen, Norway: The Influence of Climate, Glacier Geometry and Glacier Dynamics. *Annals of Glaciology, 14*, 283–287. https://doi.org/10.3189/S0260305500008764

Theakstone, W.H. & Knudsen, N. T. (1996). Isotopic and ionic variations in glacier river water during three contrasting ablation seasons. *Hydrological Processes, 10*(4), 523–539. https://doi.org/10.1002/(SICI)1099-1085(199604)10:43.0.CO;2-8

Theakstone, W.H. (2003). Oxygen isotopes in glacier-river water, Austre Okstindbreen, Okstindan, Norway. *Journal of Glaciology, 49*(165), 282–298.

https://doi.org/10.3189/172756503781830700

Theakstone, W.H. (2013). Long-term variations of the seasonal snow cover in Nordland, Norway: the influence of the North Atlantic Oscillation. *Annals of Glaciology, 54*(62), 25–34. https://doi.org/10.3189/2013AoG62A300

Thompson, W.F. (1962). Cascade alp slopes and gipfelfluren as clima-geomorphic phenomena. *Erdkunde, 16*(2). https://doi.org/10.3112/erdkunde.1962.02.01

Tonkin, T.N., Midgley, N.G., Cook, S.J., & Graham, D.J. (2016). Ice-cored moraine degradation mapped and quantified using an unmanned aerial vehicle: A case study from a polythermal glacier in Svalbard. *Geomorphology (Amsterdam, Netherlands), 258*, 1–10.

https://doi.org/10.1016/j.geomorph.2015.12.019

Waller, R.I. (2001). The influence of basal processes on the dynamic behaviour of cold-based glaciers. *Quaternary International, 86*(1), 117–128.

https://doi.org/10.1016/S1040-6182(01)00054-4

Waller, R.I., Murton, J. B., & Kristensen, L. (2012). Glacier–permafrost interactions: Processes, products and glaciological implications. *Sedimentary Geology, 255-256*, 1–28. https://doi.org/10.1016/j.sedgeo.2012.02.005

Wang, X., Wang, F., Xiang, Y., & You, H. (2021). A General Framework of Remote Sensing Epipolar Image Generation. *Remote Sensing (Basel, Switzerland), 13*(22), 4539.

https://doi.org/10.3390/rs13224539

Westoby, M.J., Brasington, J., Glasser, N.F., Hambrey, M.J., & Reynolds, J.M. (2012). 'Structure-from-Motion' photogrammetry: A low-cost, effective tool for geoscience applications. *Geomorphology (Amsterdam, Netherlands), 179,* 300–314.

https://doi.org/10.1016/j.geomorph.2012.08.021

Williams, P.J. & Smith, M. W. (1989). *The frozen earth: fundamentals of geocryology*. Cambridge University Press.

Williams, M. W., Knauf, M., Caine, N., Liu, F., & Verplanck, P. L. (2006). Geochemistry and source waters of rock glacier outflow, Colorado Front Range. *Permafrost and periglacial processes*, *17*(1), 13-33. https://doi.org/10.1002/ppp.535

Wilson, N.J. & Flowers, G. E. (2013). Environmental controls on the thermal structure of alpine glaciers. *The Cryosphere, 7*(1), 167–182. https://doi.org/10.5194/tc-7-167-2013

Winkler, S. (2003). A new interpretation of the date of the 'Little Ice Age' glacier maximum at Svartisen and Okstindan, northern Norway. *Holocene (Sevenoaks), 13*(1), 83–95.

https://doi.org/10.1191/0959683603hl573rp

WTW Weilheim GmbH (2008) *WTW Cond 3110 Operating Manual WTW_Cond_3110*. Retrieved from 10.02.22 https://usermanual.wiki/Pdf/WTWCond3110.572769824/html#pf5

Xue, S., Dang, Y., Liu, J., Mi, J., Dong, C., Cheng, Y., Wang, X., & Wan, J. (2016). Bias estimation and correction for triangle-based surface area calculations. *International Journal of Geographical Information Science: IJGIS, 30*(11), 2155–2170.

https://doi.org/10.1080/13658816.2016.1162795

Xylem Analytics Germany GmbH (2018) *Operating manual TetraCon 325/ TetraCon 325/C Standard Conductivity Measuring Cell.* Retrieved from 10.02.2022

https://www.xylemanalytics.com/en/File%20Library/Resource%20Library/WTW/01%20Manuals/ba55301e05_TetraCon_325.pdf

Yde, J. C., & Knudsen, T. N. (2004). The importance of oxygen isotope provenance in relation to solute content of bulk meltwaters at Imersuaq Glacier, West Greenland. *Hydrological Processes*, *18*(1), 125–139. https://doi.org/10.1002/hyp.1317

Yde, J.C., Knudsen, N. T., Steffensen, J. P., Carrivick, J. L., Hasholt, B., Ingeman-Nielsen, T., Kronborg, C., Larsen, N. K., Mernild, S. H., Oerter, H., Roberts, D. H., & Russell, A. J. (2016). Stable oxygen isotope variability in two contrasting glacier river catchments in Greenland. *Hydrology and Earth System Sciences, 20*(3), 1197–1210.

https://doi.org/10.5194/hess-20-1197-2016

Zuecco, G., Carturan, L., De Blasi, F., Seppi, R., Zanoner, T., Penna, D., Borga, M., Carton, A., & Dalla Fontana, G. (2019). Understanding hydrological processes in glacierized catchments: Evidence and implications of highly variable isotopic and electrical conductivity data. *Hydrological Processes, 33*(5), 816–832. https://doi.org/10.1002/hyp.13366

Østrem, G. (1959). Ice Melting under a Thin Layer of Moraine, and the Existence of Ice-cores in Moraine Ridges. *Geografiska Annaler, 41*(4), 228–230.

https://doi.org/10.1080/20014422.1959.11907953

Østrem, G. (1964). Ice-Cored Moraines in Scandinavia. *Geografiska Annaler, 46*(3), 282–337. https://doi.org/10.1080/20014422.1964.11881043

Østrem, G. & Arnold, K. (1970). Ice-Cored Moraines in Southern British Columbia and Alberta, Canada. *Geografiska Annaler. Series A, Physical Geography, 52*(2), 120–128.

https://doi.org/10.1080/04353676.1970.11879817

Østrem, G. (1971). Rock Glaciers and Ice-Cored Moraines, a Reply to D. Barsch. *Geografiska Annaler. Series A, Physical Geography, 53*(3-4), 207–213.

https://doi.org/10.1080/04353676.1971.11879847

Åkesson, H., Nisancioglu, K. H., Giesen, R. H., & Morlighem, M. (2017). Simulating the evolution of Hardangerjøkulen ice cap in southern Norway since the mid-Holocene and its sensitivity to climate change. *The Cryosphere, 11*(1), 281–302. https://doi.org/10.5194/tc-11-281-2017

Appendices

Figure A1 Water level(cm)(blue) and temperature (°C)(orange) of the lake every 30 min between 26.06.21 – 14.09.21, recorded by a diver logger placed in the lake. The water level has been adjusted to account for slight changes in position when data was retrieved from the logger.

Figure A2 Water level(cm(blue)) and temperature (°C)(orange) of stream LS every 30 min between 26.06.21 – 14.09.21, recorded by a diver logger placed in stream LS. The water level has been adjusted to account for slight changes in position when data was retrieved from the logger.

Figure A3 Water level(cm(blue)) and temperature (°C)(orange) of stream LL every 30 min between 26.06.21 – 03.08.21, recorded by a diver logger placed in stream LL.

Figure A4 Water level(cm)(blue) and temperature (°C)(orange) of stream LN1 every 30 min between 26.06.21 – 03.08.21, recorded by a diver logger placed in stream LN1.

Figure A5 Water level(cm(blue)) and temperature (°C)(orange) of stream 005 every 30 min between 09.08.21 – 14.09.21, recorded by a diver logger placed in stream 005.
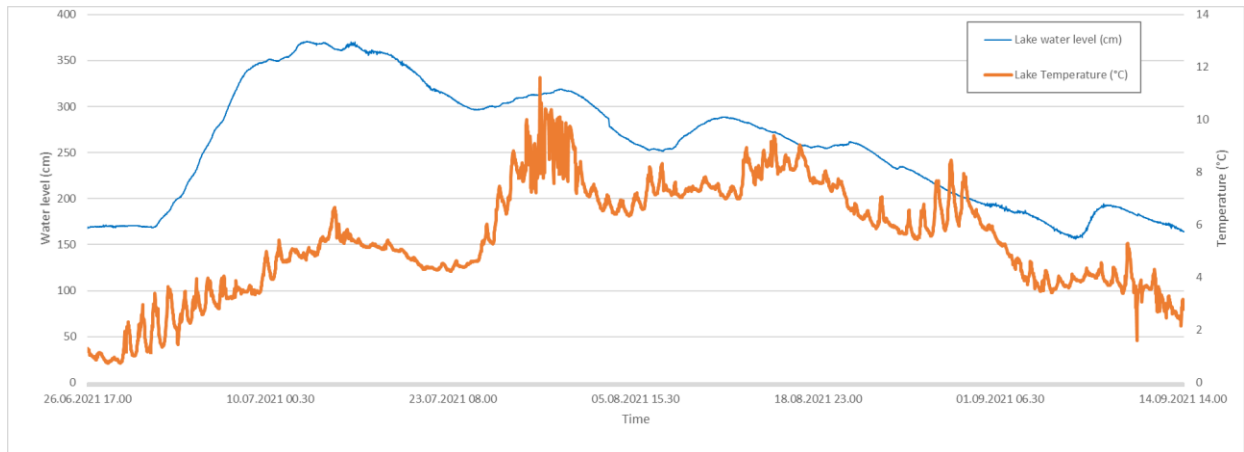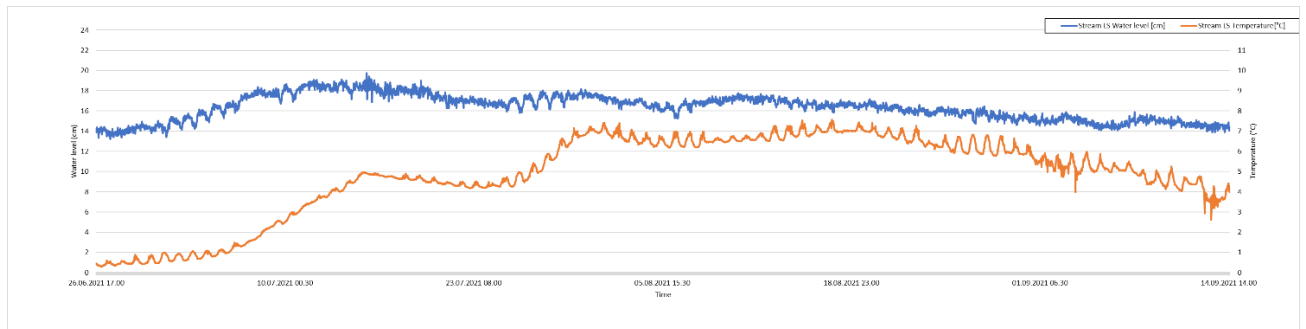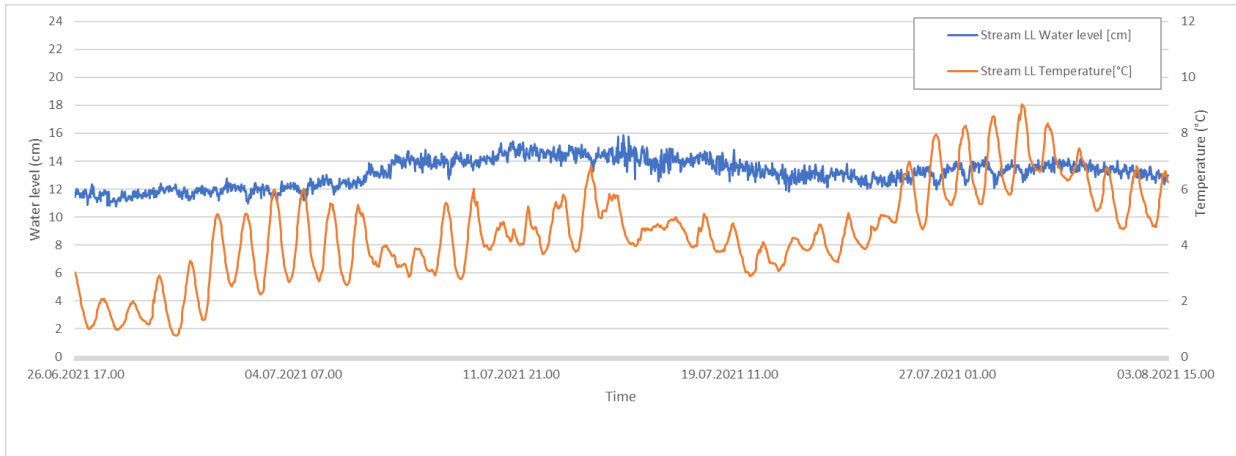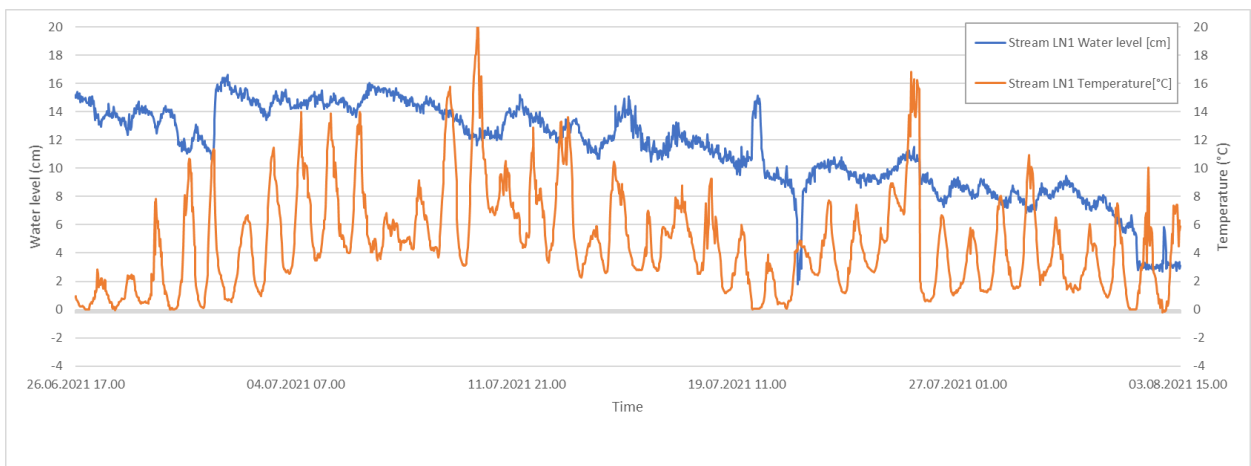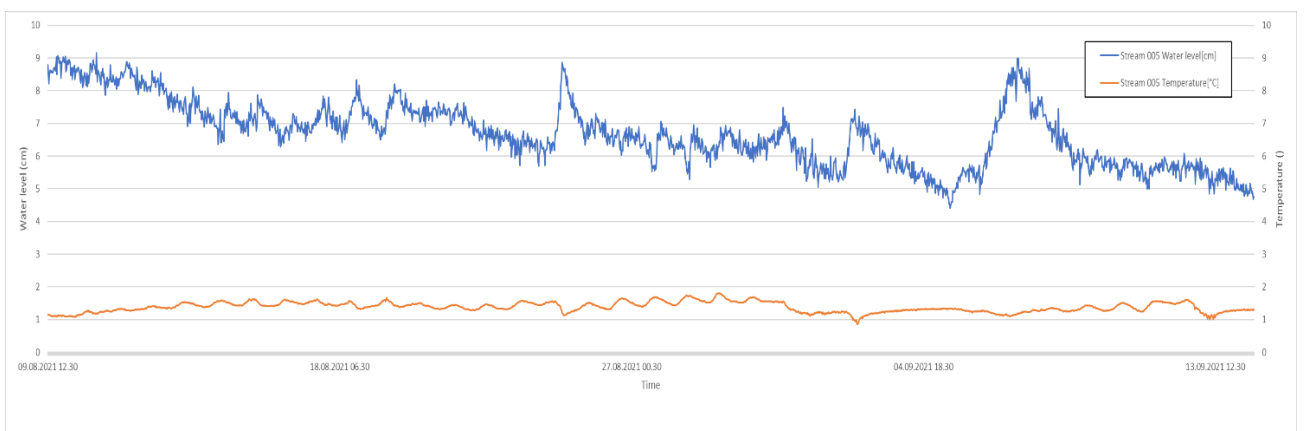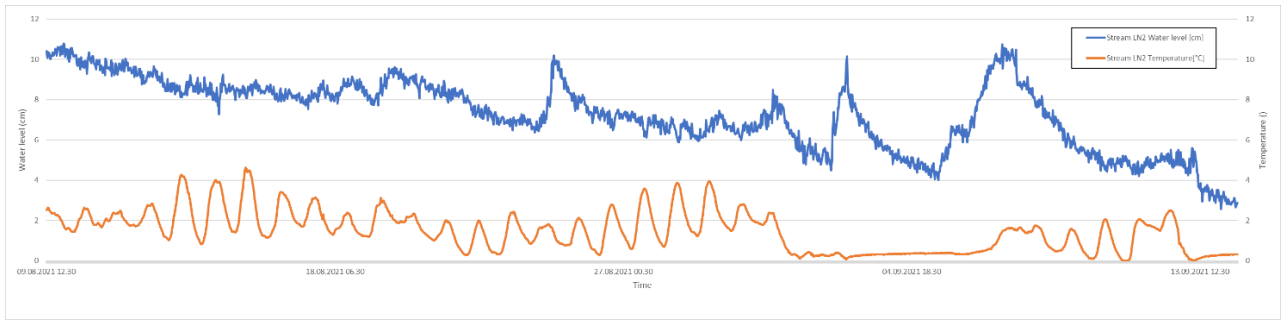
Figure A6 Water level(cm)(blue) and temperature (°C)(orange) of stream LN2 every 30 min between 09.08.21 –
14.09.21, recorded by a diver logger placed in stream LN2.

Table A1: Correlation analysis for the period 26.06 – 03.08.21 for water level and temperature of lake and
streams, in addition to air temperature and barometric pressure

	LS Water level [cm]	LS Temperature[°C]	Lake Water level [cm]	Lake Temperature[°C]	LL Water level [cm]	LL Temperature[°C]	LN 1Water level [cm]	LN1 Temperature[°C]	Air Pressure[cmH2O]	Air Temperature[°C]
LS Water level [cm]	1									
LS Temperature[°C]	0,236715462	1								
Lake Water level [cm]	0,920685372	-0,009862855	1							
Lake Temperature[°C]	0,156754244	0,914903387	-0,122758144	1						
LL Water level [cm]	0,793347905	0,561367026	0,578263572	0,541215607	1					
LL Temperature[°C]	0,054544759	0,736894645	-0,148507826	0,865659195	0,381924689	1				
LN 1Water level [cm]	0,185218471	-0,818181082	0,36346007	-0,708995827	-0,137900163	-0,549713542	1			
LN1 Temperature[°C]	0,310833485	-0,041895637	0,364500633	0,03366333	0,209904171	0,323479064	0,184292582	1		
Air Pressure[cmH2O]	0,007981496	-0,572529519	0,144921904	-0,468660259	-0,166507004	-0,215575053	0,455544356	0,324267981	1	
Air Temperature[°C]	-0,091218619	-0,117462753	-0,15864768	0,221985054	-0,00047165	0,490489379	0,199608785	0,341867984	0,404069117	1

Table A2: Correlation analysis for the period 09.08 – 14.09.21 for water level and temperature of lake and
streams, in addition to air temperature and barometric pressure

|	LS Water level[cm]	LS Temperature[°C]	Lake Water level [cm]	Lake Temperature[°C]	005 Water level[cm]	005 Temperature[°C]	LN2 Water level [cm]	LN2 Temperature[°C]	Air Pressure[cmH2O]	
LS Water level[cm]	1									
LS Temperature[°C]	0,805702205	1								
Lake Water level [cm]	0,948688235	0,833686374	1							
Lake Temperature[°C]	0,839129316	0,922548423	0,874587745	1						
005 Water level[cm]	0,779255873	0,59941271	0,727186772	0,621237503	1					
005 Temperature[°C]	0,138332469	0,384932847	0,205647546	0,456085557	-0,116552483	1				
LN2 Water level [cm]	0,764860007	0,690262383	0,717571249	0,675137867	0,930753561	-0,081281778	1			
LN2 Temperature[°C]	0,487109608	0,602601013	0,547417506	0,722255172	0,432575415	0,685512518	0,437924094	1		
Air Pressure[cmH2O]	-0,233741008	-0,060638123	-0,235238617	-0,143364031	-0,331714434	0,2195847	-0,344044683	-0,097533752	1	
Air Temperature[°C]	0,601551707	0,651696188	0,62884414	0,802921319	0,539980788	0,528898336	0,575019719	0,843779079	-0,135260524	1
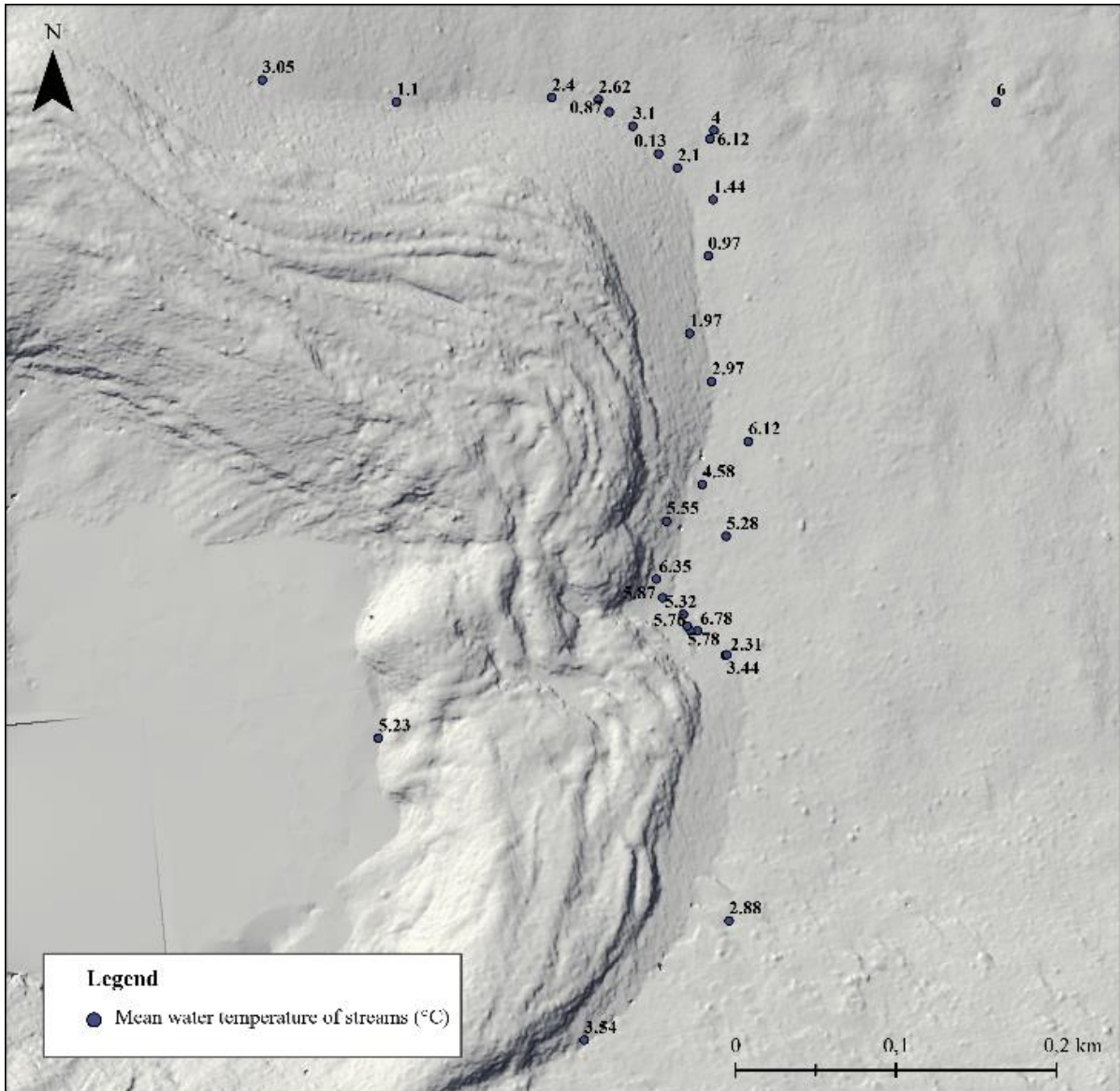
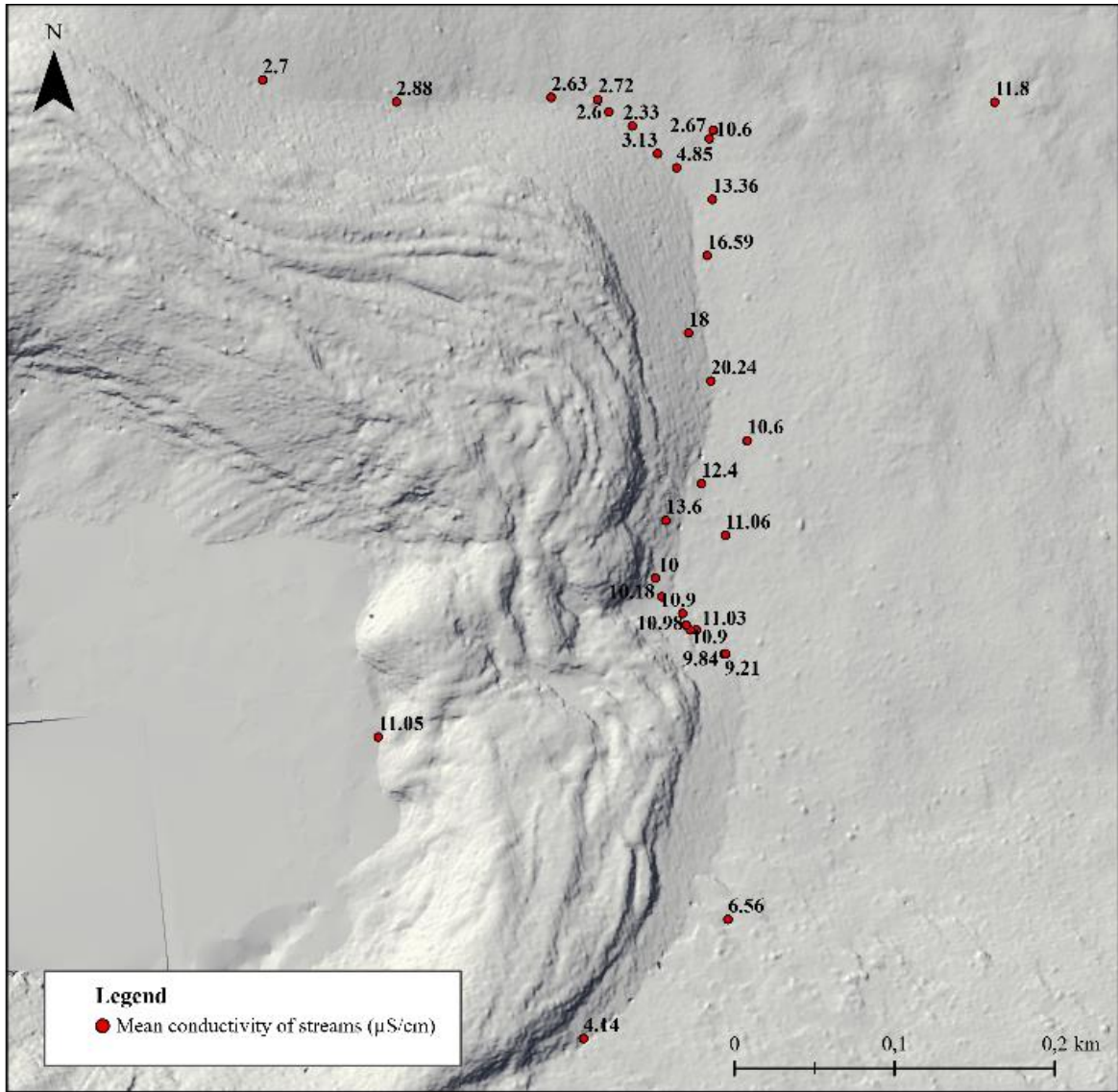*Figure A7 Mean water temperature of streams (raw data is available by request)*

Figure A8 Mean conductivity of streams (raw data is available by request

Table A3: Raw data for stable water isotopes

Name	Date	Time	d18O	d18O_u	dD	dD_u	dxs	dxs_u
Brevann	26.07.21	11.10	-12,05	0.06	-82,9	0.4	13,5	0.6
Snøprøve 2 - 10 cm v/innsjø	26.06.21		-11,39	0.06	-81,6	0.4	9,6	0.6
"Ny"Snø 6 cm 1240 moh - snoprove	26.06.21		-12,78	0.06	-92,5	0.4	9,8	0.6
"Ny"Snø 25 cm 1240 moh - snoprove	26.06.21		-13,57	0.06	-98,8	0.4	9,8	0.6
Snøfonn foran morenen 30 cm	26.06.21		-12,83	0.06	-92,1	0.4	10,6	0.6
Snøfonn 003	25.07.21	17.55	-9,53	0.05	-65,5	0.4	10,7	0.6
Elv i hoveddalen (øvre del)	30.07.21	09.30	-11,51	0.06	-80,5	0.4	11,6	0.6
Elv nedre del 0056	05.08.21	10.43	-11,79	0.06	-82,5	0.4	11,8	0.6
Lake 0023	26.06.21		-13,85	0.06	-95	0.4	15,8	0.6
Lake 0023	25.07.21	19.24	-12,78	0.06	-88	0.4	14,2	0.6
Lake 0023	05.08.21	17.46	-12,41	0.06	-86,2	0.4	13,2	0.6
Logger Bekk Nord	26.06.21		-13,53	0.06	-93,2	0.4	15,1	0.6
Logger Bekk Nord	25.07.21	17.42	-12,74	0.06	-88,1	0.4	13,8	0.6
Logger Bekk Sør	26.06.21		-13,85	0.06	-95,6	0.4	15,2	0.6
Logger Bekk Sør	25.07.21	18.38	-12,68	0.06	-88,1	0.4	13,3	0.6
Logger Bekk Sør	04.08.21	14.05	-12,59	0.06	-86,9	0.4	13,8	0.6
Logger Nedre bekk	26.06.21		-13,76	0.06	-94,8	0.4	15,2	0.6
Logger Nedre bekk	25.07.21	17.25	-12,83	0.06	-88,3	0.4	14,4	0.6
Logger Nedre bekk	04.08.21	18.30	-12,71	0.06	-87,1	0.4	14,6	0.6
0002	25.07.21	18.06	-12,35	0.06	-84,5	0.4	14,3	0.6
0002	04.08.21	14.25	-12,49	0.06	-86,6	0.4	13,3	0.6
0004	25.07.21	18.18	-12,41	0.06	-85,2	0.4	14,1	0.6
0004	04.08.21	14.35	-12,52	0.06	-85,8	0.4	14,4	0.6
0005 Ny log pos	04.08.21	15.20	-12,43	0.06	-85,1	0.4	14,3	0.6
0006	25.07.21	18.30	-12,82	0.06	-87,9	0.4	14,7	0.6
0006	04.08.21	14.30	-12,67	0.06	-86,8	0.4	14,6	0.6
0007	25.07.21	18.50	-12,94	0.06	-88,7	0.4	14,9	0.6
0007	04.08.21	13.50	-12,64	0.06	-86,9	0.4	14,2	0.6
0008	04.08.21	14.00	-12,69	0.06	-87	0.4	14,6	0.6
0009	25.07.21	20.40	-11,83	0.06	-81,5	0.4	13,2	0.6
0009	04.08.21	13.30	-12,49	0.06	-86,3	0.4	13,6	0.6
0010	04.08.21	13.35	-12,68	0.06	-86,9	0.4	14,6	0.6
0012	26.07.21	09.50	-11,79	0.06	-81,3	0.4	13,1	0.6
0012	04.08.21	15.37	-11,47	0.06	-78,3	0.4	13,5	0.6

0013	26.07.21	09.54	-12,7	0.06	-87	0.4	14,6	0.6
0013	04.08.21	15.43	-12,56	0.06	-86,2	0.4	14,2	0.6
0014	26.07.21	10.00	-12,9	0.06	-88,6	0.4	14,5	0.6
0014	04.08.21	15.50	-12,39	0.06	-85,1	0.4	14	0.6
0015	28.07.21	20.22	-11,92	0.06	-81,6	0.4	13,7	0.6
0015	04.08.21	13.22	-11,96	0.06	-82,2	0.4	13,5	0.6
0024	04.08.21	13.17	-12,09	0.06	-82,5	0.4	14,2	0.6
0025	28.07.21	20.15	-12,13	0.06	-83,6	0.4	13,4	0.6
0026	28.07.21	20.42	-11,72	0.06	-80,9	0.4	12,9	0.6
0026	04.08.21	13.40	-12,64	0.06	-86,8	0.4	14,3	0.6
0027	04.08.21	13.40	-12,8	0.06	-87,3	0.4	15,1	0.6
0028	04.08.21	13.47	-12,8	0.06	-87,4	0.4	15	0.6
0029	28.07.21	21.05	-12,95	0.06	-88,7	0.4	14,8	0.6
0029	04.08.21	14.20	-12,89	0.06	-88	0.4	15,1	0.6
0032	04.08.21	15.25	-11,88	0.06	-81,8	0.4	13,3	0.6
0033	04.08.21	15.26	-12,94	0.06	-88,7	0.4	14,7	0.6
0034	29.07.21	14.10	-11,85	0.06	-80,5	0.4	14,3	0.6
0049	04.08.21	14.08	-12,76	0.06	-87	0.4	15,1	0.6
0050	04.08.21	14.10	-12,79	0.06	-87	0.4	15,3	0.6
0051	04.08.21	14.30	-12,38	0.06	-85,2	0.4	13,8	0.6
0053	04.08.21	15.30	-11,44	0.06	-78,5	0.4	13	0.6
0055	04.08.21	15.35	-11,86	0.06	-80,5	0.4	14,4	0.6
0036 lite vann	29.07.21	16.25	-11,24	0.06	-77,1	0.4	12,8	0.6
0037 bekk fra annen bre	29.07.21	17.00	-11,5	0.06	-77,5	0.4	14,4	0.6
0038 liten bre	29.07.21	17.35	-11,71	0.06	-79,9	0.4	13,8	0.6
0040 grunnvann	29.07.21	17.46	-12,3	0.06	-85,2	0.4	13,3	0.6
0042 grunnvann	29.07.21	17.53	-12,52	0.06	-86,8	0.4	13,3	0.6
0043 kilde 1115	29.07.21	18.02	-12,74	0.06	-88,8	0.4	13,1	0.6
0044 bekk	29.07.21	18.09	-12,96	0.06	-89	0.4	14,7	0.6
0045 stor bekk, steinete	29.07.21	18.12	-13,26	0.06	-88,4	0.5	17,6	1.0
0046	29.07.21	18.18	-13,26	0.06	-88,7	0.5	17,4	0.7
0047 bekk	29.07.21	18.22	-13,25	0.06	-88,8	0.5	17,2	0.7
0048	29.07.21	16.25	-12,83	0.06	-86,5	0.5	16,2	0.7

Table A4: Summary statistics for stable water isotopes

d18O		dD		dxs	
Gjennomsnitt	-12,46746269	Gjennomsnitt	-85,79552239	Gjennomsnitt	13,9462687
Standardfeil	0,085669298	Standardfeil	0,610674801	Standardfeil	0,18866965
Median	-12,64	Median	-86,8	Median	14,2
Modus	-12,83	Modus	-88,7	Modus	13,3
Standardavvik	0,701233423	Standardavvik	4,998588675	Standardavvik	1,54432768
Utvalgsvarians	0,491728313	Utvalgsvarians	24,98588874	Utvalgsvarians	2,38494799
Kurstosis	3,597346973	Kurstosis	3,541686583	Kurstosis	1,91371816
Skjevhet	1,024188353	Skjevhet	0,721907125	Skjevhet	-0,70220887
Område	4,32	Område	33,3	Område	8
Minimum	-13,85	Minimum	-98,8	Minimum	9,6
Maksimum	-9,53	Maksimum	-65,5	Maksimum	17,6
Sum	-835,32	Sum	-5748,3	Sum	934,4
Antall	67	Antall	67	Antall	67

Table A5, size of lichen thalli in cm

Ridge and transect line - northern section

	LS11A	LS11B	LS11C	LS12A	LS12B	LS12C	LS13A	LS13B	LS13C	LS14A	LS14B	LS14C	LS15A	LS15B	LS15C	LS16	LS17
	46,8	63,8	37,2	57,2	46,6	52,4	109,2	128,0	102,9	124,0	93,2	173,1	190,0	72,6	160,0	206,0	107,8
	57,6	63,9	40,7	65,8	50,5	56,3	112,9	128,0	107,1	124,5	119,2	177,5	197,0	98,5	155,0	224,0	110,0
	58,1	65,0	46,0	66,8	55,3	60,2	113,3	148,1	115,3	126,1	159,0	185,6	199,0	101,6	134,0	231,0	113,1
	58,4	66,4	46,1	71,7	56,3	69,1	119,3	149,2	122,9	129,2	126,5	227,4	200,0	116,2	219,1	308,0	121,5
	45,7	52,0	35,5	55,0	44,8	51,3	95,7	108,0	99,6	102,8	92,8	145,0	173,0	71,5	205,0	179,0	135,4
Mean lichen size (cm)	53,3	62,2	41,1	63,3	50,7	57,8	110,1	132,3	109,6	121,3	118,1	181,7	191,8	92,1	174,6	229,6	117,6

Ridge and transect line - northern section

	LS21	LS22	LS23	LS24	LS31	LS32	LS33	LS34	LS35	LS41	LS42	LS43	LS44	LS45	LS51	LS52	LS53	LS54	LS55	LS56	LS57
	115,0	124,4	123,6	56,0	47,7	99,7	111,8	183,4	155,0	242,0	206,7	140,6	93,1	46,0	52,2	61,2	144,0	200,0	70,6	225,5	55,7
	117,2	151,0	103,4	56,2	52,2	101,6	124,9	197,1	143,9	225,0	253,6	147,5	73,2	39,8	51,0	59,9	134,9	190,1	76,7	174,0	74,4
	109,1	178,0	139,9	42,6	41,0	101,7	99,3	175,5	156,0	233,4	200,0	156,2	57,3	37,5	47,9	61,5	107,3	134,6	61,4	154,6	60,5
	94,1	121,8	126,3	44,0	39,1	121,1	95,2	186,0	143,0	235,0	183,5	117,8	77,6	44,8	49,9	65,9	111,6	163,0	83,9	179,4	67,7
	104,8	145,2	116,2	39,7	51,3	125,0	98,7	185,3	140,8	182,0	227,7	154,2	86,7	36,5	49,3	66,7	139,7	203,0	65,7	187,0	69,5
Mean lichen size (cm)	108,1	144,1	121,9	47,7	46,2	109,8	106,0	185,5	147,7	223,5	214,3	143,3	77,6	40,9	50,1	63,0	127,5	178,1	71,6	184,1	65,6

Ridge and transect line - southern section

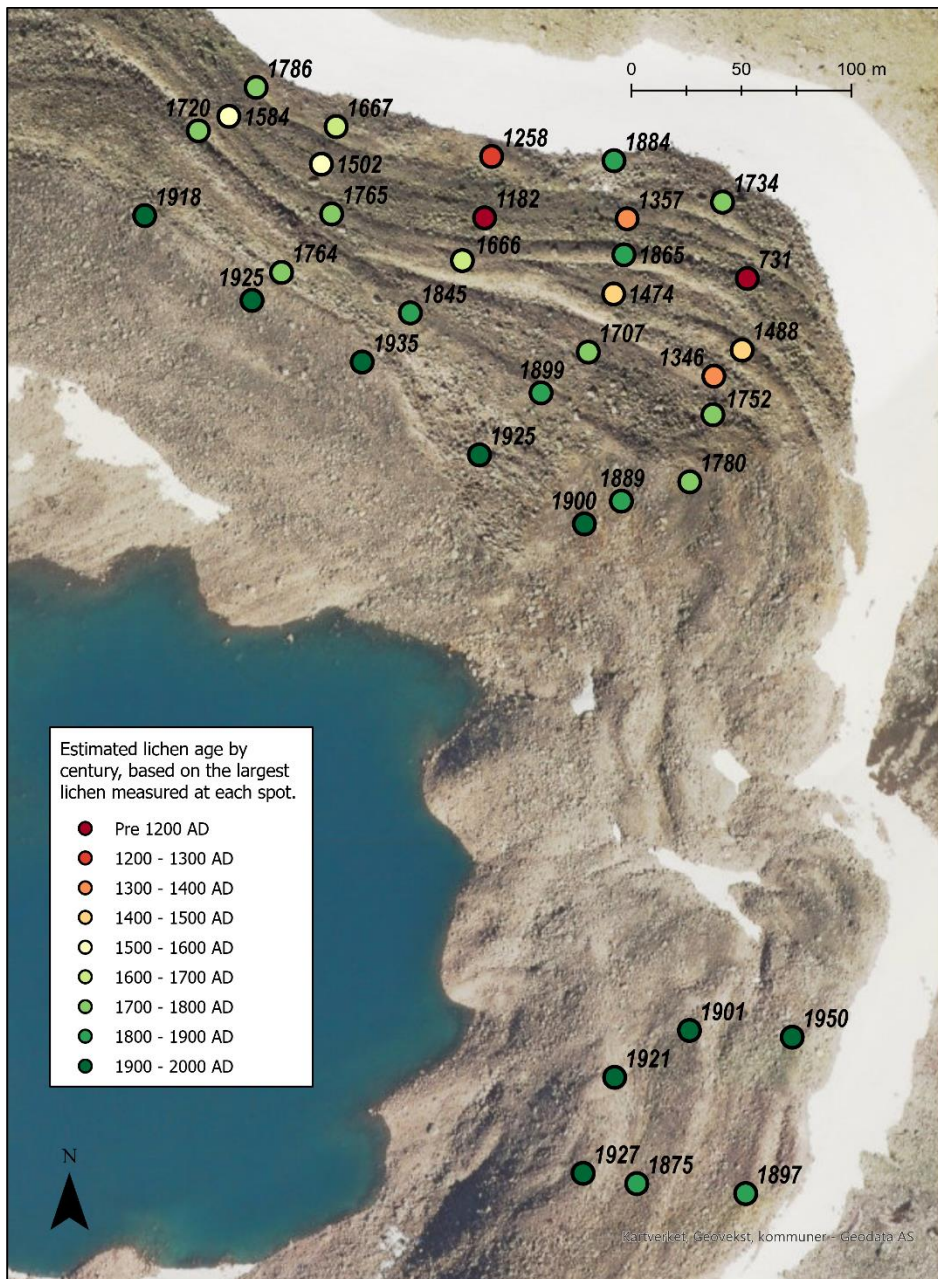|	LS61	LS62	LS63	LS71	LS72	LS73
	50,8	55,6	63,0	34,5	53,4	54,5
	37,4	67,0	61,4	33,6	51,1	47,4
	33,8	61,4	58,5	33,0	58,2	50,3
	44,1	79,2	68,0	34,0	65,8	53,5
	48,2	70,9	64,4	37,0	58,7	43,1
Mean lichen size (cm)	42,8	66,8	63,0	34,4	57,4	49,8

Figure A9 Dating of moraine ridges based on the largest lichen measured at each spot, and date estimates based an indirect lichenometric dating curve: log (y + 150) = 0.003 3 + 2.2343, by Winkler (2003) for Øvre Beiarnbre (ca. 38 km west).
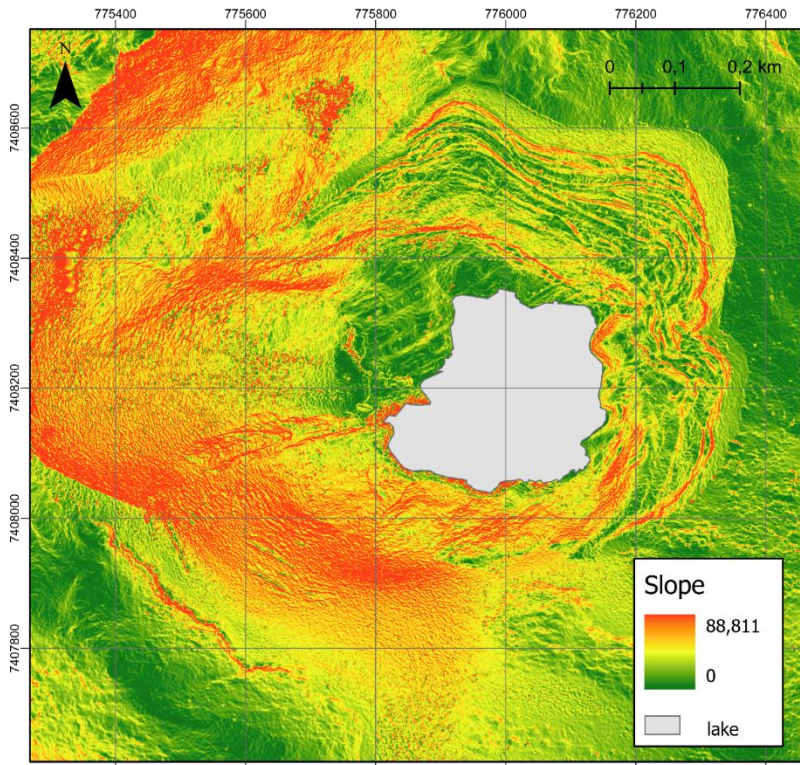
Figure A10 Slope, shows the rate of change in elevation. Calculated based on DEM from Høydedata 0,5 m resolution. Coordinate system: ETRS 1989 UTM 33N.
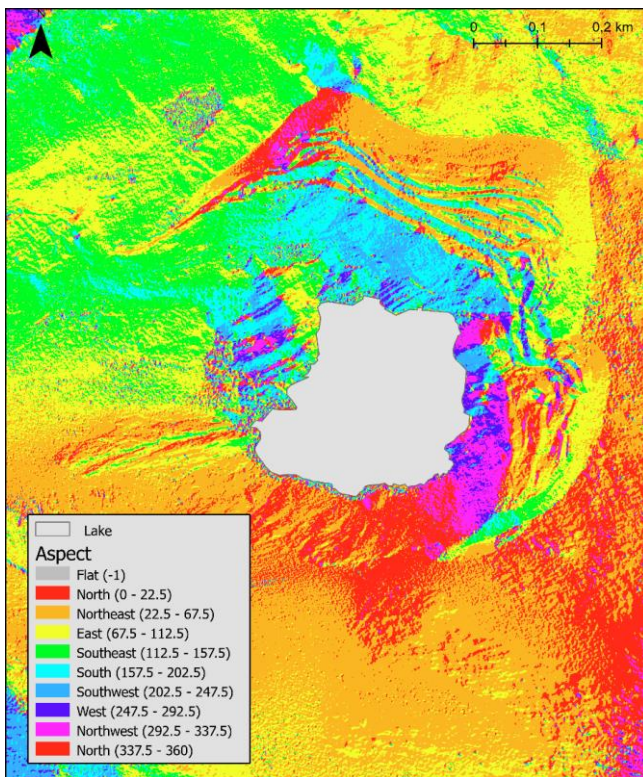

Figure A11 Aspect, Coordinate system: ETRS 1989 UTM 33N. Calculated based on DEM from Høydedata 0,5 m resolution. Coordinate system: ETRS 1989 UTM 33N.